archive

-WOSUB-
A SUBCHANNEL CODE FOR STEADY-STATE AND TRANSIENT THERMAL-HYDRAULIC ANALYSIS OF BWR FUEL PIN BUNDLES
VOLUME I
MODEL DESCRIPTION

by
L. Wolf, A. Faya, A. Levin, L. Gillebaud

Energy Laboratory Report No. MIT-EL-78-023
September 1978

Topical Report for Task 3 of the
Nuclear Power Reactor Safety Research Program

Sponsored by

New England Electric System
Northeast Utilities Service Co.

under the

M.I.T. Energy Laboratory Electric Power Program

ABSTRACT

The WOSUB-codes are spin-offs and extensions of the MATTEO-code [1]. The series of three reports describe WOSUB-I and WOSUB-II in their respective status as of July 31, 1977.

This report is the first in a series of three, the second of which contains the user's manual [2] and the third [3] summarizes the assessment and comparison with experimental data and various other subchannel codes.

The present report introduces the drift-flux and vapor diffusion models employed by the code, discusses the solution method and reviews the constitutive equations presently built into the code. Wherever applicable, possible exteriors of the models are indicated especially with due regard of the findings presented in [3].

Overall, the review of the model and the package of constitutive equations demonstrate that WOSUB-I and II constitute true alternatives for BWR bundle and PWR test bundle calculations as compared to the commonly applied COBRA-IIIC, and COBRA-IIIC/MIT codes which were primarily designed for PWR subchannel and core calculations, respectively. In fact, the incorporation of the drift flux and the vapor diffusion processes into a subchannel code has to be considered a major step towards a more basic understanding and a well balanced engineering approach without the extra burden of a true two-fluid two-phase model.

Recommendations for improvements in the various areas are indicated and should serve as guidelines for future development of this code which in light of the encouraging results presented in [3] seems to be highly warranted.

The WOSUB-code is still in the stage of evolutionary development. In this context, the review reflects the achievements as of July 1977.

ACKNOWLEDGEMENTS

The first consistent checks of the models and solution methods employed by the WOSUB-code were undertaken by Louis Guillebaud who proposed some further improvements in the constitutive equation package especially with respect to the extension of the drift velocity.

Alan Levin provided the additional subroutines for calculating the heat transfer coefficients and the critical heat flux, thus enabling WOSUB to present data beyond the scope of the MATTEO code.

A step further in this direction was done by Arthur Faya who added the fuel pin model based upon the collocation method to the code and who made the code overall operational in the state as described in the present report. Since then, he continued working on and with the code, and it is due to his expertise that this report contains the complete information in what follows.

To all these gentlemen I owe a great deal of gratitude for their tireless efforts in achieving the aforementioned goals.

Finally, I would like to express my gratitude for the financial support as well as for the encouraging discussions by the New England Electric System and Northeast Utilities

Service Company as part of the Nuclear Reactor Safety Research Program under the M.I.T. Energy Laboratory's Electric Power Program.

Lothar Wolf
Principal Investigator
Associate Professor of
Nuclear Engineering

TABLE OF CONTENTS

LIST OF FIGURES

LIST OF TABLES

1. Introduction

1.1 Formulation of the Problem

Recent advances in numerical solution techniques for systems of quasi-linear partial differential equations have led to more refined analyses of complex engineering problems. Therefore, the resulting computer programs can be used for extrapolative engineering design studies with increased confidence.

The nuclear industry employs a large number of computer codes for both steady state and transient analysis of complete nuclear steam supply systems or selected subsystems such as the primary pressure vessel, emergency core cooling system, and the reactor core. Because of the importance of the thermal-hydraulic characteristics of the core, many experimental and analytical studies have been performed on the parallel rod array geometry which is typical of the reactor core design. The study of this geometry is difficult to conduct due to the geometric complexity of the array and the two-phase flow and heat transfer involved in nuclear reactors.

The geometric complexity stems from the high degree of freedom associated with parallel rod arrays. Rod diameter, rod-to-rod pitch, rod spaces type and location, and, for arrays within shrouds, the spacing between rods and shroud as well as the shroud geometry are the principal parameters which affect the thermal-hydraulic performance of rod bundles. In addition, radial

and axial variations of the fuel rod power generation cause coolant flow rate and thermal coolant conditions to vary substantially throughout the array.

The two-phase flow situation of the coolant compounds the difficulties by introducing additional variables such as the vapor volume fraction, velocity and temperature between the phases, and distribution of the phases within the complex flow hold in the bundle.

The development of a computer program for the thermal-hydraulic core and for fuel pin bundle analysis requires the following sequence of major decisions:

1) Definition of code objectives;
2) Selection of a model for the two-phase flow;
3) Choice of primary fluid state variables;
4) Selection of component and process models;
5) Selection of computing procedures, differencing schemes and integration algorithms;
6) Decision upon code structure and programming strategies.

These decisions have been listed in the order of decreasing difficulty. It should be recognized that changing any one of the first three decisions may very well necessitate a totally new start. Naturally, there are many more decisions to be made, such as for instance, for the material descriptions, correlations for momentum and heat exchange etc. However, the aforementioned six are believed to have the greatest impact and some will be reviewed in more detail in what follows.

1.1.1 Definition of Code Objectives

In general, the transient scenario affects the definition of the objectives as well as the scope for both the analysis and the computer code development. The Loss of Coolant Accident (LOCA) and the Anticipated Transient Without Scram (ATWS) are postulated accidents with the most severe consequences. Whereas LOCA leads to high temperatures of the fuel elements in the reactor core, ATWS leads to high pressures in the primary systems. It is obvious that the elimination of the LOCA analysis as code objective will greatly simplify the task of the program development. However, besides the great significance of the transient scenario there are still other phenomena which have not been consistently simulated by common subchannel codes in steady-state BWR bundle analysis yet.

In fact, a review of the available data by Lahey and Schraub [1-1] indicated that there is an observed tendency for the vapor to get to less obstructed, higher velocity regions of a BWR fuel rod bundle. This tendency was seen in quality contours obtained from isokinetic prove sampling of adiabatic air-water flow in a 9-rod array by Schraub et al. [1-2] where it was noted that the flow quality is much higher in the more open interior center subchannels than in the corner and side subchannels. This behavior is shown in Fig. 1.1 which indicates obviously the presence of a thick liquid film on the channel wall and the apparent affinity of the vapor for the more open side and center subchannels. More

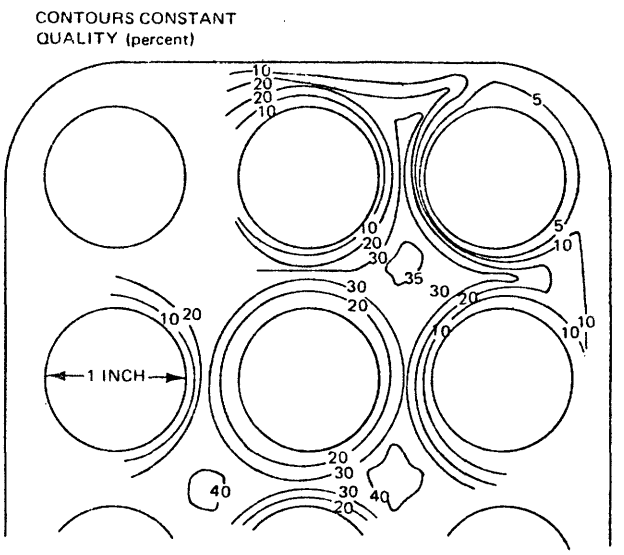

Fig. 1.1: Quality contours from isokinetic probe sampling of air-water flow in a 9-rod array

recent diabatic subchannel data by Lahey [1-3, 1-4] and Bayoumi [1-5] confirmed this observation. Fig. 1.2 clearly indicates that despite the fact that the power-to-flow ratio of the corner subchannel is the highest of any subchannel the quality in this channel is the lowest whereas that in the center subchannel is the highest. In addition, the center subchannel behaves higher-than-bundle average with respect to mass flux while the corner subchannel depicts lower-than-bundle average behavior. The enhanced turbulent two-phase mixing that occurs at the slug-annular transition point ($\bar{x} \sim 0.1$ at 1000 psia) can also be clearly seen in Fig. 1.2. This is in accordance with the observations by Rowe and Angle [1-6].

The aforementioned phenomena have been widely discussed in the open literature. For several years there was a tendency to neglect them mostly because the models incorporated into the subchannel programs then were unable to display the correct trends. Meanwhile a new awareness of these details developed which calls for more advanced modeling.

The complete quantifcation of the void drift transport remains one of the unsolved phenomena today. Therefore, to develop reliable subchannel codes, approximate void drift models must be synthesized.

In any derivation of a model to be implemented into a subchannel code, the conservation of mass, momentum, and energy in each subchannel is involved. This has not only to account for

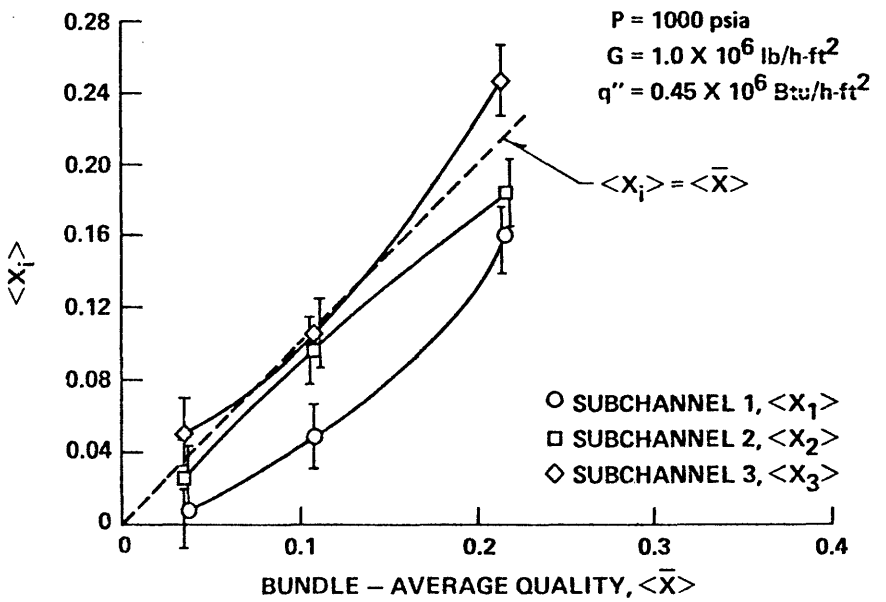

Fig. 1.2a: Variation of subchannel qualities with average quality

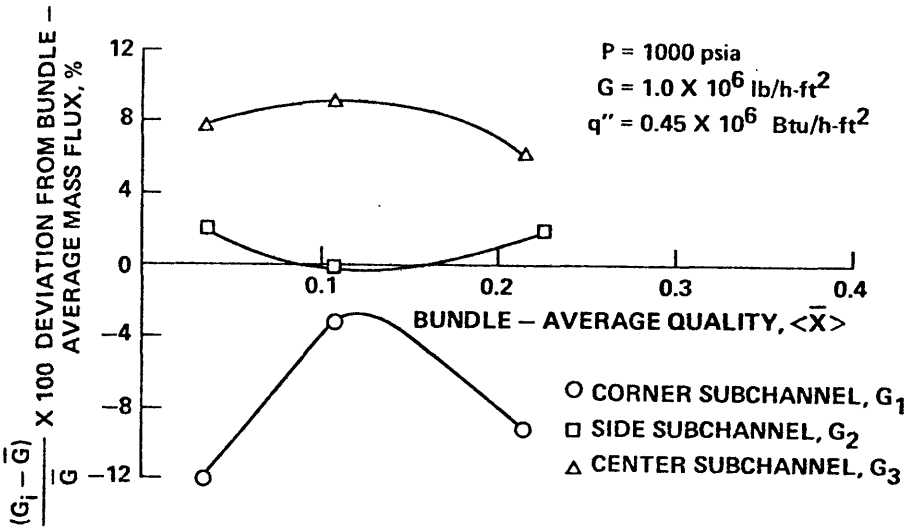

Fig. 1.2b: Comparison of subchannel flows as function of average quality

axial effects but also to consider the transverse interchange of mass, momentum, and energy across the imaginary interfaces which define the subchannels. These transverse transport phenomena are the unique features of any subchannel analysis. Usually, they are subdivided into the following elementary interchange terms according to Lahey and Moody [1-7].

1) Flow diversion occuring due to imposed transverse pressure gradients;
2) Natural turbulent mixing as a result of stochastic pressure and flow fluctuations;
3) Void drift with a strong tendency to approach equilibrium conditions.

In BWR-type fuel rod bundles, the first transverse exchange mode can be neglected because the rod-to-rod spacing is so large that only negligible transverse pressure gradients were observed by Lahey [1-8].

In conclusion, the objectives of the WOSUB subchannel code can be stated as follows:

1) It should predict the correct experimentally found trends in BWR bundle geometry;
2) It should predict the thermal-hydraulic behavior of encapsuled PWR bundles equally well;
3) It should handle most of the ATWS transients;

The following assumptions will be introduced:

a) All LOCA-related phenomena are neglected.
b) Transverse pressure gradients across the bundle are neglected.

1.1.2 Mathematical Models for Multi-Phase Flows

Most recently, several mathematical schemes have been developed in order to account for the velocity and temperature of each phase or component in multi-phase flows. The development of models for multi-phase flows starts by performing space and/or time averaging operations on the Navier-Stokes equations, usually for fluids obeying a linear stress-rate-of-strain relation. In addition, assumptions are introduced to obtain a tractable mathematical description which still contains the essential physics of the situation. These assumptions may be different for different flow situations. Naturally, the higher the complexity of the model, the more field equations are retained and the fewer assumptions are made. When field equations are removed they are replaced by constitutive equations. These simplifications change the coupling between the fields which results in changes of the characteristic curves, which in turn affects especially the prediction of choking conditions according to Bouré [1-9]. However, due to assumption (a) in the foregoing chapter these conditions have been ruled out for WOSUB.

From the two sets of three time-averaged, local phase balance equations many two-phase flow models can be formulated which differ from each other by the number of field equations retained.

The following models have resulted from this process for two-phase flows of a single component fluid [1-10, 1-11].

(1) Homogeneous Flow: The differential model equations consist of one mixture continuity equation, one mixture momentum equation, and one mixture energy equation. Unequal velocity effects are not accounted for. The presence of other phases in the flow field appears only through the friction factor correlations and these are in most cases empirical modifications of single-phase correlations. It should be recognized that many of the overall-mixture correlations are simple curve fits that do not attempt to incorporate representations of basic physical processes.

(2) Homogeneous Equilibrium Model with Slip: The set of differential model equations is exactly the same as for the homogeneous flow although it may or may not contain information about unequal velocities. Mostly this information enters the friction factor correlations which depend now on other correlations that give the velocity ratio, or the velocity difference as a function of the flow field quantities.

(3) The Drift Flux or Diffusion Model: The set of differential model equations consists of two continuity equations (arbitrary combination), one mixture momentum equation and one energy equation. These two latter equations contain differential terms which represent the difference between the sum of the phase momentum and energy fluxes and the mixture momentum and energy fluxes, respectively. Therefore, this model necessitates a constitutive equation for the velocity difference between the

two phases. The drift flux model is an extension of the homogeneous equilibrium approach but it is not as broadly applicable as the two-fluid model. The unequal temperature models have been limited in that one of the phases must be at the saturation state. This special model is called the general drift flux model and accounts for non-equilibrium effects. The four field equations are supplemented by the drift velocity relation as discussed above and by a relation for the time rate of non-equilibrium evaporation or condensation.

(4) Two-Fluid Model: The set of differential models consists of continuity, momentum and energy equations for each phase and/or component in the flow field. The interaction of each phase with all other phases and with stationary surfaces are accounted for by use of simple physical models or empirical correlations. It should be noticed that in addition to accounting for the dynamic behavior of each phase in the mixture, the constitutive equations associated with the two-fluid model allow direct incorporation of more complete descriptions of the physical processes which occur in two-phase flows. That is to say, it would seem that the empiricism which still enters the constitutive equations is introduced at a more basic level than in each of the other aforementioned approaches.

Table 1.1 summarizes the discussion above. It contains additional information about the codes which use the various models described before. A glance at this table shows clearly that the vast majority of today's subchannel computer codes employ the homogeneous model.

In light of the objectives for WOSUB as stated in the foregoing section and by fully acknowledging the shortcomings of the well-known subchannel codes as discussed later, the drift flux model constitutes a powerful compromise between simplicity and complexity. The model certainly describes the interaction between the mixture and the system better than the homogeneous models. It can be applied to all flow regimes if the constitutive equations are known. The drift flux models seem to be appropriate for solving problems with strong local coupling between the phases by lateral mixing and those with weak coupling, i.e., separated flows, where the interface between the phases can be described by simple geometries. The inherent limitations of the drift flux model follow directly from the assumptions underlying the derivation of the relations for the drift velocity and vapor generation. The model should be most effective for a dispersed two-phase flow situation since for this case the constitutive equations can be reduced to realistic forms. Even though most of these relations are derived for steady-state conditions, they can be employed as long as the local relaxation processes are much faster than the global system transients of interest.

TABLE 1.1

MODELS FOR TWO-PHASE FLOW AND HEAT TRANSFER

Model	HEM	Drift Flux	Drift Flux (non-eq.)	2-Fluid
Conservation Equations	Mixture Conti., Mixture Moment., Mixture Energy	Vapor Conti. Liquid Conti Mixture Mom. Mixture Energy	Vapor Conti. Liquid Conti. Mixture Mom. Vapor Energy Liquid Energy	Vapor Conti. Liquid Conti. Vapor Mom. Liquid Mom. Vapor Energy Liquid Energy
No. of Conservation Eqs.	3	4	5	6
Constitutive Eqs.	$T_c=T_{sat}$ $v_v=v_c$ $T_v=T_c$	$v_v-v_c=$ ( ) $T_v=T_c$	$v_v-v_c=$ ( )	
Transport Across Phase Boundary		Mass	Mass Energy	Mass Energy Momentum
Core/ Bundle Subchannel Codes Marching Technique	COBRA-IIIC, COBRA-IIIC/ MIT, COBRA-IIIP/ MIT, THINC-II, TORC, LYNX 1+2	MATTEO WOSUB		
Field Equation Sol. Technique	THINC-IV, COBRA-IV-I	COBRA-DF	COBRA-DF	SCORE COBRA-DF TRAC THERMIT
Loop Codes	RELAP, RETRAN, FLASH, RELAP3B	THOR	TRAC RELAP5	

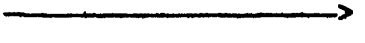

Direction of increased numerical complexity and dependence upon experimental evidence with respect to input and comparison

However, serious problems arise when the drift flux model is applied to problems with sharp density gradients as well as high-frequency transients.

Drift velocity relations and lateral void fraction distributions in vertical ducts have been published for bubbly and slug flows [1-12], for annular flow [1-13] and for dispersed droplets [1-14].

The vapor generation rate, Ψ, for thermodynamic equilibrium can be derived directly from the conservation equations [1-15]. This approach is only valid for moderate heating and flashing rates and does not hold for subcooled boiling and near breaks. In general, Ψ, contains at least time and space derivatives of the pressure field [1-16]. Non-equilibrium vapor generation has been analyzed for subcooled boiling through the prescription of the variation of the liquid enthalpy [1-17, 1-18] and by predicting interphase heat transfer in varying pressure fields [1-19]. A very good review of these issues has been presented by Jones and Saha [1-20] which summarizes the state-of-the-art constitutive relations for Ψ.

In light of the foregoing discussion and by fully acknowledging the need for an advanced modeling for the WOSUB code, the drift flux model seems to be an appropriate and justifiable choice. When coupled with a void drift model in the lateral direction as discussed previously, the combined formulation should be capable of more closely predicting experimentally observed

trends in subchannel behavior. Due to the appreciable amount of information, the implementation of appropriate constitutive equations should pose no serious problems.

1.1.3 Choice of Primary Fluid State Variables

The selection of primary fluid state variables determines to some extent the choices of computation procedure and differencing schemes. Therefore, it is important to understand the impact of the state variable selection.

For integrating the balance equations, two state variables are usually eliminated by virtue of the equations of state. For the prediction of fast transients, it is important that the pressure be retained in the governing equations thereby accounting for the close coupling between the pressure and the inertia. This choice would lend itself automatically to a boundary value problem solution. As the review of subchannel codes shows, the vast majority of them use the concept of a system reference pressure and thereby neglect any compressibility effects. It should be noticed that this choice greatly simplifies the analysis. On the other hand, together with the commonly employed marching type solution technique, it constrains the generality of boundary conditions to be analyzed and thus limits the generality of the total solution.

The next choice concerns internal energy, u, and enthalpy, h, and determines largely the efficiency of thermodynamic

property calculations. The reader is reminded that many property formulations have pressure and enthalpy as arguments. The choice between u and h depends on whether the total or only the thermal energy balance is integrated. The total energy balance is certainly the more fundamental one. Its advantage is that the mechanical stress terms appear in conservative form, i.e., only containing derivatives of products but its disadvantage lays in the introduction of the nonlinear time rate change of the kinetic energy. On the other hand, the thermal energy balance is simpler because it only contains time derivatives of enthalpy and pressure and is preferable when the change in mechanical energy is small compared to the transport of thermal energy. This seems to be valid for fuel pin bundles under normal and slightly off-normal operational conditions.

It is known that the balance equations take on very simple forms when written in a conservative manner and in terms of products like $\rho v=G$ and $\rho h=H$ and the like. However, the complexity shows up again in the calculation of extensive thermodynamic phase properties which are given in terms of mass-weighted properties.

In conclusion and by acknowledging the objectives of the WOSUB code the following choices are made concerning the state variables:

1) The system reference pressure will be employed.

2) The thermal energy equation is used.

3) The balance equations are written in conservative form.

1.1.4 Selection of Component and Process Models

There are various ways to model a core or a fuel pin bundle for the purpose of thermal-hydraulic analysis. One simple way is to smear out local details and to treat a whole bundle cross-section as one node with average physical properties as is done in the MEKIN code [1-21], and the THERMIT code [1-22]. Another alternative which accounts for local details as far as it is feasible for technical purposes is the subchannel representation. Two approaches are known. The first and more common one involves a subdivision where the imaginary subchannel boundaries are drawn at the minimum rod-to-rod and rod-to-wall gaps. This approach is known as the coolant centered subchannel model. The second approach is known as the rod centered subchannel model and was introduced by the Italians [1-23]. Although it lends itself easily for first-order approximations to the local parameters, it never received widespread attention. Due to its close resemblance with the annular geometry it seems easy to apply straightforwardly experimental evidence from annuls to rod bundle geometry as was recently done by Whalley [1-24] for strict annular two-phase flow conditions. Despite these infrequent applications, it is the coolant centered model which is employed worldwide.

In terms of the objectives of the WOSUB code development, the following choices will be selected:

1) WOSUB will employ a subchannel representation of encapsuled bundles;
2) The subchannel will be defined in terms of a coolant centered approach;
3) The balance equations will be formulated on the basis of subchannel control volumes.

1.1.5 Selection of Computing Procedures and Differencing Schemes

Most subchannel codes employ a marching type of solution for the set of conservation equations involved. Although some improvements have been introduced in the past, the underlying principle is still the marching from the inlet to the exit of the channel. As a result, only inlet flow and exit pressure boundary conditions can be handled by codes such as COBRA-IIIC [1-25]. However, there are many areas where flow reversal and recirculation have to be considered and where the lack of pressure boundary conditions at the inlet and exit is very inconvenient. These areas include the analysis of LOCA and natural circulation under very low flow conditions. The effective treatment of these phenomena is only possible with a pressure-velocity method which accepts either flow or pressure boundary conditions. Such a boundary value problem solution has been built into COBRA-IV [1-26] and is called the explicit transient option due to the temporally explicit finite differencing. Unfortunately, this method requires a strict homogeneous flow model thereby even

not allowing slip between the phases and the application of a subcooled boiling model. This means severe limitations in the physical model which outweigh the advantages of the numerical solution method.

A much better approach is offered by the THERMIT code [1-22] which combines easily both advanced two-fluid modeling and boundary value problem solution method. The only drawback of THERMIT as of now is that it has not been extended yet to subchannel methodology.

Given the aforementioned facts, and in light of the overall objectives of the code, it was decided to choose the following differencing scheme and computation procedure:

1) Application of semi-implicit spatial and temporal finite difference scheme;

2) Use of a marching type solution method.

In essence, these two selections indicated above mean that the overall solution method of the MATTEO-code [1-27] are maintained in WOSUB, because it was thought that the physical model should have higher priority than the numerical method. In retrospect, this choice seems justified on the grounds that the advanced numerical methods are available now at any desired level of sophistication.

1.2 Brief Review of Subchannel Codes

Because of the overall complexity of a thermal hydraulic analysis of fuel pin arrays, many computer programs have been developed. Representative of the codes in use are COBRA-IIIC [1-25], HAMBO [1-28], HOTROD [1-29] and THINC-II [1-30]. All of these codes are based on a fluid flow model that assumes that the rod array can be represented by parallel interconnected channels. Homogeneous flow and one-dimensional slip flow are assumed, while exchanges of mass, energy and momentum are allowed by diversion and turbulent cross flows. All of these codes are based on the equi-mass model, which means that transverse exchange processes are governed by a mass for mass exchange between the subchannels. Therefore, only momentum and energy are transported across the imaginary subchannel boundaries. Differences between the aforementioned codes exist only in the manner how the various mixing modes are coupled. In HAMBO [1-28] for instance it is assumed that diversion and turbulent crossflows are dependent upon each other. Other differences exist with respect to the treatment of transverse pressure gradients. Whereas the solution method of COBRA-IIIC is indirectly driven by those gradients, the solution methods of HOTROD and MATTEO rely on the basis that these gradients do not exist. Besides these details, all of the codes have in common that the Navier-Stokes equations have been simplified to be consistent with the assumptions and the resulting set of equations is generally solved as an initial value

problem. These simplifications usually result in an incomplete representation of the momentum component in the transverse direction as well as in an inability to handle flow reversals. Although COBRA-IV [1-26] can treat the latter, it still suffers from the first shortcoming.

A first consistent treatment of the subchannel problem was suggested by Wnek et al. [1-31] and led eventually to the SCORE-code, which was later overcome by a more advanced methodology in the TRAC-code [1-32]. However, SCORE was intended to be a subchannel code, while TRAC is a vessel code. Even the THERMIT code development stopped at the level of bundle-wide analysis simply for the reason that it has no turbulent mixing processes built in thus far. Therefore, to the author's knowledge, there is no advanced subchannel code around which substitutes SCORE and at the same time combines the various advantages of TRAC and THERMIT.

In conclusion of this brief review, one can state with confidence that the subchannel code development has not yet reached its end. Certain developments such as COBRA-IV have reached a dead end due to its overly simplistic model and inefficient numerical scheme as far as the explicit option is concerned. More recent schemes seem to have bright future potential for subchannel analysis purposes but need more efforts for realization.

On the other hand, it must be fully recognized that codes like COBRA-IIIC/MIT as single stage method and the vendors'

two stage methods which are based upon similar models and solution methods have been licensed by NRC, thus forming an engineering design basis. Therefore, from this point of view there is seemingly no incentive for improvements, unless the inherent overconservatism in these approaches becomes unbearable.

With all these imformations on hand, the remaining question to be answered is: How does the WOSUB code fit into this overall picture?

Given the objective of non-LOCA application and the need for an engineering tool rather than a benchmark code the following decisions have been made:

1) The code should operate as closely as possible with a methodology known from the other common subchannel codes.
2) Rather than following recent trends in modeling and solution technique, the emphasis should be put into the drift flux-vapor diffusion model.
3) With the help of the vapor diffusion concept some drawbacks of the treatment of the transverse exchange terms in other codes can be overcome.

1.3 Conclusions

In summary of the decisions listed in the various sections before, the following overall approach for WOSUB emerges:

1) The code should handle most of the operational transients including some ATWS transients as long as the type of boundary conditions would allow it.
2) LOCA conditions are excluded.
3) The code will employ a drift flux model for improved prediction capability of void distributions. The Zuber-Findlay formulation will be used.
4) In the transverse direction, both natural turbulent mixing and vapor drift on a volume to volume exchange basis will be considered, whereas transverse pressure gradients will be suppressed.
5) A vapor generation rate term accounts for thermodynamic non-equilibrium conditions in subcooled boiling.
6) The code will use the system reference pressure concept, thus neglecting any compressibility effects.
7) Balance equations in conservative form will be used.
8) The balance equations are derived from a control volume approach set up for a coolant centered subchannel model.
9) Fully implicit differencing schemes are applied in space and time.
10) The set of equations are solved by a marching technique.

11) Because there is no diversion crossflow involved, the concept of recirculation loop is introduced to obtain a closed set of equations.

1.4 References

[1-1] R.T. Schraub, F.A. Schraub, "Mixing,Flow Regimes and Void Fraction for Two-Phase Flow in Rod Bundles," Two-Phase Flow and Heat Transfer in Rod Bundles, ASME Booklet, 1969.

[1-2] F.A. Schraub et al., "Two-Phase Flow and Heat Transfer in Multirod Geometrics, Air-Water Flow Structure Data for a Round Tube, Concentric and Eccentric Annulus, and Nine-Rod Bundle," GEAP-5739, 1969.

[1-3] R.T. Lahey et al., "Mass Flux and Enthalpy Distribution in a Rod Bundle for Single- and Two-Phase Flow Conditions," J. Heat Transfer, 1971.

[1-4] R.T. Lahey et al., "Out-of-Pile Subchannel Measurements in a Nine-Rod Bundle for Water at 1000 psia," Progress in Heat and Mass Transfer, Vol. VI, Pergamon Press, 1972.

[1-5] M. Bayoumi et al., "Determination of Mass Flow Rate and Quality Distributions Between the Subchannels of a Heated Bundle," European Two-Phase Flow Meeting, Erlangen, Germany, 1976.

[1-6] D.S. Rowe, C.W. Angle, "Cross Flow Mixing Between Parallel Flow Channels During Boiling - Pt. III," BNWL-371, 1969.

[1-7] R.T. Lahey, F.J. Moody, "The Thermal-Hydraulics of a Boiling Water Nuclear Reactor, ANS Monograph Series, 1977.

[1-8] R.T. Lahey et al., "Two-Phase Flow and Heat Transfer in Multirod Bundles: Subchannel and Pressure Drop Measurements for Diabatic and Adiabatic Conditions," GEAP-13049, 1970.

[1-9] J.A. Bouré, "On a Unified Presentation of the Non-Equilibrium Two-Phase Flow Models," in Non-Equilibrium Two-Phase Flows, ASME, 1975.

[1-10] M. Ishii, Thermo-Fluid Dynamic Theory of Two-Phase Flow, Eyrolles, Paris, France, 1975.

[1-11] E.D. Hughes et al., "An Evaluation of State-of-the-Art Two-Velocity Two-Phase Flow Models and their Applicability to Nuclear Reactor Transient Analysis," Vol. 1: Summary, EPRI-NP-143, Feb. 1976.

[1-12] N. Zuber, A.J. Findlay, "Average Volumetric Concentration in Two-Phase Flow," J. Heat Transfer, 87, 1965.

[1-13] M. Ishii et al., "Constitutive Equations for Vapor Drift Velocity in Two-Phase Annular Flow," AIChe J, 22 (1976), 283.

[1-14] M. Ishii, "One-Dimensional Drift Flux Modeling: Vapor Drift Velocity for Dispersed Two-Phase Flow," ANL-76-15 and ANL-76-49, 1976.

[1-15] L.S. Tong, Boiling Heat Transfer and Two-Phase Flow, John Wiley & Sons, 1967.

[1-16] W. Wulff et al., "Development of a Computer Code for Thermal Hydraulics of Reactors (THOR)," Sixth Quarterly Progress Report, BNL-NUREG-50569, Jan-March 1976.

[1-17] N. Zuber et al., "Steady-State and Transient Void Fraction in Two-Phase Flow Systems," GEAP-5417, Vol. 1, 1967.

[1-18] D. Maitra, K.S. Raju, "Vapor Void Fraction in Subcooled Flow Boiling," Nucl. Engng. and Des., 32 (1972), 20.

[1-19] O.C. Jones, N. Zuber, "Evaporation in Variable Pressure Fields," 16th National Heat Transfer Conf., St. Louis, Paper No. 76-CSME/CSCME-12, 1976.

[1-20] O.C. Jones, P. Saha, "Non-Equilibrium Aspects of Water Reactor Safety," BNL-NUREG-23143, July 1977.

[1-21] R.W. Bowring et al., "MEKIN: MIT-EPRI Nuclear Reactor Core Kinetics Code," Research Project 227, CCM-1, Dec. 1975.

[1-22] W.H. Reed et al., "THERMIT: A Computer Program for Three-Dimensional Thermal-Hydraulic Analysis of Light Water Reactor Cores," Internal MIT Report, Dept. Nucl. Engng., Sept. 1978.

[1-23] G.P. Gaspari et al., "A Rod-Centered Subchannel Analysis with Turbulent (Enthalpy) Mixing for Critical Heat Flux Prediction in Rod Clusters by Boiling Water," Proc. Fifth Int. Heat Transfer Conf., Tokyo, Paper B6.12, 1974.

[1-24] P.B. Whalley, "The Calculation of Dryout in a Rod Bundle," Int. J. Multiphase Flow, 3 (1978), 501-515.

[1-25] D.S. Rowe, COBRA-IIIC: A Digital Computer Program for Steady-State and Transient Thermal Hydraulic Analysis of Rod Bundle Nuclear Fuel Elements, BNWL-1695, 1973.

[1-26] C.W. Stewart et al., "COBRA-IV: The Model and the Method," BNWL-2214, July 1977.

[1-27] G. Forti, J.M. Gonzalez-Santalo, "A Model for Subchannel Analysis of BWR Rod Bundles in Steady State and Transient," Int. Conf. Reactor Heat Transfer, Karlsruhe, Germany, 1973.

[1-28] R.W. Bowring, "HAMBO, A Computer Programme for the Subchannel Analysis of the Hydraulic and Burnout Characteristics of Rod Clusters - Pt. 2, The Equations, AEEW-R-582, Jan. 1968.

[1-29] S.G. Beus, J.H. Anderson and R.J. DeCrestofaro, "HOTROD - A Computer Program for Subchannel Analysis of Coolant Flow in Rod Bundles," WAPD-TM-1070 (1973).

[1-30] H. Chelemer et al., "Subchannel Thermal Analysis of Rod Bundle Cores," Nucl. Eng. Des. 21 (1972), 35-45.

[1-31] W.J. Wnek et al., "Transient Three-Dimensional Thermal-Hydraulic Analysis of Nuclear Reactor Fuel Rod Arrays: General Equations and Numerical Scheme," ANCR-1207, Nov. 1975.

[1-32] "TRAC-2: An Advanced Best-Estimate Computer Program for PWR LOCA Analysis, Vol. I: Methods, Models, User Information and Programming Details, Draft, Thermal Reactor Safety Group, Energy Division Los Alamos Scientific Laboratory.

2. Drift Flux, Vapor-Diffusion Model

2.1. Introduction

The main objective of the WOSUB code is to predict local flow and heat transfer conditions in the subchannels of BWR bundles and PWR test bundles during steady state and transient operations. These bundles are subdivided in the plane perpendicular to the flow direction into the commonly employed subchannels, which are considered the smallest control volumes in the analysis. The basic conservation equations for the drift-flux modeling of the two-phase flow, i.e.,conservation of mixture mass, conservation of the vapor mass, conservation of mixture energy and conservation of mixture momentum,are written down in terms of quantities which are averages over these control volumes. Due to the various transport processes in the transverse direction (i.e., in the plane perpendicular to the axial flow direction) induced by geometric changes of the coolant cross sectional areas and/or the boiling process,the individual flow channels communicate with each other in a very complex and not yet fully understood manner. These transverse mass, momentum, and energy exchange processes are accounted for in the WOSUB code in a quite different way as hitherto incorporated in the other well-known subchannel code. Figs. 2.1a through 2.1c summarize the transport phenomena between two control volumes in the axial & transverse directions.

2.2. List of Assumptions

The following assumptions will be applied through-

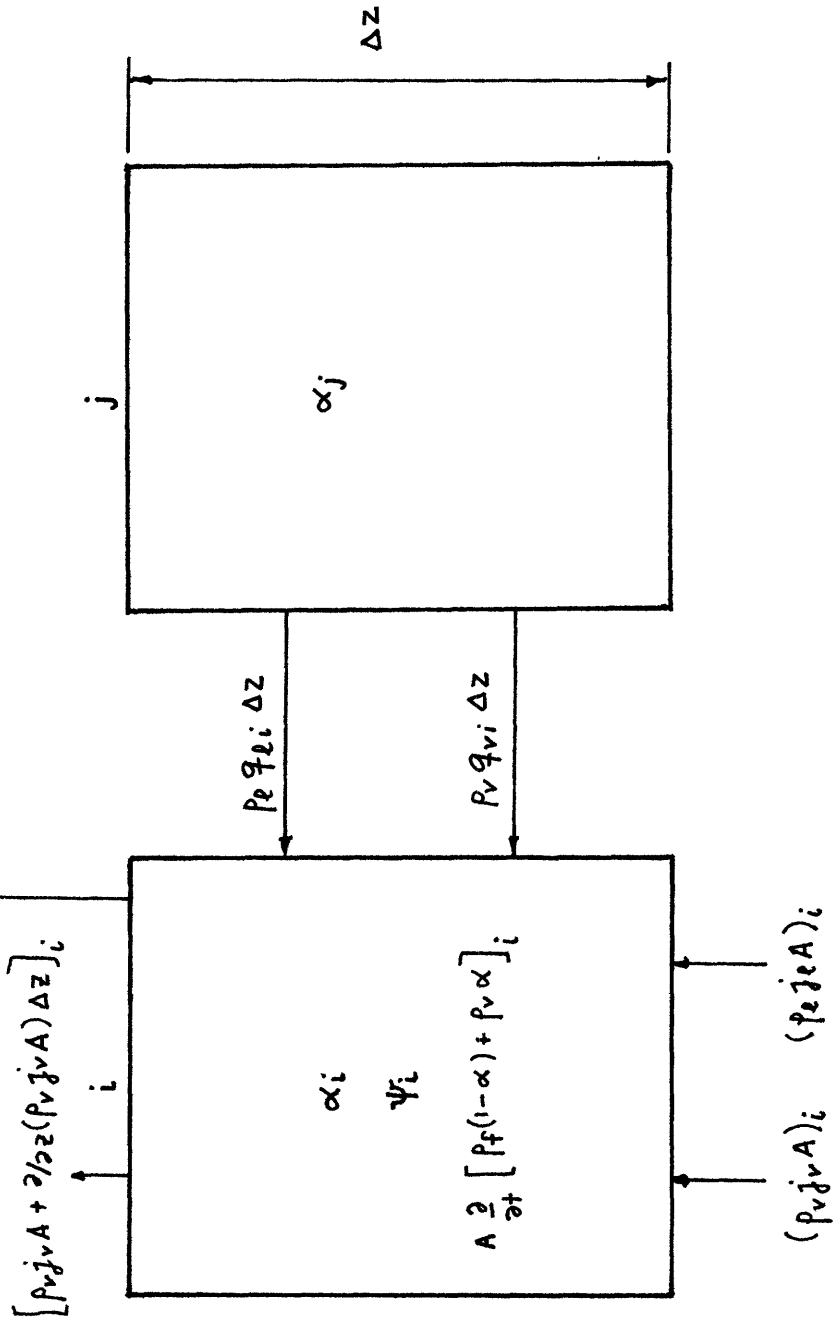

Fig. 2.1a: Control volumes used to derive the subchannel continuity equation.

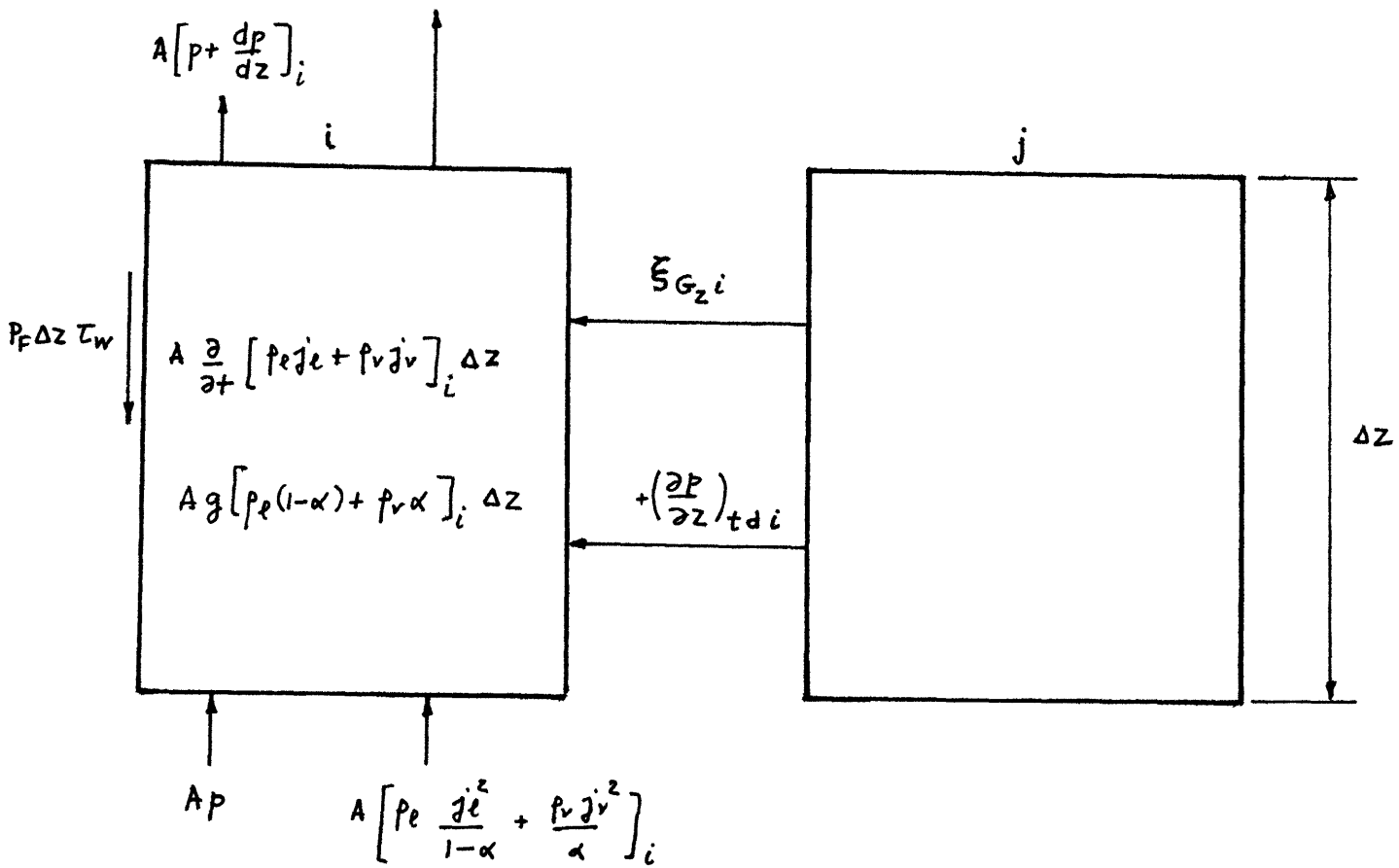

Fig. 2.1b: Control volume used to derive the subchannel axial momentum equation.

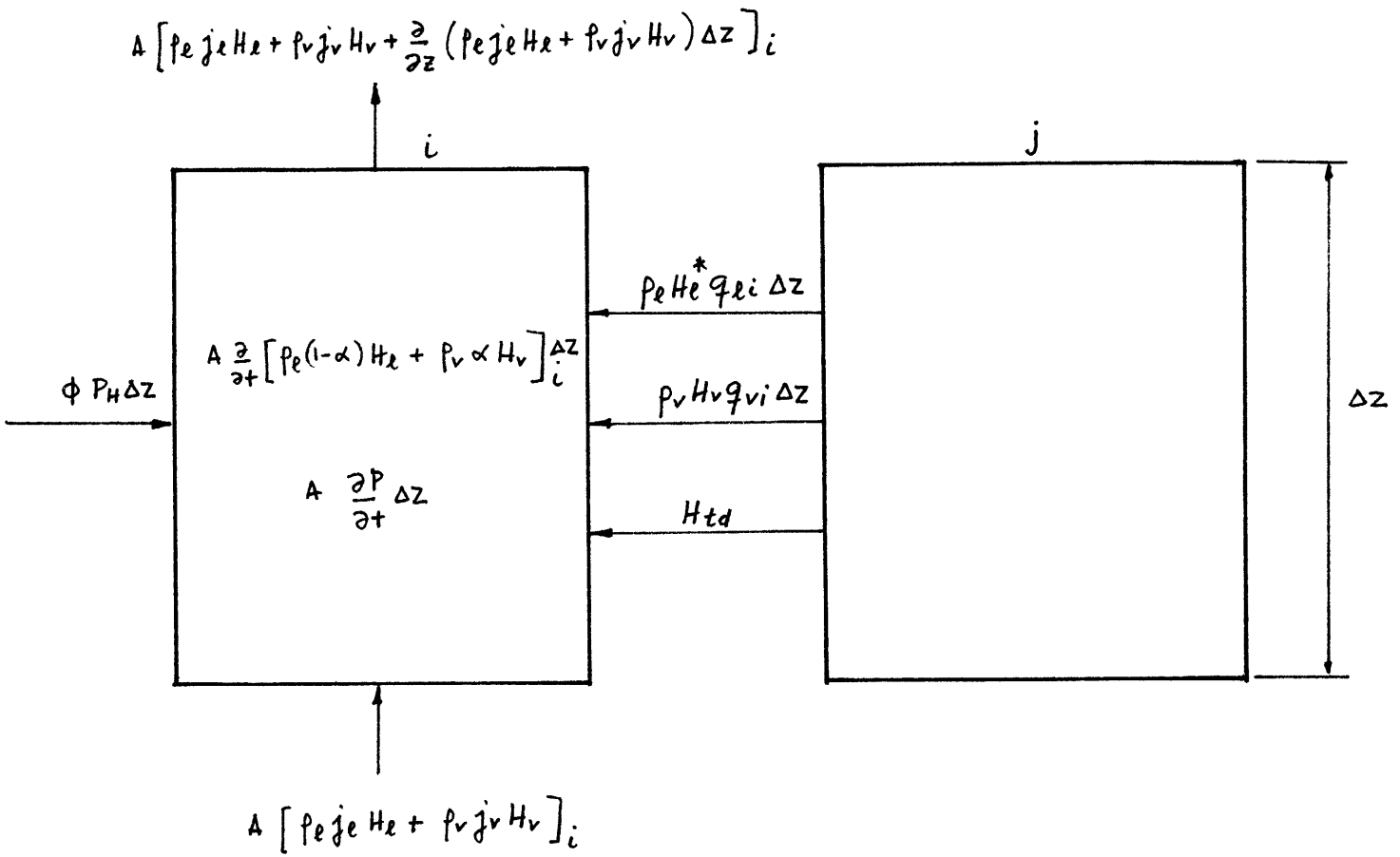

Fig. 2.1c: Control volumes used to derive the subchannel energy equation.

out the model development in order to make it more tractable:

2-1. The density of the liquid phase is assumed to be constant. Other liquid phase properties are evaluated at saturation thus leaving the system pressure as the only independent variable which is considered to be a known function of time. It is obvious that this assumption drastically simplifies the whole analysis by eliminating the effect of compressibility and thus sound wave propagation effects. This assumption is also known as the system reference pressure concept and as such is widely used in all COBRA-codes including COBRA-IV-I. Only recent developments for COBRA-DF eliminated this limitation by virtue of the ACE technique [2-1]. In practical terms, the reliance upon this assumption means that no reliable blowdown calculations can be performed with WOSUB in its present form.

Certainly, the constant liquid density assumption could be easily relaxed but it is felt that at least for BWR applications, where the inlet subcooling is usually low, no significant error is introduced.

2-2. The vapor is considered to be always saturated. Furthermore, no liquid superheat is allowed in the present version. Therefore, thermodynamic equilibrium in the bulk boiling regime is assumed to prevail. This latter assumption could be easily removed in order to allow for flashing phenomena during depressurization transients.

2-3. It is assumed that no transverse pressure gradients exist at any axial elevation in the bundle. This essentially means that all subchannels depict the same axial pressure drop at all elevations. The assumption is known as the fully ventilated channel assumption. It eliminates the diversion cross flow transport due to different subchannel pressures as used in the COBRA codes and similar other ones. This assumption plays a major role in the solution scheme of the WOSUB code and its removal would necessitate a complete reformulation.

2-4. The assumption 2-3 actually removes the transverse momentum equation in its various incomplete forms as used by various subchannel codes such as COBRA-II, COBRA-IIIC, FLICA and the like. Yet in order to maintain a determined set of equations and unknowns, the assumption is introduced that the net volume flow recirculation along closed paths is zero around the fuel pins. By virtue of this concept which has its physical counterpart in various areas of fluiddynamic theory the problem becomes completely determined. It is worthwhile mentioning that this concept is not a unique invention in WOSUB. Rather, it has been successfully used already in the HAMBO code [2-2] in the past and most recently by Whalley [2-3] in his attempt of an annular flow subchannel analysis.

2-5. The neglection of diversion cross flow does not mean that there is no transverse transport process at all. Rather, the exchange due to natural turbulence remains in effect.

On top of this, an additional vapor diffusion process on a volume-to-volume basis is introduced. This is truly a unique feature of the WOSUB model and simulates the experimentally observed tendency of the vapor to diffuse preferentially into areas with higher velocities.

2.3 Conservation Equations

The four conservation equations can be written for each subchannel i with due respect of the above listed assumptions as follows:

Continuity equation for the mixture

$$A \frac{\partial}{\partial t} (\rho_f(1-\alpha) + \rho_v \alpha \,]_i + A\frac{\partial}{\partial z} [\rho_\ell j_\ell + \rho_v j_v \,]_i = \rho_{\ell q \ell_i} + \rho_v q_{v_i} \quad (2.1)$$

Continuity equation for the vapor phase:

$$A \frac{\partial}{\partial t} (\rho_v \alpha)_i + A\frac{\partial}{\partial z} (\rho_v j_v)_i = A\rho_{v_i} \Psi_i + \rho_{v_i} q_{v_i} \quad (2.2)$$

(2.3)

Conservation of axial momentum for the mixture:

$$\frac{\partial P}{\partial z} = \left(\frac{\partial P}{\partial z}\right)_g + \left(\frac{\partial P}{\partial z}\right)_a + \left(\frac{\partial P}{\partial z}\right)_f + \frac{\partial G_z}{\partial t} - \xi_{Gz} - \left(\frac{\partial P}{\partial z}\right)_{t_d}$$

Conservation of energy for the mixture:

$$A\frac{\partial}{\partial t} [\rho_\ell(1-\alpha)H_\ell + \rho_v \alpha H_v]_i + A \frac{\partial}{\partial z} [\rho_\ell j_\ell H_\ell + \rho_v j_v H_v]_i \quad (2.4)$$

$$= A[\Phi + \frac{\partial P}{\partial t}] + \rho_\ell H_\ell q_{\ell_i} + \rho_v H_v q_{v_i} + H_{t_d}$$

The set of conservation equations constitutes only one set. Other selections could contain the continuity equations of both individual phases or the continuity equation for the mixture and that for the liquid alone. It should be noticed that all these sets are perfectly identical with respect to handling the physical situation on hand.

Due to the fact that some of the terms on the right hand side are unique to WOSUB, they are explained in some more detail in what follows.

The right hand side of the conservation equation for the mixture, Eq. (2.1), contains the two flows, q_{ℓ_i} and q_{v_i}, which are the total liquid and vapor flow, respectively, transported into subchannel i from all neighboring subchannels. Both flows appear again in connection with the energy conservation equation, where $\hat{H}^*_\ell$ is the enthalpy of the liquid transported into subchannel i. Naturally, the continuity equation for the vapor phase incorporates only the vapor flow into subchannel i together with the vapor volume generation per unit volume, Ψ_i, in this subchannel. The latter term is a unique feature of the drift-flux model and its specification is a major part of the constitutive package discussed in Chapter 3. The term H_{td} appearing in the mixture energy conservation equation, Eq. (2.4), constitutes the energy transfer due to turbulent liquid-liquid mixing in the subcooled region. Similarly, the term $(dP/dz)_{td}$ in the mixture momentum conservation equation, Eq. (2.3), presents the turbulent shear stress due to

velocity differences in the subchannels, whereas ξ_{G_z} accounts for the axial momentum transferred into subchannel i by the flow diverted from the other subchannels. Fig. 2.1 summarizes the various transport phenomena between subchannels i and j. In order to completely specify the problem the following conditions are imposed upon the volumetric diversion flows and their respective momentum transfer terms across subchannel boundaries.

$$\sum_i q_{\ell_i} = 0 \tag{2.5}$$

$$\sum_i q_{v_i} = 0 \tag{2.6}$$

$$\sum_i \xi_{G_{z_i}} = 0 \tag{2.7}$$

$$\sum_i \left(\frac{\partial P}{\partial z} \right)_{td_i} = 0 \tag{2.8}$$

In the bulk boiling regime, where the liquid and vapor are assumed to be in equilibrium at saturated conditions, the vapor volumetric source, ψ_{si}, in each subchannel i is given by the energy equation. This is discussed in more detail in Chapter 5.2.

For the subcooled region, ψ_{il} is determined by the model discussed in Chapter 3.1.2.

The different phase velocities of liquid and vapor are accounted for by a modified Zuber-Findlay relation for diabatic conditions

$$j_v = (C_{oj} + \bar{V}_{gj}) - C_o Z_e \psi_s \qquad (2.9)$$

where C_o is the distribution parameter for adiabatic flow, Fig. 2 shows C_o for different flow and concentration profiles. $\bar{V}_{gj}$ is the average vapor drift velocity for which correlations have to be supplied for the flow regimes encountered in the analysis. This point is more fully discussed in Chapter 3.3. The second term of the RHS of Eq. (2.9) accounts for the effect of heated surfaces and different geometries. Z_e has the dimension of a length and is according to Forti [2-5] of the order of the hydraulic equivalent diameter of the subchannel. It is considered a relaxation length beyond which there will be an asymptotic void distribution profile established. ψ_s is the volumetric source of vapor at the heating surface.

The volumetric flow of vapor entering each of the subchannels can be considered as the sum of two different sources. The first one is due to the preferred diffusion of vapor between differently sized subchannels and this transport process exists even under the condition of equal pressures in all channels. The second source for the volumetric vapor flow is related to the total diverted flow which can be split up into liquid and vapor part as

$$q_i = q_{vi} + q_{\ell i} \quad . \tag{2.10}$$

For the first source term, the vapor diffusion source corresponds to a vapor for liquid exchange that tends to establish a fully developed void distribution which is a function of the geometry and the overall flow conditions. Such distributions have been measured in characteristic two-subchannel arrangements by Gonzalez-Santalo [2-6]. For any pair of communicating subchannels, Forti [2-5] suggested to write this term as

$$q'_{v_{i-k}} = [R_{k,j}\ \alpha_k - R_{i,k}\ \alpha_i] \tag{2.11}$$

where the $R_{i,k}$ and $R_{k,i}$ are appropriate diffusion coefficients which depend upon the flow conditions in the respective subchannels. These coefficients will be specified in more detail in Chapter 3.2.2. The result of this diffusion process is the net vapor flow from subchannel k to subchannel i.

For the second source term the following model has been established. The divested vapor flow is considered to be a certain fraction of the total diverted flow, namely

$$q''_{v_{i,k}} = S_i\ \alpha_i\ q_{ik} \quad \text{for} \quad q_{ik} < 0 \tag{2.12}$$
(flow leaving subchannel i)

S_i is a transverse slip ratio governing the phase velocities in the transverse direction in the gap region. The following

empirical form is implemented in the code:

$$S_i = \frac{1}{0.815 + 0.835\ P} \qquad \text{for} \qquad \alpha_i > 0.2 \tag{2.13}$$

and

$$S_i = \frac{0.2}{(0.815 + 0.835\ P)_i} \quad \text{for} \qquad \alpha_i \leq 0.2 \tag{2.14}$$

For the case that diverted vapor flow enters subchannel i one obtains

$$q''_{v_{i,k}} = S_k\ \alpha_k\ q_{ik} \qquad \text{for} \qquad q_{ik} > 0 \quad \text{(flow into subchannel i)} \tag{2.15}$$

instead of Eq. (2.12).

With these two source terms specified now, the total vapor flow entering the subchannel i from all neighboring channels can be written as:

$$q_{vi} = \sum_{k(\text{joining } i)} \{R_{k,i}\ \alpha_k - R_{i,k}\ \alpha_i + \frac{1}{2}\ [S_k\ \alpha_k (q_{i,k} + |q_{i,k}|) + S_i\ \alpha_i\ (q_{i,k} + |q_{i,k}|)]\} \tag{2.16}$$

To close the system of equations for the solution, the condition for the pressure drops in each subchannel is expressed as

$$\left(\frac{dP}{dz}\right)_i = \left(\frac{dP}{dz}\right)_k \quad \text{for any i,k} \tag{2.17}$$

2.4 References

[2-1] C.W. Stewart et al., "Core Thermal Model: COBRA-IV Development and Applications," BNWL-2212, Jan. 1977.

[2-2] R.W. Bowring, "HAMBO, A Computer Programme for the Subchannel Analysis of the Hydraulic and Burnout Characteristics of Rod Clusters, Pt. 2, The Equations, AEEW-R-582, Jan. 1968.

[2-3] P.B. Whalley, "The Calculation of Dryout in a Rod Bundle," Int. J. Multiphase Flow, s(1978), 501-515.

[2-4] S.V. Lekach, "Finite Difference Solution to the 1-D Drift Flux Model for General Two-Phase Flow," BNL-50523.

[2-5] G. Forti, J.M. Gonzales-Santalo, "A Model for Subchannel Analysis of BWR Rod Bundles in Steady State and Transient," Int. Conf. Reactor Heat Transfer, Karlsruhe, Germany, 1973.

[2-6] J.M. Gonzalez-Santalo, "Two-Phase Flow Mixing in Rod Bundle Subchannels, Ph.D. Thesis, Dept. Mech. Engng., MIT, Nov. 1971.

3. Constitutive Equations

3.1. Volumetric Vapor Source Term

3.1.1. Introduction

The specification of the volumetric vapor source term is one of the foremost tasks for arriving at a successful drift-flux model. The research in this area has not led to a general constitutive formulation for general use yet. As a result, various researchers recommend the application of vastly different formulations for ψ [3-1, 3-2, 3-3].

In general, the subcooled boiling region as well as the post-CHF region are of major concern, whereas in the bulk boiling regime with the assumption of thermodynamic equilibrium for vapor and liquid phases in saturated conditions, ψ is simply given by the energy equation.

In the present version of WOSUB, the post-CHF region is not modelled. Therefore, the specification of ψ in the subcooled region remains as the only task in what follows. Obviously, this problem is tightly connected to the representation of the model for subcooled boiling in forced convection.

3.1.2. Model for Subcooled Boiling

The state of subcooled boiling is clearly characterized by the fact that thermodynamic non-equilibrium prevails. Although the phenomenon is seemingly more important in PWR's, any consistent BWR analysis requires an accurate subcooled void-quality model.

Fig. 3.1 shows schematically a typical subcooled void-fraction profile in a heated tube. As can be seen, the subcooled boiling regime can be divided into two distinct regions. Region I is usually called the region of wall voidage, meaning that the voids essentially adhere to the heated surface. Recent observations indicate that the bubbles move in a narrow layer close to the wall. This bubble boundary layer grows [3-4] under the competing effects of bubble coalescence and condensation processes until the bubble departure or detachment point, z_λ is reached. At that point bubbles are ejected in the subcooled core of liquid which is the first sign of the existence of appreciable void.

The most important aspect of any subcooled boiling model is to accurately determine the location of the bubble detachment or void departure point. Table 3.1 summarizes the most familiar and widely used bubble detachment criteria. These can be classified into two categories, one category is characterized by the use of mechanistic models, such as suggested by Griffith [3-5], Bowring [3-6], Rouhani and Axelsson [3-7], Rouhani [3-8], Larsen and Tong [3-9] and Hancox and Nicoll [3-10] among others. The second category comprises the use of what is called a profile-fit model which has been used by Zuber et al. [3-11], Staub [3-12], Levy [3-13] and Saha and Zuber [3-14]. As the model names already indicate, the first approach uses a phenomenological description of the heat transfer process whereas the second one postulates a con-

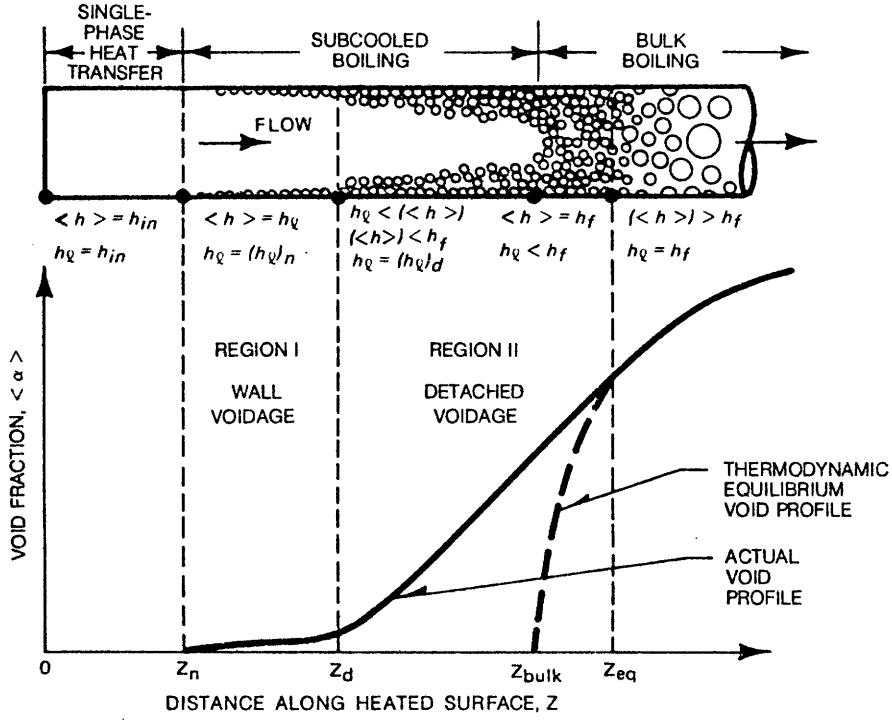

Fig. 3.1: Void fraction during forced convection subcooled boiling

TABLE 3.1: Summary of bubble detachment criteria

Criterion (Critical Subcooling, Btu/lb$_m$)	Source	Principle
$[h_f - (h_l)_d] = \dfrac{c_{p_l} q''}{5.0 H_{1\phi}}$	(Griffith et al., 1958)	Heat Transfer Model
$[h_f - (h_l)_d] = c_{p_l} \eta \dfrac{q''}{(G/\rho_f)}$, where $\eta \triangleq 0.94 + 0.00046p [156 \leq p \leq 2000, \text{psia}]$.	(Bowring, 1962)	Empirical
If: $0 \leq y_b^+ \leq 5.0$ $[h_f - (h_l)_d] = c_{p_l} \dfrac{q''}{H_{1\phi}} - \dfrac{q''}{G(f/8)^{1/2}} \text{Pr } y_b^+$ If: $5.0 \leq y_b^+ \leq 30.0$ $[h_f - (h_l)_d] = c_{p_l} \dfrac{q''}{H_{1\phi}} - \dfrac{5.0q''}{G(f/8)^{1/2}} \times \{\text{Pr} + \ln [1 + \text{Pr } (y_b^+/5.0 - 1.0)]\}$ If: $y_b^+ \geq 30.0$ $[h_f - (h_l)_d] = c_{p_l} \dfrac{q''}{H_{1\phi}} - \dfrac{5.0q''}{G(f/8)^{1/2}} \times [\text{Pr} + \ln (1.0 + 5.0 \text{ Pr}) + 0.5 \ln (y_b^+/30.0)]$, where $y_b^+ = 0.010(\sigma g_c D_H \rho_f)^{1/2}/\mu_f$.	(Levy, 1966)	Force Balance
If: $\text{Pe} \triangleq \dfrac{G D_H c_{pl}}{\kappa_l} < 70\,000$ $[h_f - (h_l)_d] = 0.0022 \dfrac{q'' D_h c_{Pl}}{\kappa_l}$. If: $\text{Pe} > 70\,000$ $[h_f - (h_l)_d] = 154\, q''/G$.	(Saha and Zuber, 1974)	Empirical

venient mathematical fit for the flow quality or liquid enthalpy profile between the bubble detachment point z_d and the point at which thermodynamic equilibrium is reached, z_{eq}. Incidentally, the most accurate of the criteria listed in Table 3.1 are those of Levy [3-13] and Saha and Zuber [3-14]; the latter constituting the latest effort in this research area. Despite this obvious success of the profile-fit models, it should be pointed out that only the mechanistic model gives an opportunity to discuss the results on the bases of basic physical models involved. For this simple reason the application of the latter should be preferred for the drift-flux and two-fluid two-phase model developments. A trend in this direction is quite apparent from recent developments.

In order to more completely substantiate the appropriate selection for the WOSUB code, the requirements for the model to be selected will be discussed in more detail below.

What is desired is a model capable of evaluating the vapor concentration and flows in interconnected channel geometry in steady state and transient situations. The problem on hand can be characterized as follows. Given a control volume as part of a heated channel at an instant in time and knowing the temperature of the heated wall, θ_w, the bulk temperature of the coolant, θ_b, as well as the flow conditions, what is the heat flux to the coolant and how much vapor is generated in this control volume or recondensed?

Whereas the first part of the problem is standard to all thermal-hydraulic codes and thus has been essentially solved although not always in a totally satisfactory manner, the second part is unique to more advanced models of two-phase flow and heat transfer modeling schemes.

By neglecting separate vapor momentum and energy conservation equations in the set of conservation equations as introduced in Chapter 2 for use in the WOSUB code, the final scope of the model in WOSUB is somewhat limited right from the onset, because very fast transients cannot be handled due to the neglection of the dynamics of bubble nucleation and transport. Rather the validity of the quasi-steady state assumption is introduced by recognizing that all relevant and reliable information which is needed for the model building process is essentially stemming from steady state measurements.

Following Forti's mechanistic model [3-1] means that a rational basis is sought instead of fitting void profiles.

Fig. 3.2 summarizes the well accepted heat flux dependence as function of the surface temperature difference to the saturation temperature. The following regimes can be identified in this map.

1) Below a certain temperature, the heat flux is well represented by the single phase convection relation

$$\phi = h\ (\theta_w - \theta_b) \qquad (3.1)$$

with the heat transfer coefficient, h, given by the familiar relationship

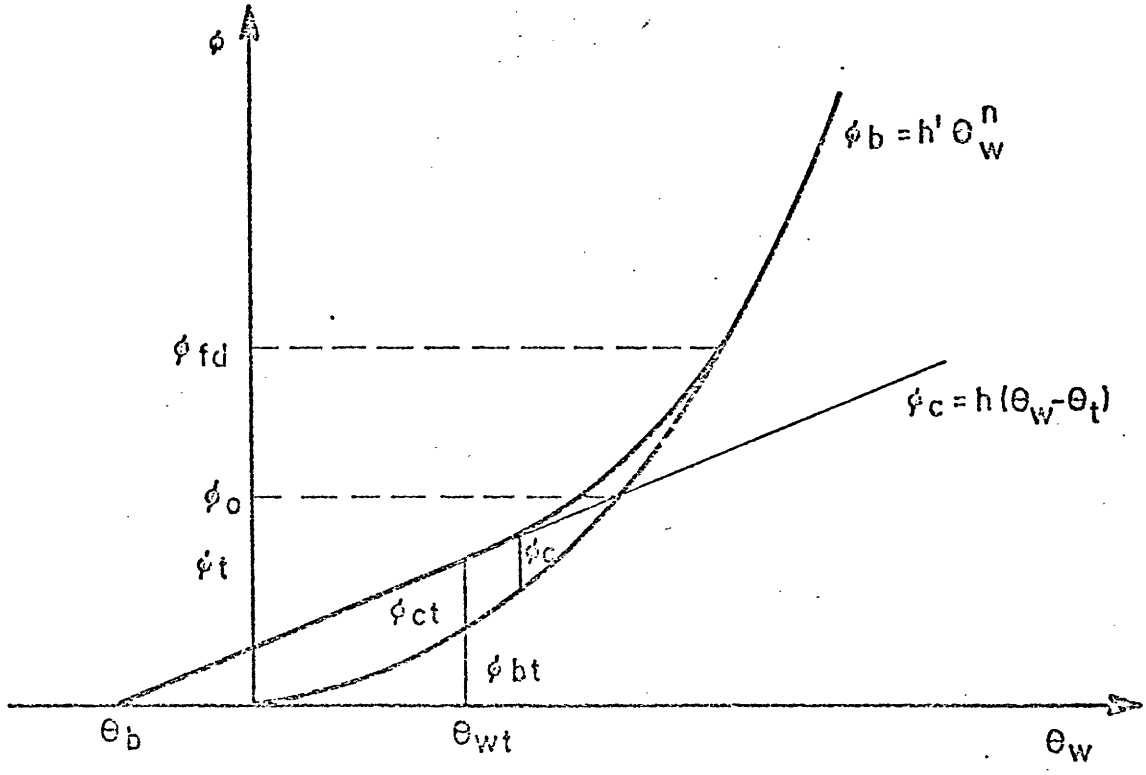

Fig. 3.2: Heat Flux as Function of Wall Overheating θ_w

$$\frac{hD}{k} = C\ Re^{a}\ Pr^{b} \qquad (3.2)$$

2) In the fully-developed nucleate boiling region the heat flux is represented by

$$\phi_b = h'\theta_w^n \qquad (3.3)$$

where h' depends only on the pressure and the exponent, n, n in the range between 3 and 4. A widely accepted correlation of the type indicated by Eq. (3.3) is that by Jens and Lottes who suggested n = 4.

3) For wall temperatures above θ_{wt} up to the fully developed nucleate boiling conditions, ϕ lies certainly above the value given by the convective heat transfer and should asymptotically approach the nucleate boiling curve. Once these circumstances have been acknowledged the task of modeling the subcooled boiling phenomenon can be subdivided into the following subtasks:

a) Finding a suitable correlation

$$\theta_{wt} = \theta_{wt}\ (h, h', \theta_b) \qquad (3.4)$$

which gives θ_{wt} as function of the channel conditions represented by h and h'.

b) Formulation of a correlation ϕ as function of θ_w for $\theta_w \geq \theta_{wt}$. A simple approach to this problem is by relying upon the general validity of the nucleate boiling correlation and to add a residual convective heat transfer term, i. e.

$$\phi = h'\theta_w^n + \phi_c \qquad (3.5)$$

c) Establish a reliable model for the volumetric vapor source ψ_S. For this process, Bowring's model [3- 6] is used,

by assuming that the vapor generated is only a fraction of the heat transferred by the whole boiling process. The latter is governed by Eq. (3.3). Thus ψ_S can be formally written as

$$\psi_S = \tau \frac{p_h}{A\rho_v h_{f_g}} \phi_b \qquad (3.6)$$

and by virtue of this assumption the problem reduces to find a reliable expression for τ as function of the coolant conditions in the channel.

d) Establish a reliable model for the volumetric vapor recondensation, ψ_b, as a function of the vapor volume fraction α and liquid bulk temperature θ_b.

3.1.2.1. Net Vapor Generation Threshold and Residual Convective Heat Transfer

The physical phenomenon of subcooled boiling as it emerges from experimental observations can be summarized as follows:

1) In the highly subcooled region, the voids stay in a layer near the heated wall. They are not attached to the wall. The location of the bubbles in terms of boundary layer thickness is supposedly in a transition region between the laminar layer and the turbulent liquid core. It can be argued that the average liquid temperature in this region must be almost at saturation because of the continuous recondensation of the bubbles. Obviously, there can be no substantial net generation of vapor in steady state because the bubbles which reach the specific layer from the heated wall vanish by recondensation in the layer.

2) Net vapor generation occurs however once the bubbles are entrained from the layer into the bulk liquid stream. This happens when the heat flux from the surface to the layer is higher than the convective heat transfer from the layer to the liquid core, because the condition allows the bubbles to grow.

3) The bubble generation at the wall leading to a bubble transport into the layer is not largely affected by the flow conditions and the liquid core temperature; rather, the only important variable is θ_w. This explains the obvious fact that the heat flux correlation in forced convection follows the pool boiling curve and leads in turn to the conclusion that a substantial amount of information about the bubble generation process can be inferred from pool boiling experiments.

4) The heat conduction process in the laminar sublayer between the wall surface and the bubble layer remains essentially unaffected by the boiling process because the nucleation centers occupy only a small fraction of the total surface.

From the aforementioned observations, it may be concluded that the convective heat transfer stays the same at its threshold value $\phi_c = \phi_{c\ \text{threshold}}$ even for wall temperatures which are higher than the threshold point for net bubble generation.

The heat transferred by the bubble ejection mechanism is given by the nucleate boiling correlation, Eq. (3.3).

$$\phi_b = h'\theta_w^n$$

At the threshold point, the following formulation should hold:

$$\phi_c + \phi_b = \phi_{\text{convection only}} \tag{3.7}$$

Thus, the residual heat transfer follows as

$$\phi_c = \phi_{c\ \text{threshold}} = h(\theta_{wt}-\theta_b)-h'\theta_{wt}^n \tag{3.8}$$

To obtain the critical threshold temperature θ_{wt}, it is assumed that the total heat flux $\phi = \phi_b + \phi_c$ must be higher than the heat flux given by forced convection only, i. e. $\phi_{\text{convection only}} = h(\theta_w-\theta_b)$, because ϕ_c is constant above the threshold. This results in the following condition for the threshold

$$\frac{d\phi}{d\theta_w} = \frac{d\phi_b}{d\theta_w} = h \tag{3.9}$$

and by substituting Eq. (3.3), it follows that

$$nh'\theta_w^{n-1} = h \tag{3.10}$$

from which finally

$$\theta_w = \left(\frac{h}{nh'} \right)^{\frac{1}{n-1}} = \theta_o \tag{3.11}$$

follows. Eq. (3.11) gives a threshold condition for the net vapor generation which is independent of the bulk liquid subcooling, $\theta_{sub} = -\theta_b$. As a result, Eq. (3.11) should be only valid for low subcoolings. For high subcooling, a dependence on θ_{sub} should exist as indicated by the following derivation.

It should be recalled that the threshold condition is reached when the convective heat transfer from the bubble layer is insufficient to completely recondense bubbles which enter

the layer from the wall. Thus, the bubbles increase in size and are eventually entrained into the main stream by the stripping process caused by turbulent shear. By comparing the boiling heat fluxes and the convective heat transfer at threshold condition for the cases of no subcooling and finite subcooling, i.e. $\theta_{sub}=-\theta_b$, the following ratio is obtained:

$$\frac{h'\theta_{wt}^{w}}{h'\theta_{o}^{n}} = \frac{h(\theta_{wt} - \theta_b)}{h\theta_o} \tag{3.12}$$

from which θ_{wt} follows as

$$\theta_{wt} = \theta_o \left(\frac{\theta_{wt} - \theta_b}{\theta_o} \right)^{1/n} \tag{3.13}$$

By assuming that θ_{wt} is approximately close to θ_o and by substituting this into the expression contained in the bracket, the following final expression for θ_{wt} is obtained

$$\theta_{wt} = \theta_o \left(1 - \frac{\theta_b}{\theta_o}\right)^{1/n} = \theta_o\left(1 + \frac{\theta_{sub}}{\theta_o}\right)^{1/n} \tag{3.14}$$

which for $\theta_{sub}\approx 0$ simplifies to Eq. (3.11).

3.1.2.2. Net Vapor Generation

According to Bowring's model not all of the heat transmitted by the bubble ejection process is directly transported by the vapor. Rather a pumping process drives liquid from the bubble layer into the main liquid core. This departing volume is replaced by liquid from the main stream. As was already argued before, the liquid in the bubble layer should be near saturation, although some recondensation may still exist

which leads to a liquid temperature in the layer somewhat lower than saturation. Usually, it is assumed that the pumping process leads to a volume-to-volume exchange of liquid and vapor. However, it should be actually greater as some additional liquid will be carried out with the bubble, so that the ratio of volume ejected to volume replaced is supposedly larger than 1. In what follows a coefficient C>1 will be used to account for this effect by setting up a formulation for ψ_S. This is essentially done by virtue of an energy balance where the net heat exchange process characterized by $P_h\phi_b$ is the result of exchange processes involving a liquid volume exchange $AC\psi_S$ at average bulk temperature θ_b, a vapor volume exchange $A\psi_S$ at the enthalpy of the bubble layer, H_{layer}, and a liquid volume exchange $A(C - \rho_v/\rho_\ell)\psi_S$ also at the enthalpy of the bubble layer, H_{layer}. In summary, the following balance is obtained:

$$P_h\phi_b = A\rho_v\psi_S H_v + (C - \rho_v/\rho_\ell)A\rho_\ell\psi_S H_{layer} - AC\rho_\ell\psi_S H_{bulk} \quad . \tag{3.15}$$

Solved for ψ_S one gets

$$\psi_S = \frac{P_h\phi_b}{A} \frac{1}{\rho_v H_v + C\rho_\ell(H_{layer} - H_{bulk}) - \rho_v H_{layer}} \quad . \tag{3.16}$$

With

$$\mu = \frac{\rho_v}{\rho_\ell}$$

together with the assumption that

$$H_{f_g} \approx H_v - H_{layer} \tag{3.17}$$

ψ_S from Eq. (3.16) becomes for the Forti model

$$\psi_S = \frac{P_h \phi_b}{A\rho_\ell} \frac{1}{\mu H_{f_g} + C(H_{layer} - H_{bulk})} \quad . \tag{3.18}$$

In comparison, Bowring's original formulation arrives finally at

$$\psi_S = \frac{1}{1+\varepsilon} \frac{P_h \phi_b}{A\rho_e \mu H_{f_g}} \tag{3.19}$$

where ε is an empirical parameter depending only on the pressure. Eq. (3.18) can be somewhat simplified by approximating H_{layer} as

$$H_{layer} \simeq H_{sat}$$

which leads to the final expression for the volumetric vapor generation

$$\psi_S = \frac{P_h \phi_b}{A\rho_\ell} \frac{1}{\mu H_{f_g} + C H_{sub}} \tag{3.20}$$

where

$$H_{sub} = H_{sat} - H_{bulk} \tag{3.21}$$

3.1.2.3 Recondensation Process

The recondensation process takes place both in the bulk liquid of the coolant core and the bubble layer. Forti simply assumes a global recondensation process as expressed by

$$\psi_b = R\alpha\theta_b \tag{3.22}$$

with R being an experimentally determined recondensation constant. Forti reports that

$$R = 0.5(\text{sec } ^\circ C)^{-1}$$

has been successfully applied to fit steady state void profiles in water. The appearance of α in Eq. (3.22) is intended to account for the effect of the interfacial area upon the recondensation process. A proportionality in α has been assumed for reasons of simplicity although the assumption of constant bubble radius would result in an $\alpha^{2/3}$ dependence.

3.1.3. Summary of Formulation

In case that the wall overheating θ_w is given what is usually the case in transients, the formulation in WOSUB is as follows depending upon whether the wall temperature is smaller or larger (equal) than the threshold temperature.

$$\phi = \phi_c + \phi_b$$

$$\text{If } \theta_w < \theta_{wt} \quad \begin{cases} \phi_c = h(\theta_w - \theta_b) \\ \phi_b = 0 \end{cases} \tag{3.23}$$

$$\text{If } \theta_w \geq \theta_{wt} \quad \begin{cases} \phi_c = \varepsilon h(\theta_{wt} - \theta_b) - h'\theta_{wt}^n \\ \phi_b = h'\theta_w^n \end{cases} \tag{3.24}$$

In case that the heat flux ϕ is given as is the case in steady state, the wall temperature for the convection only follows immediately as

$$\phi_{w_{\text{convection only}}} = \phi_b + \frac{\phi}{h} \tag{3.25}$$

and the formulation depends again whether the wall temperature is smaller or larger (equal) than the threshold temperature:

$$\text{If } \theta_{w_{\text{convection only}}} < \theta_{wt} \quad \begin{cases} \phi_c = \phi \\ \phi_b = 0 \\ \phi_w = \theta_{w_{\text{convection only}}} \end{cases} \tag{3.26}$$

$$\text{If } \theta_{w_{\text{convection only}}} \geq \theta_{wt} \quad \begin{cases} \phi_c = \varepsilon h(\theta_{wt}-\theta_b)-h'\theta_{wt}^n \\ \phi_b = \phi - \phi_c \\ \theta_w = \left(\frac{\phi_b}{h'}\right)^{1/n} \end{cases} \tag{3.27}$$

In all cases the threshold temperature is determined from

$$\theta_{wt}=\theta_o \left(\frac{\theta_{wt}-\theta_{sub}}{\theta_o}\right)^{1/n} \text{ with } \theta_o=\left(\frac{h}{nh'}\right)^{\frac{1}{n-1}}$$

the vapor generation by

$$\psi_S = \frac{P_H \phi_b}{A\rho_\ell} \frac{1}{\mu H_{f_g}+CH_{sub}}$$

and the recondensation by

$$\psi_b = -R\alpha\theta_{sub}=R\alpha\theta_b.$$

The net vapor generation follows from the addition of the last two equations, i. e.

$$\psi = \psi_S + \psi_b \tag{3.28}$$

The multiplier ε has been introduced into Eqs. (3.24) and (3.27) in order to reduce linearly the convective heat transfer contri-

bution to zero when

$$\phi_{fd} = 1.4\ \phi_o \tag{3.29}$$

is reached. Again, it must be differentiated between the wall temperature and wall heat flux cases. Thus

θ_w given: $$\varepsilon = \frac{\phi_{fd} - \phi_b}{\phi_{fd} - \phi_{bt}} \tag{3.30}$$

ϕ given: $$\varepsilon = \frac{\phi_{fd} - \phi}{\phi_{fd} - \phi_t} \tag{3.31}$$

where

$$\phi_{fd} = 1.4\ h'\theta_l \tag{3.32}$$

$$\theta_l = \left[\frac{h}{h'}\ (\theta_l - \theta_b)\right]^{1/n} \tag{3.33}$$

$$\phi_{bt} = h'\ \theta_{wt} \tag{3.34}$$

$$\phi_t = h(\theta_{wt} - \theta_b) \tag{3.35}$$

3.2. Vapor Diffusion Model

3.2.1. Introduction

At this point, it should be recalled that the set of conservation equations contained in the WOSUB code does not include a transverse momentum equation. Thus any phase exchange between adjacent subchannels is assumed to occur in the absence of tranverse pressure gradients. Therefore, no diversion cross-flows in the usual sense appear in this model. Rather, the whole

exchange process between subchannels is considered to be of diffusional character. Contributors to this diffusion process are the turbulent eddy diffusivity effect and a postulated diffusion of the vapor against a potential. Thus, the formulation of the model relies upon the following assumptions:

1) No diversion cross flows due to transverse pressure gradients exist.

2) The postulated diffusion process is the effect of turbulent transport properties which are in two-phase flow regime dependent.

3) The vapor has an affinity for the higher velocity regions in the bundle.

4) The vapor phase diffuses against a velocity potential into adjacent subchannels.

It is apparent that a totally different transport model as commonly employed in well known subchannel codes evolves as a result of these postulated assumptions which are more or less based and inferred from experimental observations such as the GE bundle tests reported by Lahey *et al.* [3-15] and the Columbia test [3-16].

3.2.2. Model Formulation

According to the aforementioned assumptions, the vapor exchange between two adjacent subchannels i and j through the gap of dimension Δy_{ij} is assumed to be of the form

$$q_{v_{mix\ i,j}} = [R_{ji}\alpha_j - R_{ij}\alpha_i] \qquad (3.36)$$

where R_{ij} represents a global diffusion coefficient for the vapor in subchannel i through the gap Δy_{ij} and is postulated to be of the form

$$R_{ij} = \varepsilon \chi V \frac{\Delta y_{ij}}{\ell} \quad . \tag{3.37}$$

ε represents the single-phase turbulent eddy diffusivity for momentum transport; χ is a two-phase multiplier, V the velocity potential and ℓ is the distance between the centroids of the subchannels.

3.2.2.1. Eddy Diffusivity

The expression for the single phase turbulent eddy diffusivity follows the recommended formula given by [3-17] in the form

$$\varepsilon \frac{\Delta y_{ij}}{\ell} = k'' j D_e = 0.0264 \sqrt{f/2} \quad \frac{G}{\rho D_e} \tag{3.38}$$

3.2.2.2 Two-Phase Flow Multiplier

The two-phase flow multiplier, χ, is a correction to the single-phase turbulent eddy diffusivity and expresses the experimental evidence, that the mixing in the two-phase flow regime strongly depends on the specific flow regime encountered. As a result, χ should be at least a function of the quality, x. Experiments by Rowe and Angle [3-18]as well as Gonzalez-Santalo [3-19]indicated that the two-phase mixing is maximum around the transition from slug to annular flow. (See Figs. 3.3, 3.4, 3.5.) In order to construct a meaningful empirical correlation, some more information must be known. That is

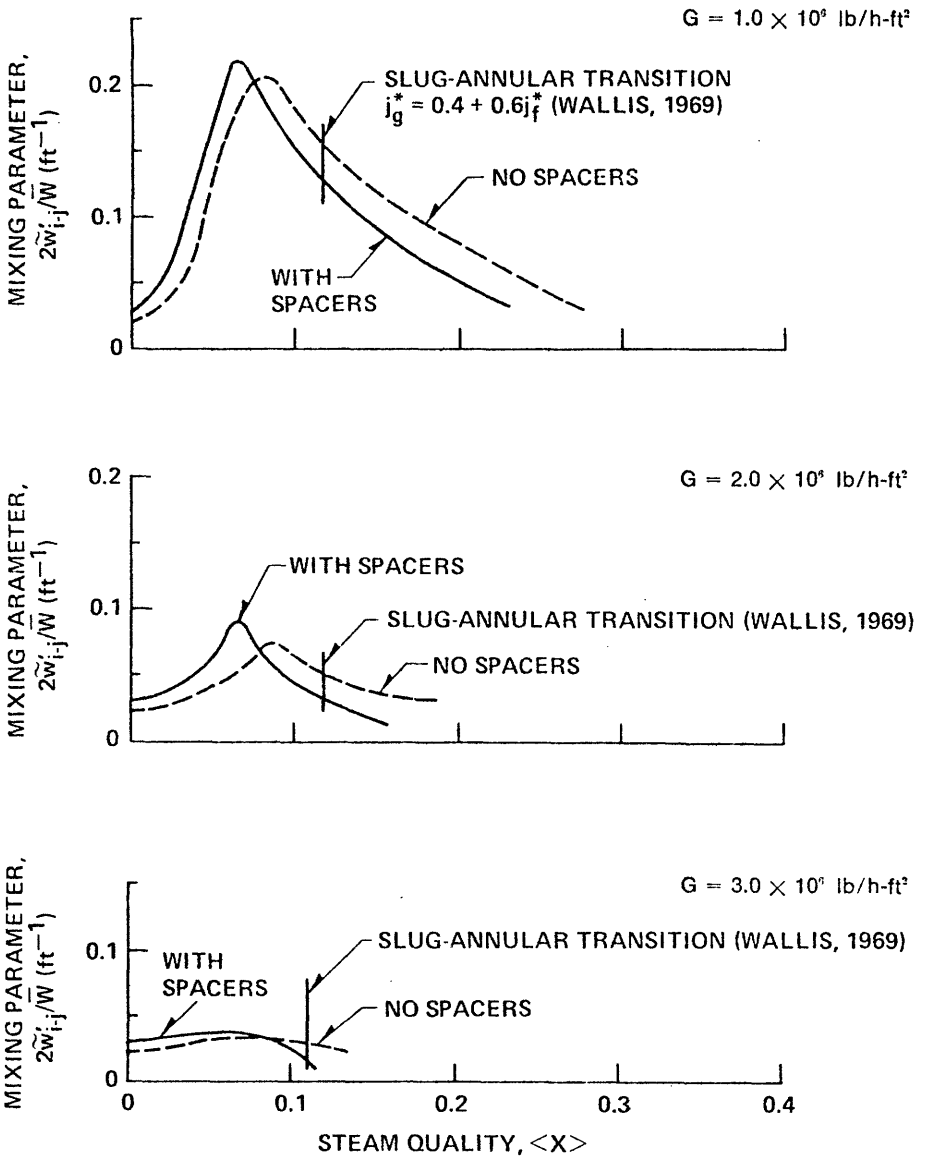

Fig. 3.3: The effect of flow regime on turbulent two-phase mixing (Rowe and Angle)

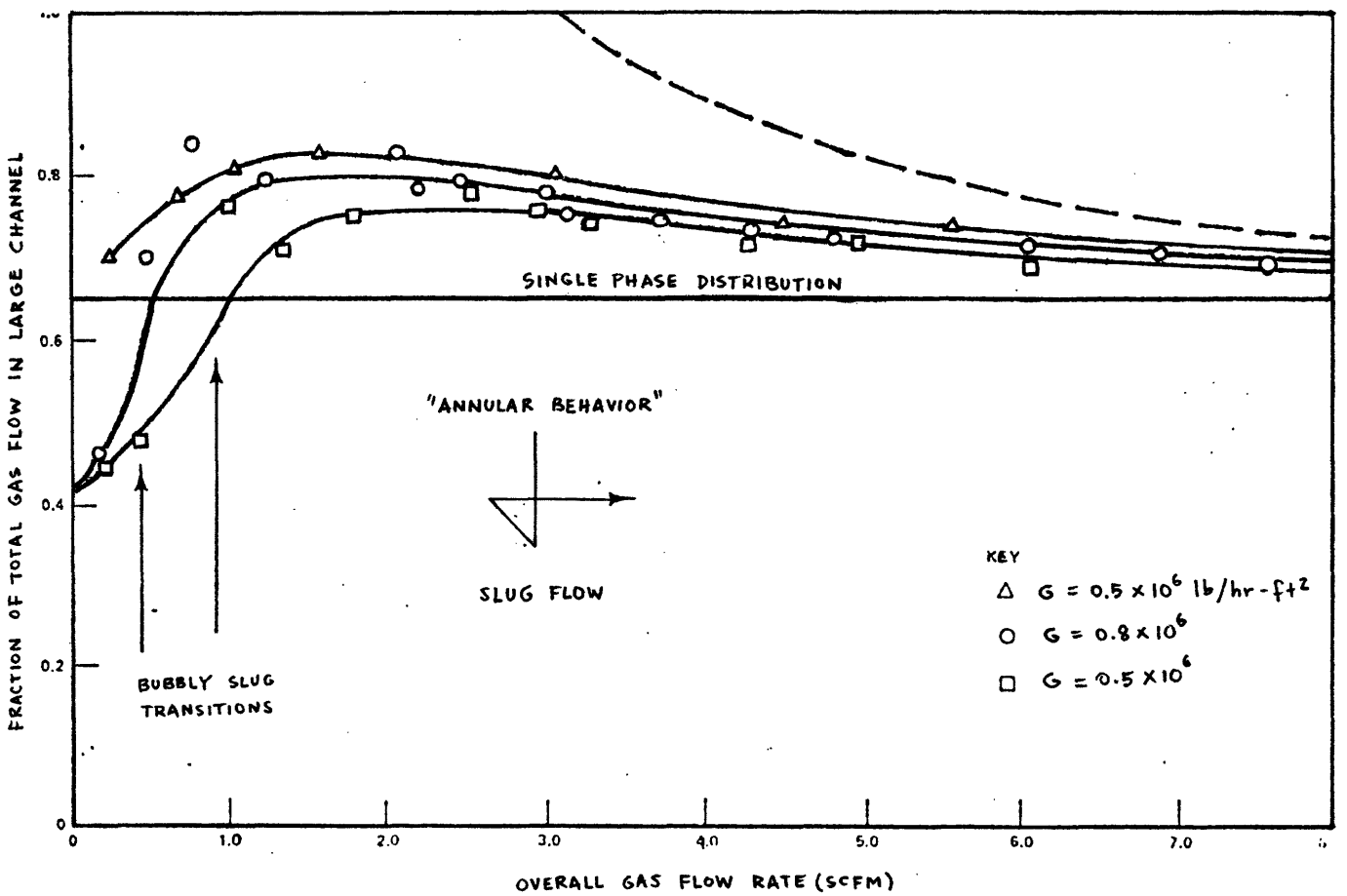

Fig. 3.4: Fully developed gas flow distribution, test section 1 (Gonzalez-Santalo)

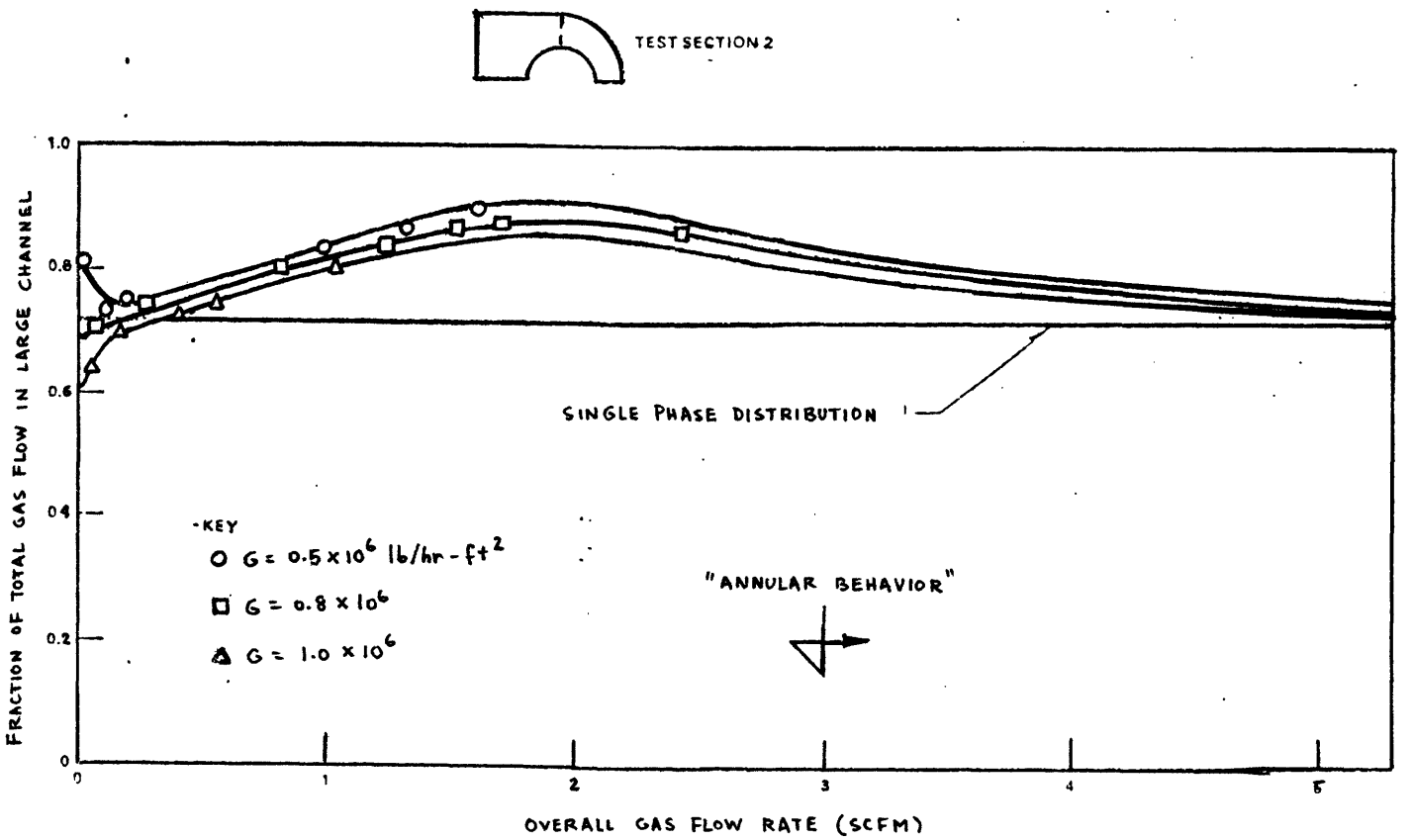

Fig. 3.5: Fully developed gas flow distribution, test section 2 (Gonzalez-Santalo)

given by the fact that both at very low and very high qualities χ should approach one which leaves the single phase turbulent mixing without samplification. Furthermore, for very high flow rates, χ should again approach asymptotically one because for these cases the flow pattern will be dispersed flow.

The empirical correlation for χ formulated by Forti [3-20] on the basis of the experiments performed by Gonzales-Santalo [3-19]

$$\chi = 1 + (1-x_o)\, f(G) \tag{3.39}$$

where $f(G) = 1$ for $G<G_o = 3.8 \times 10^6$ lb/ft^2

and $$f(G) = e^{-2\frac{G-G_o}{G_o}} \quad \text{for } G>G_o \tag{3.40}$$

Furthermore, the values for x_o are given as follows:

$$\begin{aligned} x_o &= 1 + (x_s - 1)\frac{\alpha}{\alpha_1} && \text{for } \alpha<\alpha_1 \\ x_o &= x_s && \text{for } \alpha_1<\alpha<\alpha_2 \\ x_o &= 1+(x_s-1)\tfrac{1}{2}\,[1+\cos\{\pi(\alpha-\alpha_2)/(1-\alpha_2)\}] && \text{for } \alpha>\alpha_2 \end{aligned} \tag{3.41}$$

where

α_1: void fraction for the transition bubbly to slug flow, taken as 0.37 in the code

α_2 void fraction for the transition slug to annular flow, calculated as $\alpha_2 = 0.775 - 0.0504G - 0.0171G^2$ in the code (G in Mlb/ft^2).

It should be noticed that the curve fit suggested above is only one of the possible forms which may be used to display the trend of the data.

3.2.2.3 Velocity Potential Term

The velocity potential term, V, is an important parameter in the model because it accounts for the geometric effects on the vapor drift. Forti suggested employing the following relation:

$$V = e^{-k\frac{V_{max}-V_{gap}}{V_{max}}} \tag{3.42}$$

By considering that for turbulent flow and within the range of Reynolds' number of practical interest, the velocity profile from the wall follows the one over seventh order law, V can be reformulated as

$$V = e^{-k\left[1-\frac{q_{v_i,k}}{D_i}\right]^{1/7}} \tag{3.43}$$

where

$$k = 30e^{-\sqrt{G/G_o}} \tag{3.44}$$

and G_o is given again as $G_0 = 3.8 \times 10^6$ lb/ft^2.

The constant value 30 was adjusted to fit GE subchannel data and agrees also fairly well with data presented by Gonzalez-Santalo for his two subchannel adiabatic air-water system at void fractions above the transition from bubbly to slug flow regime.

In view of the fact that the velocity potential term as specified through Eq. (3.43) is a unique feature of the MATTEO and WOSUB codes, some additional comments seem to be in order.

Gonzalez-Santalo suggested in his thesis a direct formulation of the void fraction corresponding to fully developed distributions. This seems to be a very natural way to look at that problem especially for him, because he was only concerned about pairs of subchannels. In practice, though, the disadvantage of this approach is that a single channel is connected to many others and thus it is not possible to define a single void fraction under fully developed conditions for each of the subchannels, unless a special model is synthesized which would account automatically for each possible channel layout. On the other hand, if different fully developed void distributions are maintained for each pair of subchannels in the layout, no global equilibrium distribution can be obtained and the solution scheme would probably become unstable.

All this indicates certainly a dilemma in the model-building process and shows the limitation of the empirical model selected. From the physical point of view the model leaves a lot to be desired. On the other hand, it should have become clear by now that two-subchannel experiments are indeed only of limited value, too, because there is no easy way to synthesize those results into a reliable model to be used in multi-pin geometries.

3.3 Drift Flux Model

3.3.1 Basic Definitions

As discussed in the Introduction, the drift flux model reduces substantially the complexity of the two-fluid formulation. Although the two phases are considered separated, the relative motion of the vapor phase is defined with respect to the motion of the mixture by virtue of a constitutive equation. For this purpose, the WOSUB code uses the Zuber and Findlay drift flux model [3-21].

It should be noticed that the velocity fields are expressed in terms of the mixture center of mass velocity and the drift velocity of the vapor phase, which is the vapor velocity with respect to the volume center of the mixture. A thorough discussion of these issues is presented by Lahey and Moody [3-22].

Since the response of the volumetric vapor fraction to changes of pressure, flow, and power is to be determined, it seems to be advantageous to formulate the problem in terms of the velocity of the center of volume, j, and of the drift velocities V_{gj} and $V_{\ell j}$ of the vapor and of the liquid with respect to j.

With v_ℓ and v_g as being the local liquid and vapor velocities, and α the local volumetric concentration of the vapor, the volumetric flux densities of the liquid, j_ℓ, and of the vapor, j_g, are defined as

$$j_\ell = (1-\alpha)v_\ell \tag{3.45}$$

$$j_g = \alpha v_g \tag{3.46}$$

The volumetric flux density of the mixture is

$$j = j_\ell + j_g \tag{3.47}$$

which can be rewritten with Eqs. (3.45) and (3.46) as

$$j = (1-\alpha)v_\ell + \alpha v_g \tag{3.48}$$

It should be noticed that Eq. (3.48) can be interpreted as the local volumetric flux of the mixture or the velocity of the center of volume of the mixture.

In analogy with the kinetic theory of gases, the local drift velocities with respect to the center of volume of the mixture are defined as follows

$$V_{\ell j} = v_\ell - j \tag{3.49}$$

$$V_{gj} = v_g - j \tag{3.50}$$

The relative velocity between the phases is given by

$$v_r = v_g - v_\ell \tag{3.51}$$

By means of the foregoing equations, the drift velocities can be expressed as

$$V_{\ell j} = -\alpha v_r \tag{3.52}$$

$$V_{gj} = (1-\alpha)v_r \tag{3.53}$$

$$V_{gj} - V_{\ell j} = v_r \tag{3.54}$$

As can be seen from the last three equations, if

$$v_r = 0$$

$$\text{then} \quad V_{gj} = V_{fi} = 0 \tag{3.55}$$

and it follows from Eqs. (3.48) and (3.51) that

$$v_g = v_\ell = j$$

and this means that the two phases have the same velocity which is equal to the volumetric flux density of the mixture.

3.3.2 Average Velocity and Weighted Mean Velocity of the Vapor

In two-phase flow, it is advantageous to consider the average value of a quantity F over the cross-sectional flow area, i.e.,

$$\langle F \rangle = \frac{1}{A} \int F dA \tag{3.56}$$

Introducing v_g given by Eq. (3.46) into this equation results in the average vapor velocity, v_g

$$\langle v_g \rangle = \left\langle \frac{j_g}{\alpha} \right\rangle = \langle j \rangle + \langle V_{gj} \rangle \tag{3.57}$$

Rather than using this equation, it seems to be more appropriate for the designer and experimenter to work directly with the average volumetric fluxes because these are already defined conveniently by system parameters as

$$\langle j_g \rangle = \langle \alpha v_g \rangle = \langle \alpha j \rangle + \langle \alpha V_{gj} \rangle = \frac{Q_q}{A} \tag{3.58}$$

Another important relation in this context is the weighted mean value of a quantity, defined by

$$\overline{F} = \frac{\langle \alpha F \rangle}{\langle \alpha \rangle} = \frac{\frac{1}{A} \int_A \alpha F dA}{\frac{1}{A} \int_A \alpha dA} \tag{3.59}$$

Applying this formula to the local vapor velocity, v_g, results in the weighted mean velocity $\overline{v}_g$

$$\overline{V}_g = \frac{\langle V_g \alpha \rangle}{\langle \alpha \rangle} = \frac{\langle j_g \rangle}{\langle \alpha \rangle} \tag{3.60}$$

3.3.3 General Expression for the Vapor Average Volumetric Concentration

By using Eqs.(3.58) and (3.60), $\overline{V}_g$ can be written as follows

$$\overline{V}_g = \frac{\langle \alpha j \rangle}{\langle \alpha \rangle} + \frac{\langle \alpha V_{gj} \rangle}{\langle \alpha \rangle} \tag{3.61}$$

Multiplying and dividing the first term on the RHS of this equation by $\langle j \rangle$ one obtains

$$\overline{V}_g = \frac{\langle jg \rangle}{\langle \alpha \rangle} = C_o \langle j \rangle + \frac{\langle \alpha V_{gj} \rangle}{\langle \alpha \rangle} \tag{3.62}$$

with the distribution parameters C_o defined as

$$C_o = \frac{\langle \alpha j \rangle}{\langle \alpha \rangle \langle j \rangle} = \frac{\frac{1}{A} \int \alpha j dA}{[\frac{1}{A} \int_A \alpha dA][\frac{1}{A} \int_A j dA]} \tag{3.63}$$

Bankoff [3-23] was the first who used the inverse of C_o and called it the flow parameter k.

Eq. (3.62) can be brought into a dimensionless form by dividing both sides with <j>, which gives

$$\frac{<\beta>}{<\alpha>} = C_o + \frac{<\alpha V_{gj}>}{<\alpha><j>} \tag{3.64}$$

where the average volumetric flow concentration <β> is defined as

$$<\beta> = \frac{<jg>}{<j>} = \frac{Q_q}{Q_q + Q_\ell} \tag{3.65}$$

Finally, general expressions for the vapor average volumetric concentration can be derived by starting either from Eq. (3.62) of Eq. (3.64)

$$<\alpha> = \frac{<jg>}{C_o j + \frac{<\alpha V_{gj}>}{<\alpha>}} \tag{3.66}$$

or

$$<\alpha> = \frac{<\beta>}{C_o + \frac{<\alpha V_{gj}>}{<\alpha><j>}} \tag{3.67}$$

This concludes the derivation of the most important relationships for the drift flux model. Discussions about C_o and V_{gj} follow below.

It should be pointed out that the final two expressions are applicable to any two-phase flow regime. The analysis takes into account:

a) the effects of the non-uniform flow;

b) concentration profiles;

c) temperature profiles, i.e., thermodynamic non-equilibrium;

d) the effect of local relative velocity.

Points (a) and (b) are accounted for by the distribution parameter C_o. Point (c) is accounted for by the volumetric flux of the mixture and point (d) is effectively described by the weighted mean drift velocity $\langle \alpha V_{gj} \rangle / \langle \alpha \rangle$.

Finally, it is important to point out that $\langle \alpha \rangle$ can be readily determined for each flow regime as long as appropriate expressions for C_o, $\langle \alpha V_{gj} \rangle / \langle \alpha \rangle$, $\langle j \rangle$ and $\langle j_g \rangle$ are available. Those will be discussed in what follows.

3.3.4 Distribution Parameter C_o

In order to more easily comprehend the importance of C_o and to evaluate the effect of radial void and flow profiles on $\langle \alpha \rangle$ Fig. 3.6 shows schematically the variation of these profiles along a uniformly heated duct.

At sufficiently high inlet subcooling, no bubbler will be present at Station 1. Therefore $\langle \alpha \rangle = 0$, while the volumetric flux profile of the mixture will correspond to the velocity of the liquid only.

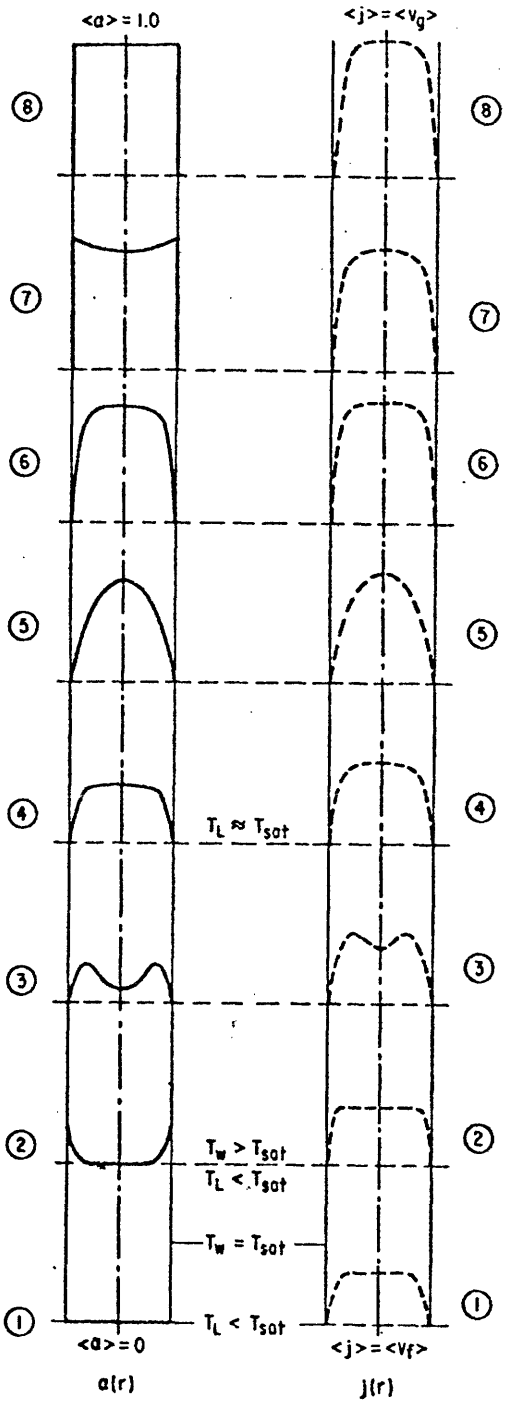

Fig. 3.6: Variation of Concentration and Flow Profiles along a Uniformly Heated Duct.
(a) Volumetric Concentration of the Vapor,
(b) Volumetric Flux Density of the Mixture

Following the nucleation process, bubbles start to grow on the heated surface. Due to the still highly subcooled bulk liquid condition, the bubbles will collapse. Therefore, the vapor concentration profile will decrease from a given value at the wall to zero at the centerline at Station 2. The bubbles will contribute to the axial volumetric flux density of the mixture especially at the vicinity of the wall which results in a flatter $j(r)$ profile at Station 2 than at Station 1.

As the temperature increases at Station 3, the rate of bubble collapse decreases. Due to the radial temperature distribution in the liquid and because of the tendency of the bubble to migrate toward the center, the concentration profile will probably show two maxima and one minimum. At pressure where $\rho_v << \rho_\ell$, the volumetric flux density of the mixture will be primarily affected by that of the vapor which should result in a $j(r)$ profile similar to that of $\alpha(r)$.

At Station 4 where the bulk temperature reaches saturation, the bubble collapse ends, while their migration toward the centerline will continue. Consequently, the α-profile will flatten more and more as the bubbly flow regime develops further downstream.

As the evaporation process continues along the duct, the vapor void fraction and volumetric flux increases, whereas the flow regime will change from bubbly churn turbulent to annular. As a consequence of this change in interfacial geometry and

redistribution of phases, the concentration as well as the flux profiles flatten at Station 6.

When droplets become entrained in the vapor core the flow regime changes to annular-mist flow. The liquid film may even dry out completely if the duct is long enough. In this case, the highest vapor concentration is at the heated wall as shown at Station 7. Note, the flux profile does not change curvature due to the requirement of no slip at the wall.

If, at Station 8, complete vaporization is encountered, α becomes unity, whereas the flux profile of the mixture becomes equal to the velocity profile of the vapor phase only.

3.3.5 Zuber's Quantitative Considerations for Circular Ducts

Experimental results show that in axially symmetric flow through a circular duct the void profile can be approximated by

$$\frac{\alpha-\alpha_c}{\alpha_c-\alpha_w} = 1 - \left(\frac{r}{R}\right)^n \tag{3.68}$$

Furthermore, Zuber *et al.* [3-24] assumed that the volumetric flux profile can also be expressed as

$$\frac{j}{j_c} = 1 - \left(\frac{r}{R}\right)^m \tag{3.69}$$

In both equations, the subscripts c and w refer to values evaluated at the centerline and at the wall, respectively.

By substituting the above expressions into Eq. (3.63) one obtains C_o for circular ducts as

$$C_o = 1 + \frac{2}{m+n+2}\left[1 - \frac{\alpha_w}{\langle\alpha\rangle}\right] \tag{3.70}$$

when expressed in terms of the volumetric concentration α_w at the wall or

$$C_o = \frac{m+2}{m+n+2}\left[1 + \frac{\alpha_c{}^n}{\langle\alpha\rangle(m+2)}\right] \tag{3.71}$$

when expressed in terms of the volumetric concentration α_c. Another alternative is to formulate C_o in terms of both α_c and α_w which gives

$$C_o = 1 + \frac{2}{m+n+2}\left[1 - \frac{\alpha_w(n+2)}{n\alpha_c+2\alpha_w}\right] \tag{3.72}$$

This equation was used by Zuber [3-24] to construct the curves in Fig. 3.7 for different values of the exponents n and m.

The following conclusions can be drawn for some interesting cases. If

$$\alpha_w = \alpha_c = \langle\alpha\rangle$$

then $C_o = 1$

If $\alpha_c < \alpha_w$

then

$$C_o < 1$$

If

$$\alpha_c > \alpha_w$$

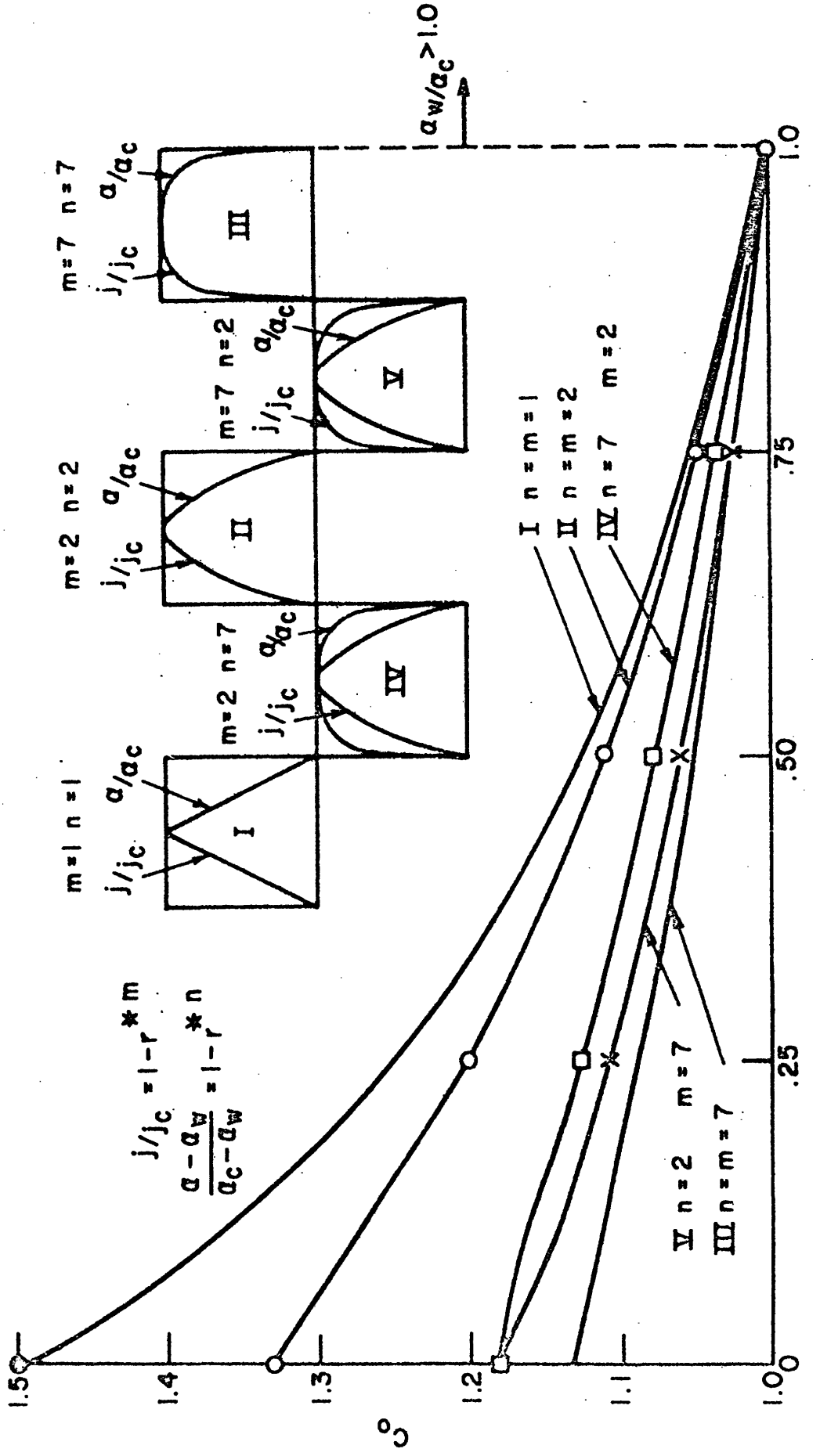

Fig. 3.7: Values of the Distribution Parameter Co as a Function of the Exponents of the Flow and Concentration Profile Curves for Axisymmetric Vertical Upflow Through Circular Ducts

then

$$C_o > 1$$

For pronounced parabolic profiles, Fig. 3.7 indicates that $C_o = 1.5$ whereas for flat profiles C_o approaches unity.

A similar analysis has been performed for rectangular ducts by Zuber et al. [3-24] and resulted in the following range for C_o

$$1 < C_o < 1.78$$

which indicates that the distribution parameter C_o is larger in rectangular ducts than in circular ducts.

3.3.6 Vapor Drift Velocity

It must be expected that the drift velocity varies when changes in the topology of the two-phase mixture occur. Consequently, in order to determine the correct drift velocity it is necessary to look at each two-phase flow regime separately. In accordance with Eq. (3.67), a change in the drift velocity will affect $\langle\alpha\rangle$, which means an effect in addition to that already discussed with respect to C_o.

3.3.7 Qualitative and Quantitative Considerations for Bubbly Flow

Experiments revealed the existence of three bubbly flow regimes, namely a turbulent one, a laminar regime and a transition regime. Fig. 3.8 shows the experimental results with a

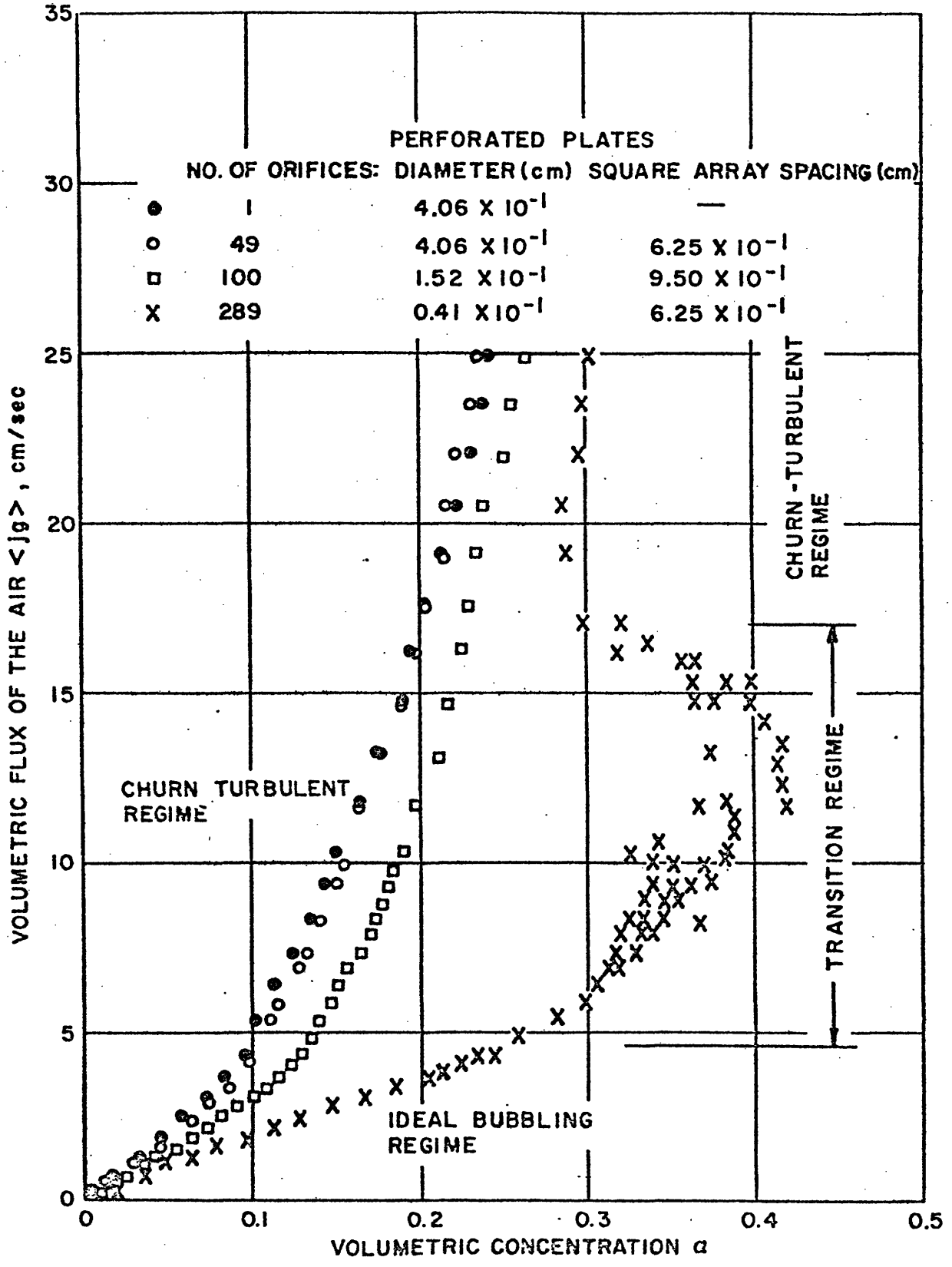

Fig. 3.8: Various Regimes with Air Bubbling Through Porous and Perforated Plates into Stagnant Water

bubbling batch system, where air was bubbling through porous or perforated plates into stagnant water. The three flow regimes have the following characteristics:

Laminar bubbling regime: Bubbles are uniformly distributed across the test section and rise with uniform velocity. They do not affect each other and have nearly equal diameter. As a result no two-dimensional effects occur because the bubbles do not generate wakes. Therefore no gross motion of the liquid is initiated in the batch.

Transition bubbling regime: As gas flow increases, bubble diameters start to increase and become non-uniform which in turn leads to non-uniform bubble rise velocity. Bubble wake flow starts and the non-uniform bubble rise velocity induces a liquid velocity profile with a maximum. This regime,which is characterized by a larger scatter of data, is caused mainly due to bubble agglomeration.

Churn turbulent bubbly regime: This is characterized by a stable, single valued void fraction for a given flow rate. The void fraction increases at a much slower rate than in the laminar regime. The main characteristics of this regime are that wake flows are produced due to non-uniform bubble distribution of non-uniform bubble sizes which in turn generate turbulent convection currents. This leads to a net

upward transport of liquid in the core of the duct. This flow has certainly three-dimensional character. The bubble form is of the cap-type. An important feature of the churn turbulent regime is that it can occur at any gas flow rate.

Eq.(3.50) shows that the local drift velocity represents the local bubble velocity with respect to the local volumetric flux of the liquid. The simplest way to find an expression for the drift velocity is by assuming that it is unaffected by the concentration. Under this assumption the local drift velocity is equal to the terminal velocity of a bubble which rises in an infinite medium.

For the churn turbulent bubbly regime, it is assumed that the assumption introduced above is valid because the effects of turbulent liquid eddies are presumably much larger than the effect of the concentration in distorting the flow.

Therefore, the local drift velocity for the churn turbulent bubbly regime implemented into WOSUB is given by

$$V_{gj} = v_g - j = 1.53 \left[\frac{\bar{v}g(\rho_\ell - \rho_g)}{\rho_\ell^2}\right]^{0.25} \qquad (3.73)$$

where the constant 1.53 is due to Harmathy [3-25]. Zuber et al. [3-24] recommend 1.41 which was deduced by Levich [3-26] and falls between the value given by Harmathy and that by Peebles and Garber [3-27] which is 1.18. It is interesting to note that

Eq. (3.73) is not dependent on the bubble diameter which is naturally not known a priori. This makes its application very convenient.

No other flow regime is modeled in WOSUB right now. Fig. 3.9 shows how well experimental data are bitted by the churn turbulent formula and indicates that the slug flow equation as well as the homogeneous flow equation do not apply.

The weighted mean drift velocity for the churn turbulent regime can be shown to become

$$\bar{V}_{gj} = \frac{\langle \alpha V_{gj} \rangle}{\langle \alpha \rangle} = 1.53 \left[\frac{\bar{\sigma} g (\rho_\ell - \rho_v)}{\rho_\ell^2} \right]^{0.25} \tag{3.74}$$

Eq. (3.66) can be solved for $\langle j_g \rangle$ to give

$$\langle j_g \rangle = \alpha (C_o \langle j \rangle + \bar{V}_{gj}) \tag{3.75}$$

In WOSUB, Eq. (3.75) has been corrected in order to account for diabatic flow conditions, namely

$$\langle j_g \rangle = \alpha (C_o \langle j \rangle + \bar{V}_{gj}) - C_o Z_\ell \Psi_s \tag{3.76}$$

where Z_ℓ is a relaxation length and Ψ_s the volumetric vapor source at the heated surface. The corrective term accounts also for geometric changes from those of a circular duct and is thought to be applicable in this form for subchannel analysis.

Finally, it should be pointed out that the formulation implemented into WOSUB is not capable of handling annular flow

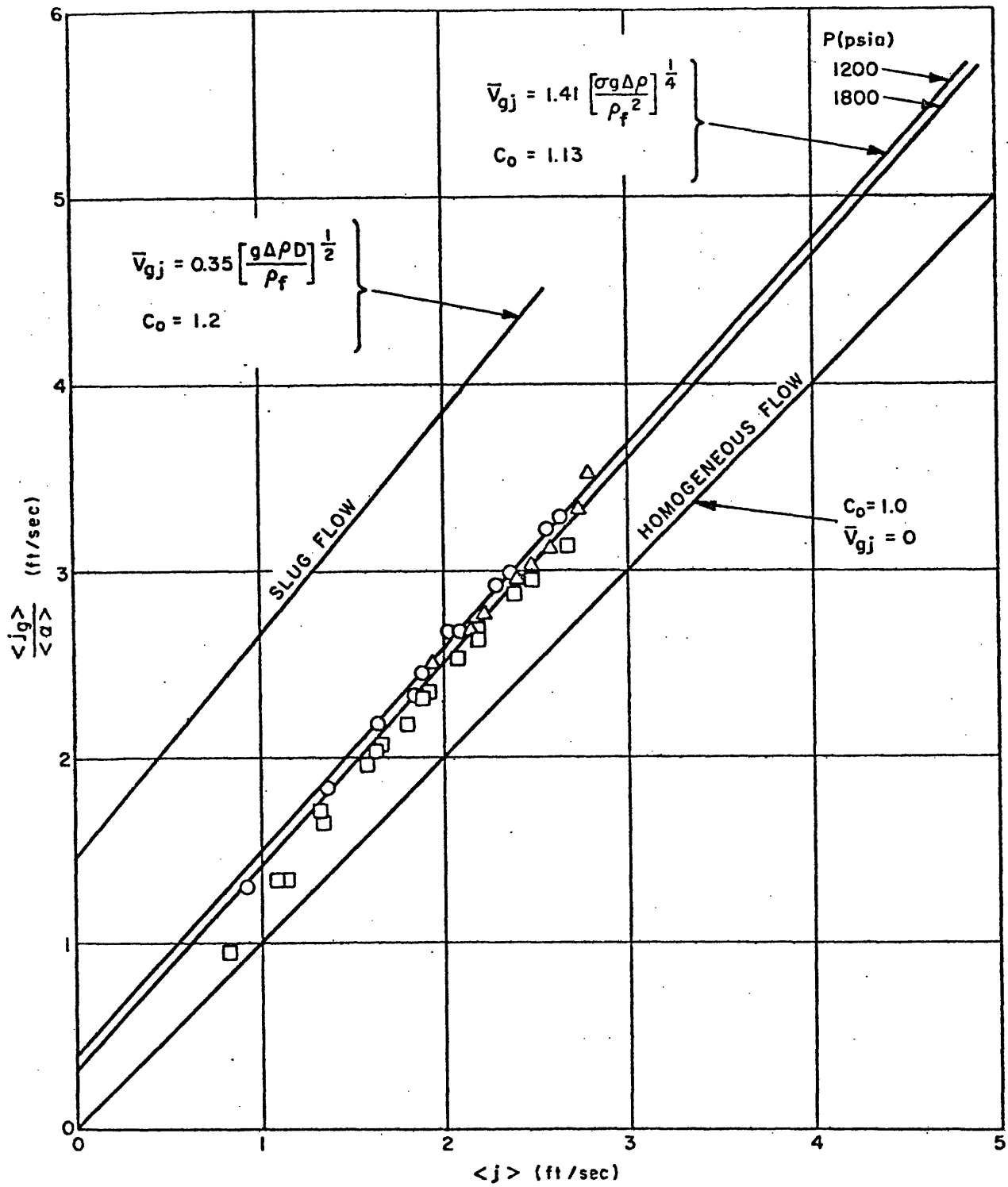

P (psia)	G (lb/sec ft^2)	x
O 1200	24.5-61.5	0.0476-0.1571
Δ 1400	51.2-74.5	0.050-0.118
☐ 1800	24.5-63.5	0.032-0.192
ID = 6.625 in.		

Fig. 3.9: Plot of the Experimental Data in the Velocity-flux Plane. Experimental Data [3-28] for Water at High Pressures

because no correlation for this regime has been built into the code. Appendix B discusses the possible implementation of an equation for annular flow as derived by Ishii et al. [3-29].

3.4 Friction Factors

3.4.1 Single-Phase Flow Friction Factor

For single-phase flow the friction factor in WOSUB is given as a function of roughness and Reynolds number in terms of the following fit of the Moody graph:

$$f = 0.0055 \left[1 + (2 \times 10^4 e + 10^6/Re)^{1/3}\right] \tag{3.77}$$

3.4.2 Two-Phase Flow Friction Factor

The two-phase flow multiplier in Eq. (5.9) is represented as

$$\phi_{\ell_o} = 1 + x(A + Bx) \tag{3.78}$$

where x = quality

and the coefficients A and B are given below

$$A = 155.044(1 - 0.014517\ P + 5.021 \times 10^{-5}\ P^2) \tag{3.79}$$

$$B = -132.322(1 - 0101135\ P + 4.3716 \times 10^{-5}\ P^2) \tag{3.80}$$

3.5 References

[3-1] G. Forti, "A Dynamic Model for the Cooling Channels of a Boiling Nuclear Reactor with Forced Convection and High Pressure Level," EUR-4052e, 1968.

[3-2] N. Zuber, F.W. Staub, "The Propagation and the Wave Form of the Vapor Volumetric Concentration in Boiling Forced Convection Systems Under Oscillatory Conditions," Int. J. Heat Mass Transfer, 9(1966).

[3-3] R.T. Lahey, "Two-Phase Flow in Boiling Water Nuclear Reactors," NEDO-13388, 1974.

[3-4] G.E. Dix, "Vapor Void Fractions for Forced Convection with Subcooled Boiling at Low Flow Rates," NEDO-10491, 1971.

[3-5] P. Griffith, A. Clark, W.M. Rohsenow, "Void Volumes in Subcooled Boiling Systems," ASME paper 58-HT-19.

[3-6] R.W. Bowring, "Physical Model Based on Bubble Detachment and Calculations of Steam Voidage in the Subcooled Region of a Heated Channel," HPR-10, 1962.

[3-7] S.Z. Rouhani, E. Axelsson, "Calculation of Void Volume Fraction in Subcooled and Quality Boiling Regions," Int. J. Heat Mass Transfer, 13(1970).

[3-8] S.Z. Rouhani, "Void Measurements in the Region of Subcooled and Low-Quality Boiling, Pt. 2," AE-RTL-788, 1966.

[3-9] P.S. Larson, L.S. Tong, "Void Fractions in Subcooled Flow Boiling," Trans. ASME, 91(1969).

[3-10] W.T. Hancox, W.B. Nicoll, "A General Technique for the Prediction of Void Distributions in Non-Steady Two-Phase Forced Convection," Int. J. Heat Mass Transfer, 14(1971).

[3-11] N. Zuber, F.W. Staub, G. Bijwaard, "Vapor Void Fractions in Subcooled Boiling and Saturated Boiling Systems," Proc. 3rd Int. Heat Transfer Conf., Chicago, 1966.

[3-12] F.W. Staub, "The Void Fraction in Subcooled Boiling -- Prediction of the Initial Point of Net Vapor Generation," Trans. ASME, 90(1968).

[3-13] S. Levy, "Forced Convection Subcooled Boiling -- Prediction of Vapor Volumetric Fraction," GEAP-5157, 1966.

[3-14] P. Saha, N. Zuber, "Point of Net Vapor Generation and Vapor Void Fraction in Subcooled Boiling," Proc. Fifth Int. Heat Transfer Conf., Vol. IV, 1974.

[3-15] R.T. Lahey et al., "Mass Flow and Enthalpy Distribution in a Rod Bundle for Single- and Two-Phase Flow Conditions," J. Heat Transfer, 93(1971), 197.

[3-16] F.S. Castellana, J.E. Casterline, "Subchannel Flow and Enthalpy Distributions at the Exit of a Typical Nuclear Fuel Core Geometry," Nucl. Eng. Des., 22(1972), 3-18.

[3-17] J.T. Rogers, R.G. Rosehart, "Mixing by Turbulent Interchange in Fuel Bundles, Correlations and Inferences," ASME paper 72-HT-53, 1972.

[3-18] D.S. Rowe, C.W. Angle, "Cross Flow Mixing Between Parallel Flow Channels During Boiling -- Pt. III," BNWL-371 Pt. 3, 1969.

[3-19] J.M. Gonzalez-Santalo, "Two-Phase Flow Mixing in Rod Bundle Subchannels," Ph.D. Thesis, Dept. Mech. Engng., MIT, 1971.

[3-20] G. Forti, J.M. Gonzalez-Santalo, "A Model for Subchannel Analysis of BWR Rod Bundles in Steady-State and Transient," Proc. Int. Reactor Heat Transfer Conf., Karlsruhe, Germany, 1973.

[3-21] N. Zuber, J.A. Findlay, "Average Volumetric Concentration in Two-Phase Flow Systems," J. Heat Transfer, 1965.

[3-22] R.T. Lahey, F.J. Moody, The Thermal-Hydraulics of a Boiling Water Nuclear Reactor, ANS Monograph Series, 1977.

[3-23] S.G. Bankoff, "A Variable Density Single-Fluid Model for Two-Phase Flow with Particular Reference to Steam-Water Flow," J. Heat Transfer, 82(1960).

[3-24] N. Zuber et al., "Steady State and Transient Void Fraction in Two-Phase Flow System," GEAP-5417, Jan. 1967.

[3-25] T. Harmathy, "Velocity of Large Drops and Bubbles in Media of Infinite and of Restricted Extent," AICHE J., 6(1960), 281.

[3-26] V.G. Levich, Physical Chemical Hydrodynamics, Prentice-Hall, New York, 1962.

[3-27] F.N. Peebles, H.J. Garber, "Studies of Motion of Gas Bubbles in Liquids," Chem. Engr. Progress, 49(1953),88.

[3-28] T.A. Hughes, "Steam-Water Mixture Density Studies in a Natural Circulation High Pressure System," B&W Report 5435, Feb. 1958.

4. Heat Transfer and Critical Heat Flux

4.1 Heat Transfer Package

4.1.1 Introduction

The heat transfer calculations are performed by the subroutine CHEN, which centers around the Chen correlation [4-1]. A flowchart of this subroutine is displayed in Fig. 4.1. The following options are now available in the code:

1) Single-phase forced convection
2) Single-phase natural convection
3) Two-phase forced convection
4) Two-phase natural convection (pool boiling)
5) Subcooled boiling forced convection
6) Subcooled pool boiling.

These options are believed to cover completely the operational and slightly off-operational conditions of BWR bundles. The extension of this package to include transition and film boiling regimes should, however, pose no special problems.

4.1.2 Correlations

4.1.2.1 Single-Phase Flow Heat Transfer Coefficient

The Dittus-Boelter correlation is applied for the single phase flow heat transfer

$$h_{sp} = 0.023\ Re^{0.8}\ Pr^{0.4}\ \frac{K}{D_e} \qquad (4.1)$$

For cases where the mass flux turns out to be less or equal to

zero, the finite heat transfer coefficient of

$$h = 50 \frac{W}{cm^2\ grd} \tag{4.2}$$

has been built into the code in order to avoid a breakdown of the calculation.

4.1.2.2 Chen Correlation

A method for calculating the two-phase heat transfer coefficient for known conditions of the heat flux, mass velocity, and quality has been derived by Chen [4-1, 4-2], since he found that previous correlations were less successful. The data include those for water in the pressure range of 1 to 35 atm with liquid flow velocities up to 14.7 ft/sec, heat flux up to 760,000 Btu/(hr/ft^2), and quality up to 71%.

Chen expressed the heat transfer coefficient h_{TP} as the sum of a nucleate boiling coefficient h_{NB} and a forced convective coefficient h_{FC}

$$h_{TP} = h_{NB} + h_{FC} \tag{4.3}$$

The single-phase heat transfer coefficient, h_{FC}, is the standard Dittus-Boelter correlation

$$h = 0.023\ Re_{TP}^{0.8}\ Pr_{\ell}^{0.4}\ \frac{k_{\ell}}{D_e} \tag{4.4}$$

evaluated for saturated liquid conditions at the mass flux of the liquid phase and multiplied by a correction parameter, F,

FIGURE 4.1 LOGIC FOR THE EVALUATION OF THE HEAT TRANSFER COEFFICIENT

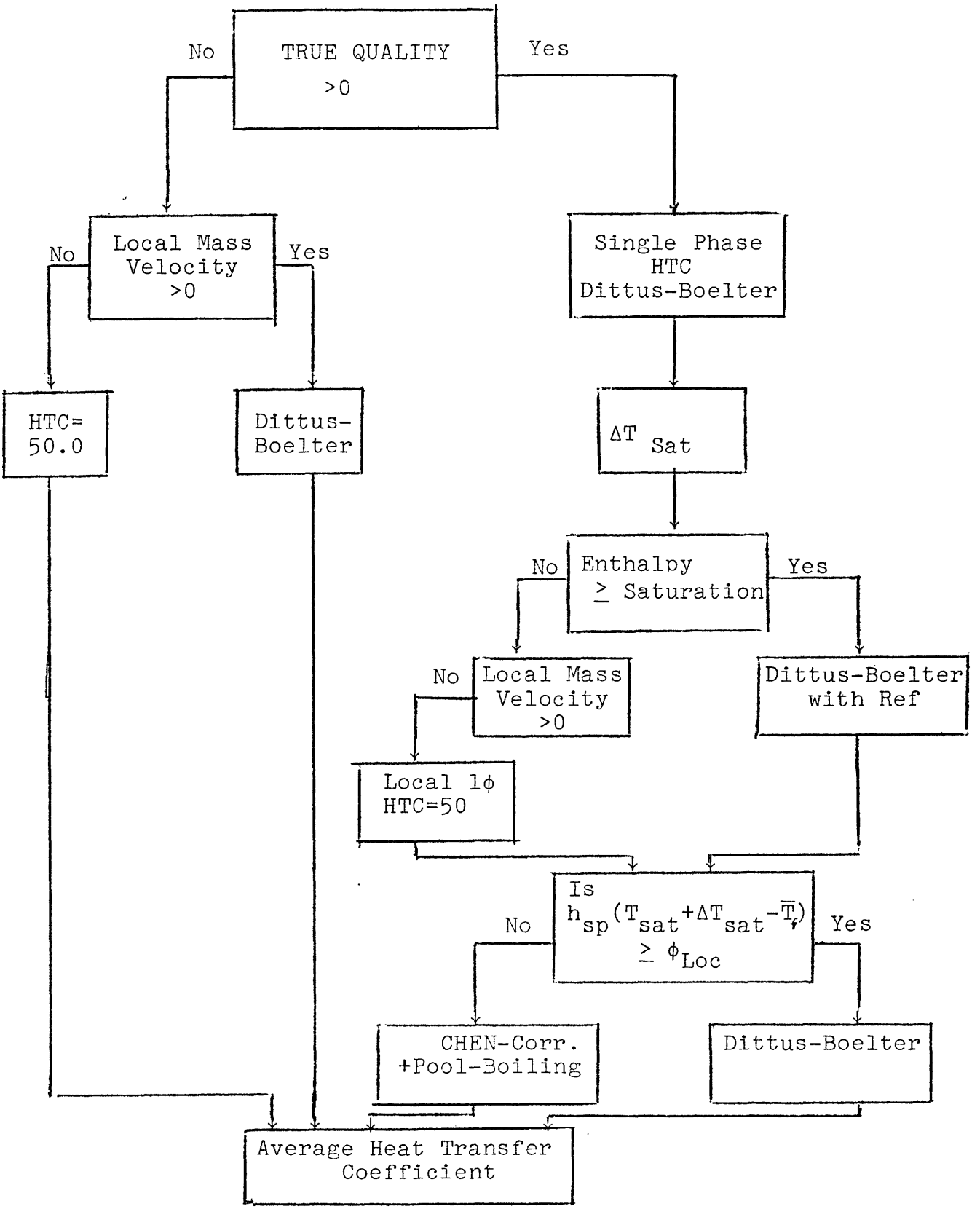

given by

$$F = \left[\frac{Re_{TP}}{Re_{\ell}}\right]^{0.8} \tag{4.5}$$

where

$$Re_{\ell} = \frac{G(1-x)\, D_H}{\mu_{\ell}} \tag{4.6}$$

Therefore, h_{FC} becomes finally

$$h_{FC} = 0.023 \left[\frac{G(1-x)\, D}{\mu_{\ell}}\right]^{0.8} \left[\frac{\mu C_p}{k}\right]_{\ell}^{0.4} \left(\frac{k_{\ell}}{D}\right) F \tag{4.7}$$

It should be noticed that the parameter F can be recognized as the ratio of an effective two-phase Reynolds number to the Reynolds number used to obtain h_{FC}. This parameter is plotted versus the Martinelli parameter , X_{tt} in Fig. 4.2. For computational purposes F must be curve-fitted versus X_{tt}.

For the two-phase nucleate boiling heat transfer coefficient, h_{NB}, Chen developed a form similar to the Forster-Zuber correlation times a nucleation suppression factor, S, i.e.,

$$h_{NB} = 0.00122 \left[\frac{k_{\ell}^{0.79}\, C_{p\ell}^{0.45}\, \rho_{\ell}^{0.49}}{\sigma^{0.5}\, \mu_{\ell}^{0.29}\, h_{fg}^{0.24}\, \rho_g^{0.24}}\right] x$$

$$x\, (\Delta T_{sat}^{0.24}\, \Delta P_{sat}^{0.75}\, S) \tag{4.8}$$

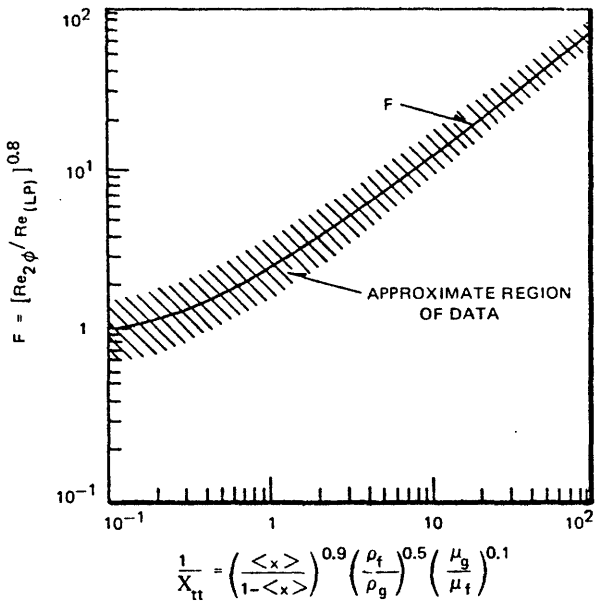

Fig. 4.2: Reynolds number factor, F

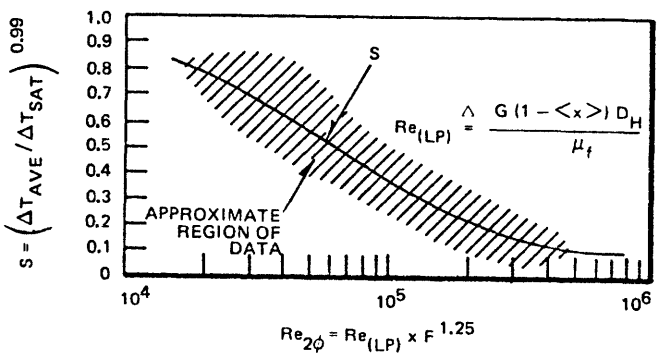

Fig. 4.3: Suppression factor, S

S is defined as

$$S = \left[\frac{\Delta T_{av}}{(T_W - T_{sat})}\right]^{0.99} \tag{4.9}$$

where ΔT_{av} is the effective radial average superheat in the liquid film. The suppression factor is displayed in Fig. 4.3 as a function of the effective two-phase Reynolds number, Re_{TP}

ΔT_{sat} in Eq. (4. 8) is given by

$$\Delta T_{sat} = T_W - T_{sat}$$

which can be developed by using Clapeyron's equation

$$\Delta T_{sat} = \frac{T_{sat}}{h_{fg}} \cdot \frac{\Delta P_{sat}}{\rho_{fg}}$$

Therefore, h_{NB} can be presented in the following form

$$h_{NB} = 0.00122 \left[\frac{k_\ell^{0.79} C_{p\ell}^{0.45} \rho_\ell^{0.49}}{\sigma^{0.5} \mu_\ell^{0.29} h_{fg}^{0.24} \rho_g^{0.24}}\right] \left(\frac{h_{fg}}{v_{fg} T_{sat}}\right)^{0.75} x$$

$$x\ (T_W - T_{sat})^{0.99} S \tag{4.10}$$

Eqs. (4.3), (4.7), and (4.8) can be used in conjunction with Figs. 4.2 and 4.3 or their respective curve fits to evaluate the two-phase heat transfer coefficient. However, it should be carefully noticed that the Chen correlation is <u>implicit</u> in $(T_W - T_{sat})$ and therefore requires an iterative

procedure which is possibly one reason that it has not been widely used in subchannel codes thus far although it is recommended throughout the nuclear industry.

Fig. 4.4 compares several of the popular boiling heat transfer correlations, namely the Chen, Jens-Lottes, and Dengler and Addoms correlations for a typical value of ΔT_{sat} = 10°F. It becomes obvious from this graph that the Chen correlation tends to merge with the Jens-Lottes correlation for nucleate boiling conditions and with the Dengler and Addoms correlation for forced convection vaporization. Characteristic of the suppression of nucleate boiling is the increase of the heat transfer coefficient with quality as depicted in Fig. 4.4.

From the above it follows that Chen's correlation, which is for saturated boiling, should be applicable to flow regimes from slug flow through annular flow, i.e. it covers the most important ones for the thermal-hydraulic analysis of fuel pin bundles. Furthermore, it provides a smooth transition from the nucleate-boiling dominated heat transfer mode to all forced convection where boiling is suppressed. An additional interesting and possible extension would be to set the parameters S and F such that F approaches one of the correlations based on Martinelli's parameters in the high-quality range (for instance Dengler and Addoms or Bennett) while S will be zero when the criterion for the boiling suppression is satisfied.

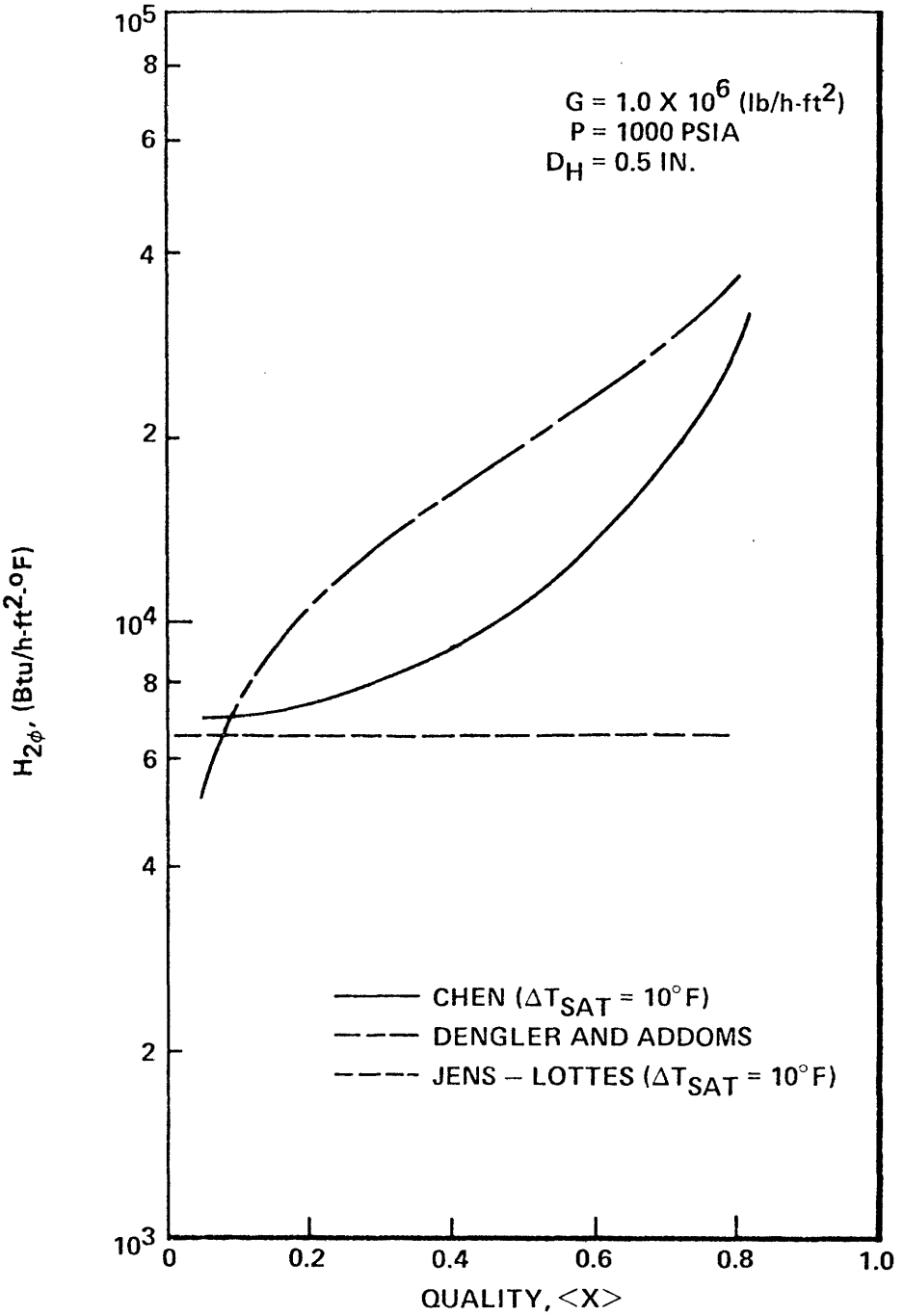

Fig. 4.4: Comparison of some convective boiling heat transfer correlations

4.1.2.3 Curve Fits to the Parameters F and S

For computational purposes the parameters F and S must be fitted to appropriate curves as mentioned before.

As depicted in Fig. 4.2 the parameter F must be represented as

$$F = f\left(\frac{1}{X_{tt}}\right)$$

where the Martinelli factor, X_{tt}, is given by Collier [4-2] as

$$X_{tt} = \left(\frac{1-x}{x}\right)^{0.9} \quad \left(\frac{\rho_g}{\rho_\ell}\right)^{0.5} \quad \left(\frac{\mu_\ell}{\mu_g}\right)^{0.1} \tag{4.11}$$

The approximation for F follows a procedure developed by McClellan [4-3] where F is considered to be approximately a straight line for $\frac{1}{X_{tt}} > 0.5$ and given by a second order polynomial for $\frac{1}{X_{tt}} < 0.5$. At $\frac{1}{X_{tt}} = 0.5$, F is assumed to have the value of 1.6. An additional constraint for the functional relationship is given by the fact that F must approach one when the quality approaches zero.

The mathematical relationship developed reads

$$F = 0.5\left(\frac{1}{X_{tt}}\right)^2 + 0.95\left(\frac{1}{X_{tt}}\right) + 1.0 \quad \text{for} \quad \frac{1}{X_{tt}} < 0.5$$

and (4.12)

$$F = 1.6\left(\frac{2}{X_{tt}}\right)^{0.738} \quad \text{for} \quad \frac{1}{X_{tt}} \geq 0.5$$

and these formulas have been implemented into WOSUB after they have been successfully tested [4-4] against data given by Collier.

It is interesting to note that Butterworth [4-5] developed similar fits in the meantime, i.e.

$$F = 1.0 \qquad \text{for } \frac{1}{X_{tt}} \leq 0.1$$

$$F = 2.35 \left(\frac{1}{X_{tt}} + 0.213\right)^{0.736} \qquad \text{for } \frac{1}{X_{tt}} > 0.1 \tag{4.13}$$

No attempts have been made to compare both formulations.

The suppression factor S was approximated by McClennan [4-3] in a similar manner. Two straight lines were used which are intersecting at Re_{TP} equal to 3.0×10^5. At this point, S is estimated as 0.17. As a result of this selection the factor S was fitted as

$$S = 1 \qquad Re_{TP} = 0$$

$$S = 0.17 - 0.232 \ln \left(\frac{Re_{TP}}{3.0x10^5}\right) \qquad 2x10^4 \leq Re_{TP} \leq 3x10^5$$

$$S = 0.17 - 0.0617 \ln \left(\frac{Re_{TP}}{3.0x10^5}\right) \qquad 3x10^5 \leq Re_{TP} \leq 10^6 \tag{4.14}$$

Independent of these fits presented above, Butterworth [4-5] presented the following formula for S

$$S = \begin{cases} [1-0.12\ (Re'_{TP})^{1.14}]^{-1} & Re'_{TP} < 32.5 \\ [1+0.42\ (Re'_{TP})^{0.78}]^{-1} & 32.5 \quad Re_{TP} < 70.0 \\ 0.1 & Re'_{TP} \geq 70 \end{cases} \tag{4.15}$$

In conclusion of this section it should be pointed out that the Chen correlation displays smooth transitions between the heat transfer regimes in the pre-CHF region. This is certainly not the case for the combination such as the Thom-Schrock-Gossman correlations which as part of the RELAP4/MOD5 heat transfer package is commonly used.

In summary then, the Chen correlation is applicable for the following conditions:

1) low and high qualities
2) low and high flow rates
3) forced convection (saturated nucleate boiling, forced convection vaporization in annular flow)
4) pool boiling
5) transforms to Forster-Zuber pool boiling correlation at low flow.

4.1.2.4 Programming Considerations

The major two-phase heat transfer evaluation in the subroutine CHEN proceeds roughly as follows:

1) Calculate single phase heat transfer coefficient
2) Evaluate F

3) Obtain h_{FC}

4) Calculate Re_{TP}

5) Evaluate S

6 Determine h_{NB} in several steps.

As mentioned already before, step 6 mandates an iterative scheme. For this purpose all terms but ΔP_{sat} and ΔT_{sat} in Eq. (4.8) are calculated. If the wall temperature is greater than the saturation temperature of the fluid, then the iterative scheme is required to find the wall temperature and corresponding pressure. This is accomplished by a Newton's method type of procedure, whereby successive guesses of the wall temperature produce heat fluxes which are compared to the actual heat flux, and the error is presumably successively reduced until it is within a preset limit. This limit is set at 1% in the code, now.

The heat transfer coefficient subroutine is presently set up to compute the heat transfer coefficient at each axial step for each subchannel, resulting in four heat transfer coefficients for each rod at each axial step which are then averaged in order to find one heat transfer coefficient for each rod at each step. but needs also quite a substantial amount of computer core storage. However, this procedure as it stands now allows for the possibility of generating enough local information in order to perform an approximate 2-D fuel pin temperature calculation.

4.1.3 Conclusions

It is believed that the implementation of the Chen correlation as described above offers a high degree of flexibility and reliability to the evaluation of the heat transfer in the pre-CHF region.

The addition of special correlations such as for instance for natural turbulent convection and the like should be of no problem. Neither should the extension of this package into the post-CHF regime be of any problem. For this purpose, the application of a best estimate heat transfer package as introduced by Bjornard [4-6] and applied by Massoud [4-7] is advised.

4.2 Critical Heat Flux Package

4.2.1 Introduction

The point at which the heat transfer coefficient deteriorates more or less rapidly is known by various names, listed by Lahey and Moody [4-8] as follows:

1) Boiling crisis
2) Critical heat flux (CHF)
3) Departure from nucleate boiling (DNB)
4) Burnout (BO)
5) Dryout

Whereas the term DNB is most frequently used to describe the high-pressure, high-flow phenomena characteristic of PWR rod bundle behavior, the term CHF seems to be preferred for the general characterization of this phenomenon and will be also used here in what follows. However, the reader should be fully aware of the possible misleading nature of this term when applied to BWR conditions. For instance, as Lahey and Moody [4-8] pointed out, CHF has generally the connotation that it is the local heat flux that determines the onset of transition boiling. However, under BWR conditions this "local condition hypothesis" does not work in all generality. For these reasons the authors prefer the term boiling transition (BT) to describe correctly the event.

No matter how the event is actually called, from a physical point of view at the qualities of interest to BWR technology it is primarily governed by the dryout of the liquid film on the

heated surface. As described by Hewitt and Hall-Taylor [4-9] as well as Collier [4-2] and Tong [4-10] this phenomena is always associated with two-phase annular flow conditions. The interested reader is referred to Lahey and Moody for a review on simple mechanistic description of the film dryout process.

The interpretation and representation of BWR fuel rod bundle CHF data are of greatest interest to the WOSUB development. Of special interest to reactor engineering applications is the complicated impact of nonuniform axial and transverse (rod-to-rod) heat flux profiles upon boiling tansition, i.e., CHF.

Collier [4-2] and Tong [4-10] have summarized various techniques which are commonly used in correlating nonuniform axial heat flux data. There are two basic methods available; the local conditions hypothesis and the integral approach. The former essentially states that only the local heat flux and local quality determine CHF, which means that the upstream effect is important, i.e., how the quality at some axial position is distributed across the channel.

Generally it has been accepted that the integral approach should be applied to BWR conditions and the associated heat flux profiles. The axial heat flux profile governs essentially the so-called "upstream memory effect" which depends on the flow regime and thus the quality. Among the various integral schemes available in the open literature the Tong F-factor is certainly the most widely used scheme applied especially for PWR conditions today. Lahey and Moody [4-8] studied carefully the

possibility of applying the same concept to BWRs and concluded that the exponential weighting as employed by the F-factor method for the upstream history although important for low-quality conditions is not nearly as important for BWR bundle analysis.

An alternate integral scheme for the CHF in the higher quality annular flow regime has been introduced by Bertoletti et al. [4-11] at CISE in Milan, Italy. This CISE-type correlation was the first one which used the concept of the critical quality-boiling length representation where the upstream history enters implicitly into the critical boiling length. Fig. 4.5 shows the boiling boundary, λ, the critical boiling length, L_{Bc}, and the critical quality, X_c. As can be seen from this figure the boiling length is the length over which bulk boiling occurs and is measured from the boiling boundary, λ. L_{Bc} measures then just the distance between this boundary and the point at which CHF occurs. Experience by the CISE group shows that nonuniform axial heat flux data as shown in Fig. 4.6 in the q_c''-x plane can be most conveniently collapsed into one curve in the X_c-L_{Bc} plane as depicted in Fig. 4.7. In this way the problem of nonuniform axial heat flux profile is easily taken care of.

Lahey and Moody [4-8] showed that the Tong-F-factor approach and the generalized critical quality-boiling length approach are equivalent. As pointed out, the main difference between the two approaches boils down to the different treatment of the upstream history. Whereas the F-factor modifies

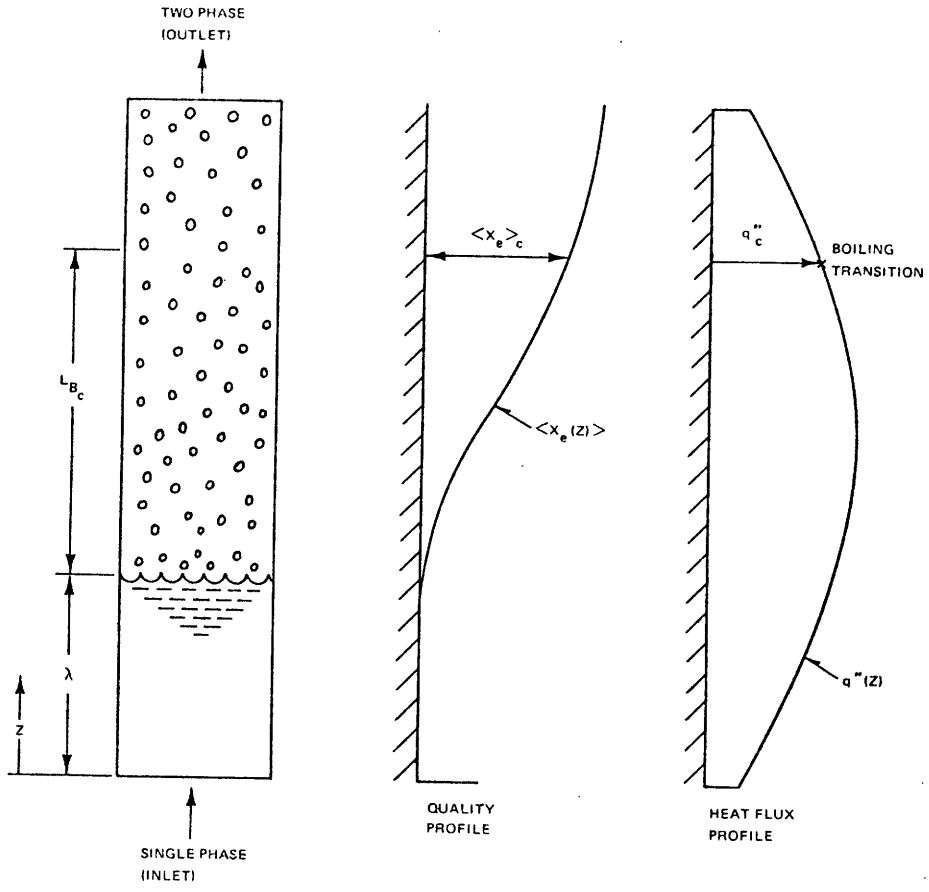

Fig. 4.5: Definition of the boiling length

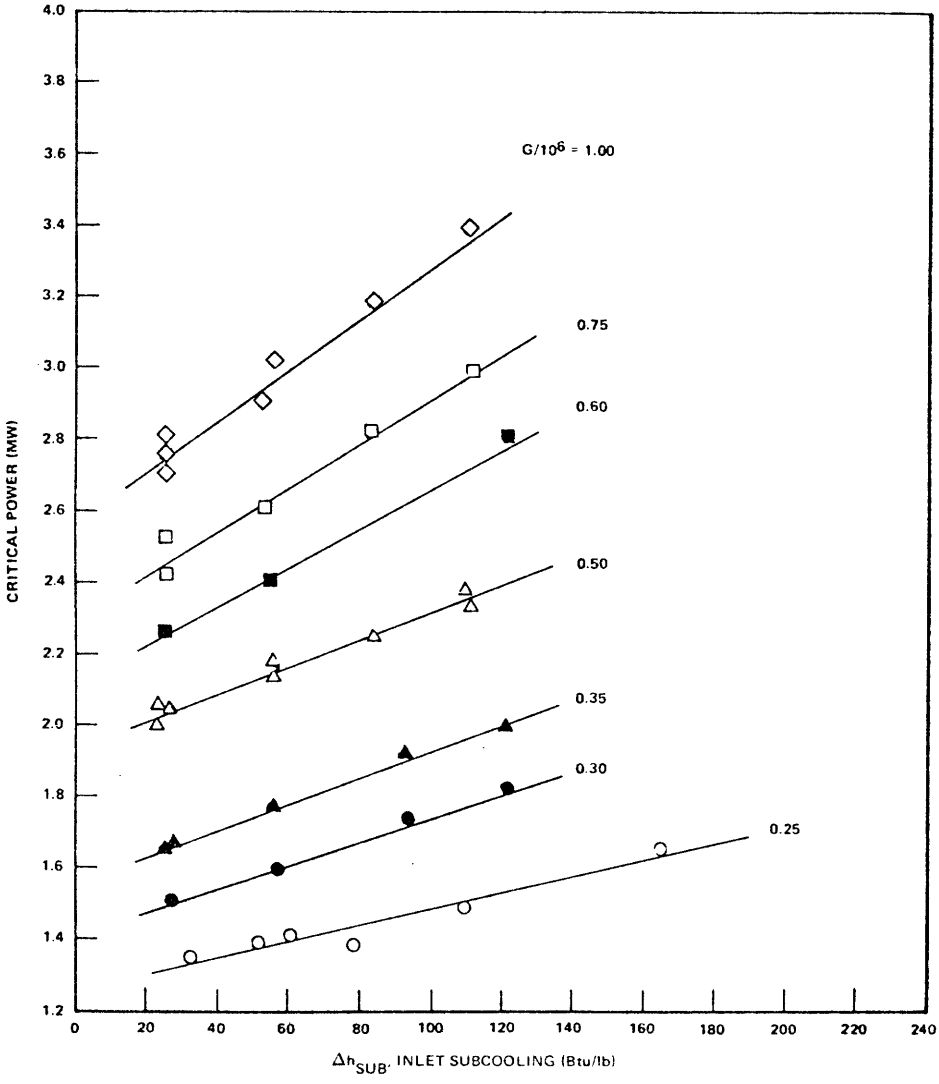

Fig. 4.6: Critical power versus inlet subcooling, 16 rod x 12-ft cosine, uniform local peaking, 1000 psia, various flow rates

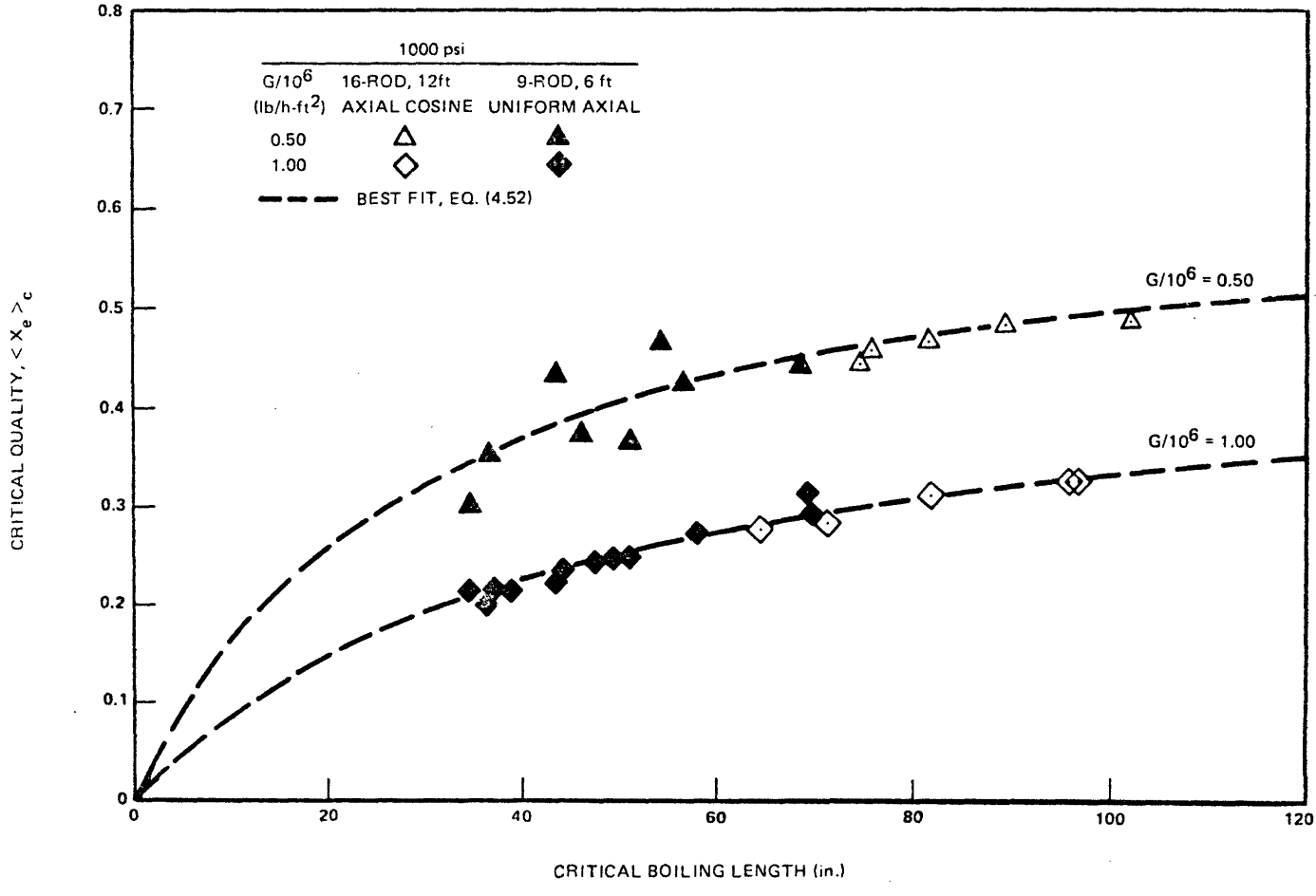

Fig. 4.7: 9- and 16-rod critical quality versus boiling length, 1000 psia

the uniform axial CHF correlation the critical quality-boiling approach modifies the heat balance $q''(x)$ to yield the appropriate correlation for the nonuniform axial heat flux profile. However, it is important to understand that both procedures are equivalent and lead to the same thermal margin. The latter is of special importance for the design and the licensing process. The most common measure for thermal margin is certainly the CHFR which is defined as the ratio of CHF given by a correlation to the local heat flux at a given quality. As noticed by several authors, this concept does not give a true picture of the thermal margin. Therefore, it has been suggested recently to employ the critical power ratio (CPR) which is defined as the ratio of the critical power to the operating power. This ratio is of direct practical use and can be easily interpreted.

There are two approaches for establishing the required design. The first concerns the construction of a limit line in the flux-quality plane whereas the second one uses the critical quality-critical boiling length plane. The first set of limit lines employed by GE was devised by Janssen and Levy [4-12]. This set was later improved by Hench and Levy [4-13] when more data for rod bundles became available. Despite these efforts, the concept of the limit line where no data points should fall below this line is uncapable to display the correct axial heat flux effect. For this reason this concept has been given up by GE for the integral technique in terms of critical quality-boiling length. This development led to the so-called GEXL

correlation which is a main part of the design procedure GETAB naturally proprietary. The form of the GEXL correlation reads

$$X_c = f\ (L_{Bo}\ ,\ G,\ P,\ L_H,\ D_q,\ R) \qquad (4.16)$$

where D_q is the thermally equivalent diameter and R is a synthesized local peaking pattern factor.

The important feature of this new correlation is that it still uses cross-sectional bundle average parameters as the limit line approaches do. It should be recognized though that a lot of proprietary and empirical information enters into the synthesis of R. Furthermore it is worth mentioning that the GEXL correlation is a best fit to the experimental data base which includes full-scale 49- and 64-rod data. This development parallels other recent efforts to apply more and more best estimate knowledge as substitute for the conservative approach used in the past. In addition, GEXL is used in GETAB in the context of a statistical treatment of the required thermal margin. This too is in perfect agreement with recent trends in thermal hydraulic analysis.

As shown in Fig. 4.8,the heat balance curve which touches the GEXL correlation determines the critical power. It is obvious that this process involves an iterative procedure. The critical power curve is associated with a minimum critical power ratio (MCPR) of one which reduces the critical quality defect, i.e., difference, ΔX_c, as shown in the figure to zero.

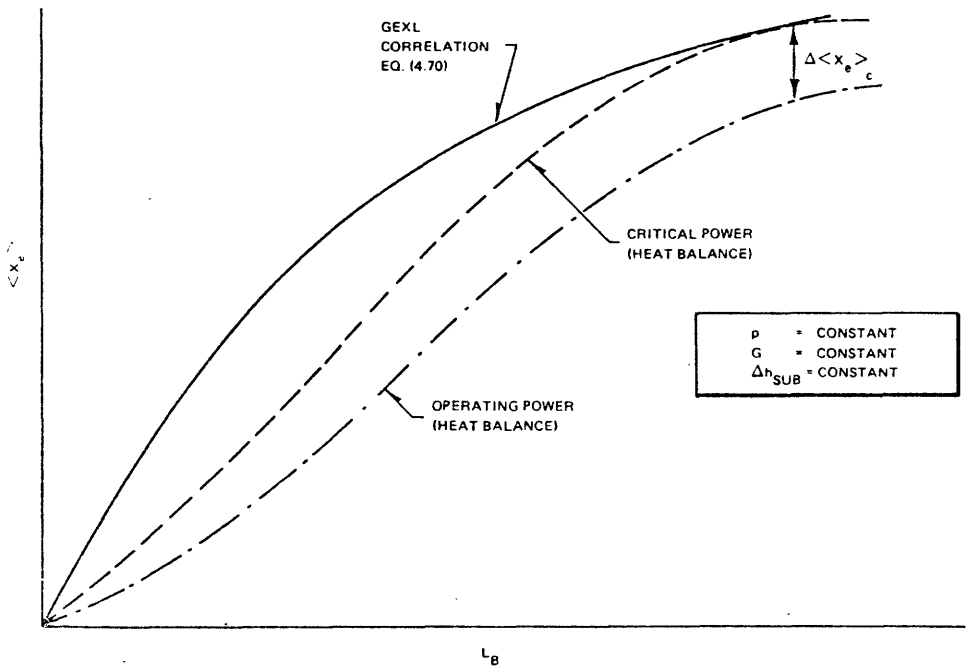

Fig. 4.8: GEXL correlation and BWR heat balance curves

From a design point of view MCPR=1 is associated with a 50% probability that CHF would be experienced on 0.1% of the fuel pins in the core.

With this background information in mind, the reader may more easily comprehend the actual selection of the correlations built into the WOSUB code as discussed below in more detail.

4.2.2 Correlations

In light of the aforementioned facts and changes in BWR design philosophy whose underlying correlations are proprietary, it was decided to provide the user of WOSUB with a wide spectrum of CHF correlation options including the following:

1) Barnett correlation
2) Israel correlation
3) Janssen-Levy limit line
4) CISE correlation with evaluation of the critical power.

It is thought that these correlations cover most of the material discussed in the foregoing chapter. Furthermore, it is believed that the implementation of the CISE correlation being a critical quality-critical boiling length correlation is an important step into the right direction as set forth by GE's new procedure. However, the user should be fully aware of the fact that this implementation of the CISE correlation constitutes a preliminary step and it cannot be expected that its results match perfectly those by GE. Much more work must be devoted into this area in the future.

The Janssen-Levy limit line and the Israel rod bundle correlation are based on bundle-averaged mass velocity and quality. On the other hand, the Barnett correlation is based on an equivalent annulus concept and contains in its implemented form in WOSUB a correction for nonuniform axial heat flux which is based on equivalent thermodynamic equilibrium quality. The basic CISE correlation is based on an annulus correlation and thus the effect of unheated walls in a bundle renders the correlation useless. Therefore, it was decided to use it only for center subchannels which are bounded by fluidic boundaries only.

4.2.3 Barnett Correlation

The data for annuli can be correlated by means of a Mcbeth-type correlation and this has been done by Barnett [4-14]. This correlation reads

$$\frac{q''_{crit}}{10^6} = \frac{A + B\,(H_{sat}-H_{in})}{C+z} \tag{4.17}$$

where for the pressure of 69 bar (1000 psia) the coefficients are given as follows

$$\begin{aligned} A &= 67.45\, D_h^{0.68}\,(Gx10^{-6})^{0.192}\,[1-0.744\exp(-6.512\, D_e(Gx10^{-6}) \\ B &= 0.2587\, D_h^{1.261}(Gx10^{-6})^{0.817} \\ C &= 185.0\, D_e^{1.415}\,(Gx10^{-6})^{0.212} \end{aligned} \tag{4.18}$$

where

D_i is defined as D_r, the rod diameter, and

$D_o = [D_r(D_r+D_h^*)]^{1/2}$ (inches), $D_h^* = \frac{4 \times (\text{Flow area})}{S \times (\text{heated rod perimeter})}$, where

$S = \sum_{\text{rods}} \frac{\text{local rod power}}{\text{maximum rod power}}$. Note that for an annulus,

$D_e = D_o - D_i$

$D_h = (D_o^2 - D_i^2)/D_i$

The correlation is given in the British system of units and covers the following range of parameters:

p = 600-1400 psia

z = 24-108 in

$G/10^6$ = 0.14-6.2 $lb/hr\ ft^2$

$(H_{sat}-H_{in})$ = 0-412 Btu/lb

D_o = 0.551-4.006 in

D_i = 0.375-3.798 in

For pressures other than 69 bar (1000 psia), Barnett suggests to multiply the coefficient A in Eq. (4-18) by $(h_{fg}/649)$. A. Levin has also successfully used this correlation at pressures up to 1500-2500 psia, which means that with the range of inlet subcooling, this correlation is applicable to both PWR's and BWR's.

A correction for nonuniform axial heat flux has been developed by A. Levin and used with good results. Radially nonuniform patterns are handled through the S-factor which appears in the formula for the equivalent heated diameter. This S-factor given by Collier [4-2] originally as

$$\sum_{\text{rods}} \frac{q''_{loc}}{q''_{max}}$$

is interpreted here somewhat differently for nonuniform axial heat flux. Instead of using the heat flux ratio the power ratio is applied. By bearing in mind that $\dot{q}_{max}$ is a constant, and that for a bundle, $\dot{q}_{avg}$ is also constant, the correction term becomes

$$\sum_{\text{rods}} \frac{\dot{q}_{loc}}{\dot{q}_{avg}} \cdot \frac{\dot{q}_{avg}}{\dot{q}_{max}}$$

The term $(\dot{q}_{avg}/\dot{q}_{max})$ is the inverse of the largest radial peaking factor in the bundle, whereas the term $\sum_{\text{rods}} (\dot{q}_{loc}/\dot{q}_{avg})$ is simply the number of rods in the bundle, since $\dot{q}_{avg}=(\Sigma\ \dot{q}_{loc})/n$. Therefore, the S-factor reduces to the number of rods in the bundle divided by the maximum radial peaking factor. This interpretation due to A. Levin allows the Barnett correlation to be used for nonuniform axial heat flux profiles and the results obtained in analytical test cases have been encouraging.

4.2.4 Israel Correlation

Another method is that of taking bundle-averaged conditions. An example for this approach is the rod-bundle correlation devised by Israel [4-15] which reads:

$$q''/10^6 = \left[0.688+0.144(\bar{G}/10^6)^{1.4}\right] - \left[0.831+0.221\left(\bar{G}/10^6\right)^{2.72}\right]\bar{x}_{exit} \quad (4.19)$$

where $\bar{G}$ and $\bar{x}_{exit}$ are bundle-averaged quantities. This correlation should be valid over the following range of system parameters:

p = 1000 psia

$\bar{G}/10^6$ = 0.5-1.8 lb/hr ft^2

4x4 rod bundle, 0.56-in. rods

L = 72 in.

$\bar{x}_{exit}$ = 0.07-0.40

The Israel correlation is applicable in the form as presented. However, the user must be careful in using the bundle average mass velocity and exit quality for this correlation.

4.2.5 The Janssen-Levy Limit Line

The first set of limit lines used by GE and devised by Janssen and Levy [4-12] were based on single-rod annular CHF data having uniform axial heat flux. For this reason it should not surprise when the correlation is now considered to be obsolete. However, it was the only set of limit lines publicly

available at the beginning of this research. The correlation is actually priced together from three straight lines whose intersections are specified in terms of qualities which are dependent on the mass flux. Accordingly the correlation reads as follows:

For 1000 psia

$$
\begin{aligned}
q''/_{10^6} &= 0.705 + 0.237\ (G/_{10^6}) && \text{for } x<x_1 \\
&= 1.63 - 0.270\ (G/_{10^6}) - 4.71x && \text{for } x_1<x<x_2 \\
&= 0.605 - 0.164\ (G/_{10^6}) - 0.653x && \text{for } x>x_2
\end{aligned}
\tag{4.20}
$$

where the qualities, x_1 and x_2

$$
\begin{aligned}
x_1 &= 0.197-0.108\ (G/_{10^6}) \\
x_2 &= 0.254-0.026\ (G/_{10^6})
\end{aligned}
\tag{4.21}
$$

This correlation should be valid over the following range of system parameters

p = 600-1450 psia

$G/_{10^6}$ = 0.4-6 lb/hr ft^2

x_{exit} = Negative-0.45

D_e = 0.245-1.25 in

L = 29-108 in.

For pressures other than 1000 psia, the following pressure correction has been recommended

$$q''(p) = q''_{1000\ psia} + 440(1000-p) \qquad (4.22)$$

Moreover, for hydraulic diameters greater than 0.6 in. the correlation should be modified according to Lahey and Moody [4-2] by subtracting

$$2.19 \times 10^6 \left(D_H^2 - 0.36\left[x - 0.0714\left(\frac{G}{10^6}\right) - 0.22\right]\right) \qquad (4.23)$$

This correction has not been implemented into WOSUB yet. As Lahey and Moody [4-2] point out, the validity of the Janssen-Levy correlation was essentially based on the hypothesis that the corner rod in a multirod bundle resembles geometrically the annular configuration. However, when more multirod CHF data became available some adjustment to the old limit lines appeared in order and led to the Hench-Levy limit lines [4-13], which were previously proprietary but have been published [4-8] meanwhile GE adopted the GEXL correlation.

For future extension of WOSUB it is recommended to replace the old Janssen-Levy correlation by the more realistic Hench-Levy limit lines although the user should bear in mind that neither is presenting the state-of-the-art.

4.2.6 The CISE Critical Quality-Critical Boiling Length Correlation

Due to the unavailability of the GEXL correlation, and yet by recognizing the need for a critical quality-critical boiling length correlation to meet present standards, the CISE correlation, being the starting point of GE's own development, was chosen for implementation as a first step. The general functional form of the correlation reads

$$x_c = \frac{a(p,G)L_{Bc}}{[b\ (p,G,D_H) + L_{Bc}]} \tag{4.24}$$

although Gaspari [4-16]suggests to apply a quadratic form of the correlation to obtain a better data fit. The CISE correlation which is built into the code has the following specific form

$$\frac{\hat{W}_{bl}}{GAh_{fg}} = \frac{\dot{q}_{avg}}{\dot{q}_{\substack{rod\\local}}} \frac{1-P/P_{crit}}{(1.35G/10^6)^{1/3}} \times \frac{L_{bl}}{L_{bl}+168\left[\frac{P_{crit}}{P}-1\right]^{0.4}\left(\frac{G}{10^6}\right)D_e^{1.4}} n \frac{A_i}{A_{tot}} \tag{4.25}$$

where the subscript bℓ refers to the boiling length. It should be noticed that the expression at the left-hand side of this equation represents the critical quality.

This correlation applies over the following range of parameters:

P = 720-1000 psia

$G/10^6$ = 0.8-3.0 lb/hr ft^2

n = 7-37 rods

Rod O.D. = 0.0333-0.065 ft

L = 2.5-12 ft

The critical bundle power is calculated by finding the minimum boiling length critical power for the bundle on a subchannel basis and adding it to the power needed to bring the bundle to zero equilibrium quality.

The following must be kept in mind when the CISE correlation is used. First of all, it was set up for rod-centered subchannels whereas WOSUB operates on the basis of coolant centered subchannels. Furthermore, this correlation is based on an annulus correlation which actually led the Italians to devise the rod centered subchannel approach. In order to apply this correlation in a meaningful way, it was thought that it should be only used for interior center channels. The reasoning behind this recommendation is that since side and corner subchannels include portions of the essentially unheated bundle wall in the coolant-centered subchannel scheme (whereas this is not the case with a rod-centered scheme), the hydraulic diameters of these channels will be too small in comparison to their annular counterparts. In addition, the presence of the cold bundle walls severely affects the boiling length of the subchannel. An interior subchannel, however, has none of the cold wall effects. Therefore, its hydraulic diameter will

be the same in the coolant-centered as well as in the rod-centered subchannel schemes so that the correlation can be safely applied. In addition to this interpretation the term for the correction of radially nonuniform heat fluxes needs to be modified. This factor appears as $\dot{q}_{avg}/\dot{q}_{loc}$ in the correlation but can be simply interpreted as just the inverse of the radial peaking factor in a rod-centered subchannel. However, for a coolant-centered subchannel, which contains one quarter of each of four possibly differently heated rods, this factor must be modified. One option which has been proposed by A. Levin is

$$\frac{\dot{q}_{avg}}{\dot{q}_{loc}} = \frac{\sum_{rods} \frac{\dot{q}_{avg}}{\dot{q}_{loc}}}{n}$$

where n=4 is the number of associated rods in a center subchannel. The use of this modified correlation gave good results in analytical tests.

4.2.7 Conclusion

It is thought that the correlations presented above offer the user quite a broad spectrum of different approaches. However, it must be recognized that none of the aforementioned options is perfect when it comes to a comparison with GE's proprietary GEXL correlation. Nevertheless, the implementation of the CISE correlation offers the user an option which is equivalent to GE's approach from a methodology point of view.

Future work on WOSUB should include the implementation of the Hench-Levy set of limit lines as a substitute for the Janssen-Levy correlation as well as the extension of the CISE correlation to the CISE-IV correlation which includes now energy transfer with neighboring subchannels thereby reducing the overconservatism described in Volume III of this report [4-17].

4.3 References

[4-1] J.C. Chen, "A Correlation for Boiling Heat Transfer to Saturated Fluids in Convective Flow," ASME paper 63-HT-34, 1963.

[4-2] J.G. Collier, Convective Boiling and Condensation, McGraw-Hill Book Co., London, 1972, p. 208-234.

[4-3] M.S. McClennan, "Flow Stability in BWR Cooland Channels During Transients," S.M. Thesis, Dept. Mech. Engng., M.I.T., 1974.

[4-4] M.S. McClellan, "Programming the Chen Correlation," unpublished MEKIN-Note, 1975.

[4-5] Butterworth, personal communication, 1977.

[4-6] T.A. Bjornard, "Blowdown Heat Transfer in a Pressurized Water Reactor," Ph.D. Thesis, Dept. Mech. Engng., M.I.T., Aug. 1977.

[4-7] M. Massoud, "Comparison of Conservative and Best Estimate Heat Transfer Packages with COBRA-IV-I, N.E. Thesis, Dept. Nucl. Engng., M.I.T., Aug. 1978.

[4-8] R.T. Lahey, F.J. Moody, The Thermal-Hydraulics of a Boiling Water Nuclear Reactor, ANS Monograph Series, 1977.

[4-9] G.F. Hewitt, N.S. Hall-Taylor, Annular Two-Phase Flow, Pergamon Press, Oxford, 1970.

[4-10] L.S. Tong, "Boiling Crisis and Critical Heat Flux," TID-25887, 1972.

[4-11] S.G. Bertoletti et. al, "Heat Transfer Crisis with Steam-Water Mixtures," Energ. Nucl., 12 (1965)3.

[4-12] E. Janssen, S. Levy, "Burnout Limit Curves for Boiling Water Reactors," APED-3892, 1962.

[4-13] J.M. Healzer et. al, "Design Basis for Critical Heat Flux Condition in Boiling Water Reactors," APED-5286, 1966.

[4-14] P.G. Barnett, "The Prediction of Burnout in Non-uniformly Heated Rod Clusters from Burnout Data for Uniformly Heated Round Tubes," AEEW-R362.

5 Method of Solution

5.1 Introduction

In this chapter, the finite difference equations and the overall solution scheme in the WOSUB code are discussed. The conservation equations as presented in Chapter 2 are developed with the help of a backward finite difference form in both space and time, which means that the numerical scheme is designed to be fully implicit for stability purposes.

Overall the solution scheme proceeds in the following manner. Once the pressure drop is calculated at a given axial elevation for each subchannel, an iterative scheme will be used to solve for the inverted volumetric crossflows which satisfy the required condition of a zero transverse pressure gradient as indicated by Eq. (2.17). For this purpose a convergence criterion is selected which compares the subchannel pressure drop to the mass flow weighted average pressure drop at the given axial position. A value of 0.001 for this criterion has been implemented into the code right now, and it is thought to be tight enough to insure sufficient accuracy of the IBM machines. This is in perfect agreement with earlier experiences with the COBRA-IIIC code.

Fig. 5.7 shows a flow chart of the pressure drop-diverted flow solution. In order to insure total flow continuity, a renormalization is performed at each axial step.

It should be noticed that there exists no absolute stability proof for this method. However, no problems have been encountered with the solution method thus far. In order to accelerate the convergence of the iterative process, an underrelaxation parameter has been introduced.

5.2 Finite Difference Formulation

The equations to be solved are written in backward finite difference form in space and time. This insures numerical stability independent of the time step selection which is an important factor since slow transients may take hundreds of seconds realtime.

A marching type of solution method from subchannel inlet to exit at each time step is performed similarly to all other well-known common subchannel codes. This scheme comprises an initial value problem set up. Flow reversals cannot be treated in this way. Rather, they would call for a solution of a boundary value problem by a field equation method.

Without going into great detail of the derivation, the set of sequential equations for the unknowns will be given below together with some explanations how to derive them from the basic conservation equations.

In a first step the conservation equations, Eqs. (2.1) through (2.4) are put into a backward finite difference form. In order to solve for the volumetric vapor generation rate, Ψ,

the vapor continuity equation is multiplied by H_{vi} and is substituted in to the energy equation. The resulting equation is divided by $\rho_{\ell i}$ and the ratio $\gamma = \frac{\rho_v}{\rho_\ell}$ is introduced. Similarly, multiplying the liquid continuity equation by $H_{\ell sat}$ and dividing by $\rho_{\ell i}$, then adding to the equation which was obtained previously by handling the vapor continuity equation yields, upon rearranging Ψ for each subchannel generated over Δz as follows:

For equilibrium bulk boiling conditions:

$$\Psi = \frac{1}{\gamma H_{fg} \Delta z}\left[\frac{\Delta z}{\rho_{\ell i}}\left(\frac{q'' P_H}{A} + \frac{\partial P}{\partial t}\right) - \frac{\Delta z}{\Delta t}\gamma \bar{\alpha}_i \left(H_{v_{sat}} - \bar{H}_{vi}\right)\frac{\bar{\rho}_{vi}}{\rho_{vi}}\right.$$

$$-\frac{\Delta z}{\Delta t}\left(1 - \bar{\alpha}_i\right)\left(H_{sat} - \bar{H}_{\ell i}\right) - j_{\ell_{i-1}}\left(H_{\ell sat} - H_{\ell_{i-1}}\right)$$

$$\left.+\frac{\Delta z}{A} q \left(H_\ell - H_{sat}\right) + \frac{\Delta z H_{zd}}{\rho_\ell A}\right] \qquad (5.1)$$

i: top of control volume and i-1: bottom of control volume.

For subcooled boiling:

$$\Psi = \Psi_s + \Psi_b \qquad (5.2)$$

A special model has been developed for subcooled boiling conditions and will be discussed in detail in Chapter 3.1.2.

In order to understand the final form of Eq. (5.1), it is necessary to keep the following points in mind:

a) For reasons of simplicity it is assumed that the enthalpy level is taken as the enthalpy of the saturated liquid at the end of the time interval.

b) The density of the liquid is assumed to be a constant, and the other water properties are evaluated at saturation which leaves the system pressure as the only independent variable which is a known function of time. This assumption is thought to be a good approximation for BWR conditions of technical interest where the inlet subcooling is not too high. However, for the analysis of PWR test bundle cases this assumption may lead to erroneous results. There should be no difficulties involved by removing this assumption.

c) The vapor is always considered saturated and no liquid superheat is allowed. The first assumption eliminates the necessity of solving two energy equations. The second assumption could be easily removed by treating this situation in a similar manner as the subcooled boiling if there were enough informations available for flashing time constants.

An expression for the total mass conservation in terms of volumetric flux can be obtained as follows

$$j_i = j_{\ell i} + j_{vi} = j_{i-1} + \Delta z[(1-\gamma)\Psi + \frac{q}{A}] - \frac{\Delta z}{\Delta t}(1-\frac{\rho_v}{\rho_v})\alpha - \quad (5.3)$$

By utilizing the drift flux formulation for the void fraction corrected for diabatic conditions results in

$$\alpha = \frac{j_v/C_o}{j+\bar{V}_{gj}/C_o} + \frac{Z_e \Psi_s}{j+\bar{V}_{gj}/C_o} \tag{5.4}$$

and allows the formulation of the vapor continuity equation in terms of the previously obtained results

$$j_v = \frac{j + \frac{\bar{V}_{gj}}{C_o}}{j+\frac{\bar{V}_{gj}}{C_o} + \frac{1}{C_o}\frac{\Delta z}{\Delta t}} \left[j_{v_{i-1}} + z\left(\Psi + \frac{q_v}{A}\right) + \frac{\Delta z}{\Delta t}\frac{\bar{\rho_v}}{\rho_v}\bar{\alpha} - \frac{\Delta z}{\Delta t}\frac{Z_e \Psi_s}{j+\bar{V}_{gj}/C_o} \right] \tag{5.5}$$

Once j and j_v are known, the liquid flux can be calculated from

$$j_\ell = j - j_v \tag{5.6}$$

The enthalpy rise of the subcooled liquid, H_ℓ, is obtained from the equation which resulted from the combination of the energy equation and the vapor continuity equation as previously discussed.

$$H = \left[j + \frac{z}{t}(1-\alpha)\right]^{-1} \left[\frac{\Delta z}{\rho_\ell}\frac{q'' P_M}{A} + \frac{\partial P}{\partial t} + j_{\ell_{i-1}} H_{\ell_{i-1}} - \gamma H_v \Delta z \Psi \right.$$

$$\left. + \frac{H^*_\ell q_\ell \Delta z}{A} + \frac{\Delta z}{\Delta t}(1-\bar{\alpha})\bar{H}_\ell - \gamma \frac{\Delta z}{\Delta t}\frac{\bar{\rho_v}}{\rho_v}\alpha(H_v - \bar{H_v}) + \frac{H_{td}\Delta z}{\rho_\ell A} \right] \tag{5.7}$$

This concludes the treatment of the continuity and energy equations in the WOSUB code. What remains then is the numerical representation of the mixture momentum equation. Starting point for this is the following balance equation.

$$\Delta P = \Delta P_f + \Delta P_g + \Delta P_{acc} + \Delta P_{exch} + \Delta P_{local} \tag{5.8}$$

where the individual pressure drop contributions are presented numerically as follows:

<u>friction</u>:

$$\Delta P_f = \phi^2_{\ell_o} f \frac{\Delta z}{2D_H} \rho_\ell [j_e + \gamma j_v]^2 \tag{5.9}$$

<u>gravitation</u>:

$$\Delta P_g = g\rho_e \Delta z[1-\alpha(1-\gamma)] \tag{5.10}$$

<u>acceleration</u>:

$$\Delta P_{acc} = \rho_\ell [\frac{M_\ell j^2_\ell}{(1-\alpha)} + \frac{\gamma M_v j^2_v}{\alpha} - (\frac{M_\ell j_{\ell_{i-1}}}{(1-\alpha)} + \frac{\gamma M_v j^2_{v_{i-1}}}{\alpha})$$

$$+ \frac{\Delta z}{\Delta t} \rho_\ell (j_\ell + \gamma j_v - \bar{j} - \gamma \bar{j_v}) \tag{5.11}$$

<u>exchange</u>:

$$\Delta P_{exch} = - \frac{\rho_\ell}{A_i} \sum_j \pm \{q_{\ell_{ij}} (\frac{j_\ell}{1-\alpha})_k + \gamma q_{v_{ij}} (\frac{j_v}{\alpha})_k\}$$

$$+ \frac{\Delta z}{A_i} \sum_j R_e S_{ij} \Delta Y_{ij} \tag{5.12}$$

The plus sign (+) has to be taken for k=j if $g_{ij} > 0$.
The minus sign (-) has to be taken for k=i if $g_{ij} < 0$.

local:

Specific loss coefficients are supplied as input for local grid and blockage pressure drop calculations.

5.3 Solution Scheme

The major part of the solution method as shown in the flow charts presented in Figs. 5.1 through 5.5 is the subroutine SWEEP. The solution in WOSUB proceeds in the following steps:

(1) All total volumetric flows are initialized to zero, i.e.,

$$q_{\ell_i} = 0 \quad \text{for all i} \tag{5.13}$$

(2) All liquid and vapor volumetric cross flows are initialized to zero, i.e.,

$$q_{\ell_i} = 0 \quad \text{and} \quad q_{v_i} = 0 \quad \text{for all i} \tag{5.14}$$

(3) Calculation of the enthalpy of the liquid transferred to subchannel i from all other subchannels

$$\hat{H}^*_{\ell} = \frac{1}{q_{\ell_i}} \sum_j q_{\ell_{ij}} H_{\ell_{k(in)}} \quad \text{for all i} \tag{5.15}$$

(4) Calculation of the energy transfer due to liquid-liquid turbulent mixing in the subcooled region

$$H_{td} = \rho_\ell \sum_j \varepsilon_y (H_{\ell_{ij}} - H_{\ell_i}) \qquad \text{for all } i \qquad (5.16)$$

(5) Determination of the vapor generation rate, Ψ, by using Eq. (5.1).

(6) Evaluation of the total volumetric flux, j, from Eq. (5.3).

(7) Evaluation of the vapor volumetric flux, j_v, from Eq.(5.5).

(8) Calculation of the void fraction, α, from Eq. (5.4).

(9) Computation of the liquid volumetric flux by using the relationship

$$j_\ell = j - j_v$$

(10) Computation of the subcooled flow enthalpy rise H_ℓ as given by Eq. (5.7).

(11) Calculation of the pressure drop ΔP_i from Eq. (5.8).

(12) Iteration on q_i to obtain $\Delta P_i = \Delta P$. Note that this iterative procedure is discussed in full detail in the context of the recirculation loop concept in Section 5.4. The iteration uses the following steps:

$$\Delta P^{(n-1)} = \frac{1}{\sum_i A_i G_i} \sum_i A_i G_i \Delta P_i^{(n-1)} \tag{5.17}$$

$$\varepsilon_i^{(n-1)} = \Delta P_i^{(n-1)} - \Delta P^{(n-1)} \tag{5.18}$$

$$q_i^{1(n)} = q_i^{(n-1)} - \lambda_r \varepsilon_i^{(n-1)} \frac{q_i^{(n-1)} - q_i^{(n-2)}}{\varepsilon_i^{(n-1)} - \varepsilon_i^{(n-2)}} \tag{5.19}$$

where λ_r is an underrelaxation parameter adjustable by the uses.

In order to account for total flow continuity, the following renormalization is performed after each iteration.

$$Q = \sum_i q_i^{1(n)} \tag{5.20}$$

$$q_i^{(n)} = q_i^{1(n)} - \frac{Q A_i}{\sum A_i} \tag{5.21}$$

The first iterate is obtained by setting

$$q_i^{1(1)} = 0.5 \frac{i^{(0)} j_i A_i}{P_i^{(0)}} \tag{5.22}$$

(13) By virtue of

$$q_{ij} = M^{-1} q_i \tag{5.23}$$

the total flow into each subchannel is split into net cross flows among pairs of neighboring subchannels. This is discussed in detail in Section 5.4. It should be recalled that M reflects the geometric layout of the subchannels and of the recirculation paths among them.

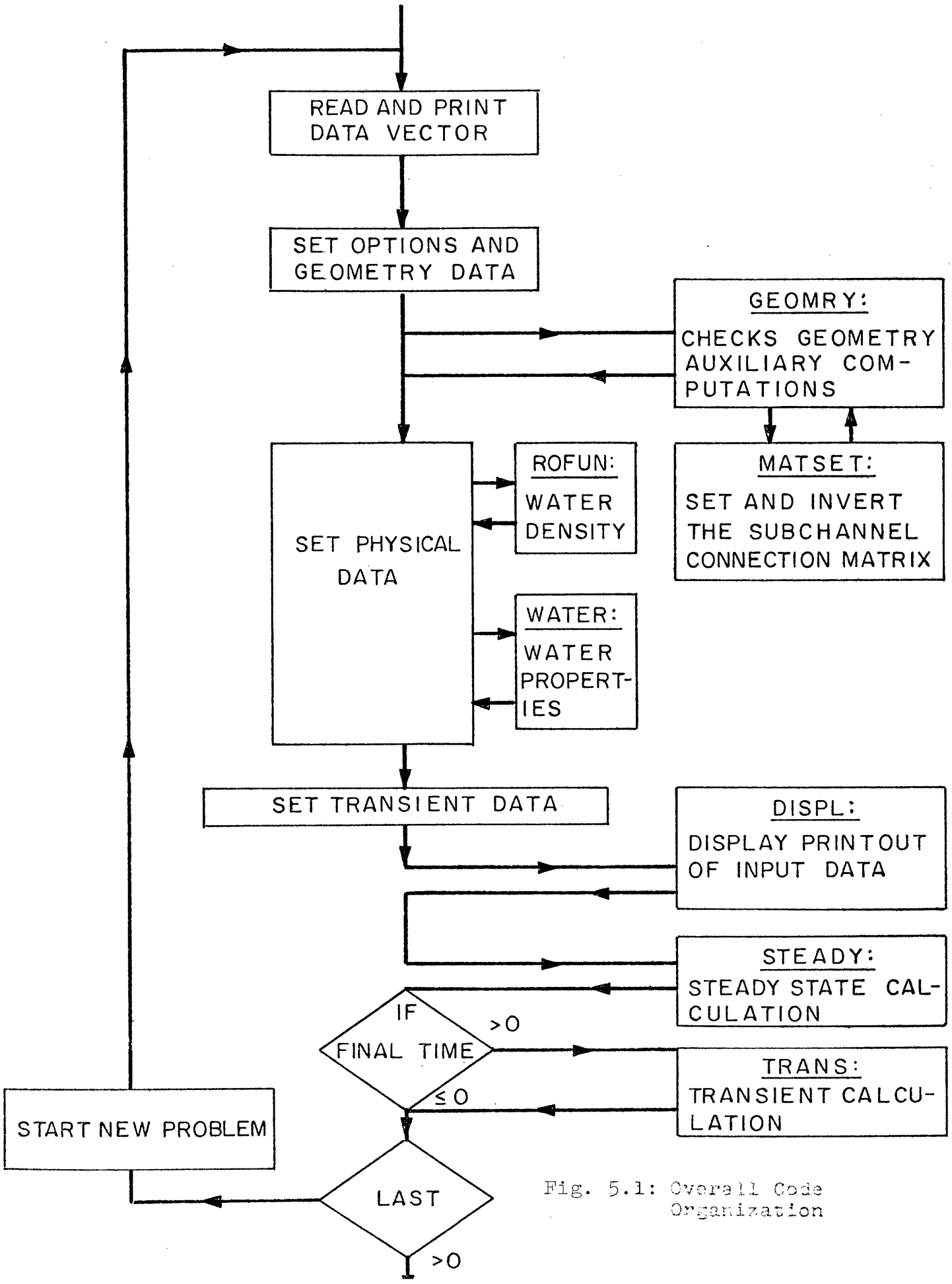

Fig. 5.1: Overall Code Organization

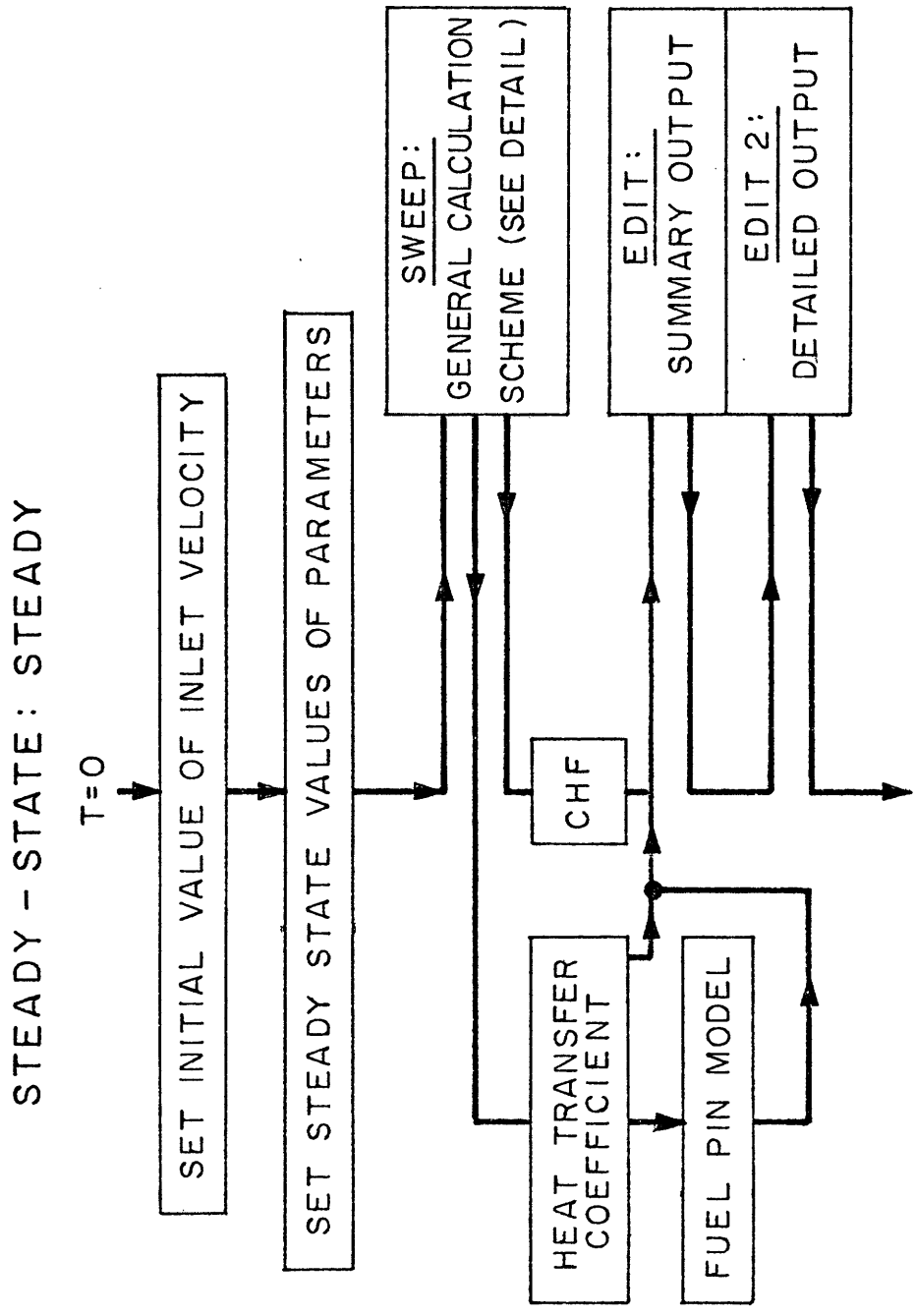

Fig. 5.2: Subroutine STEADY

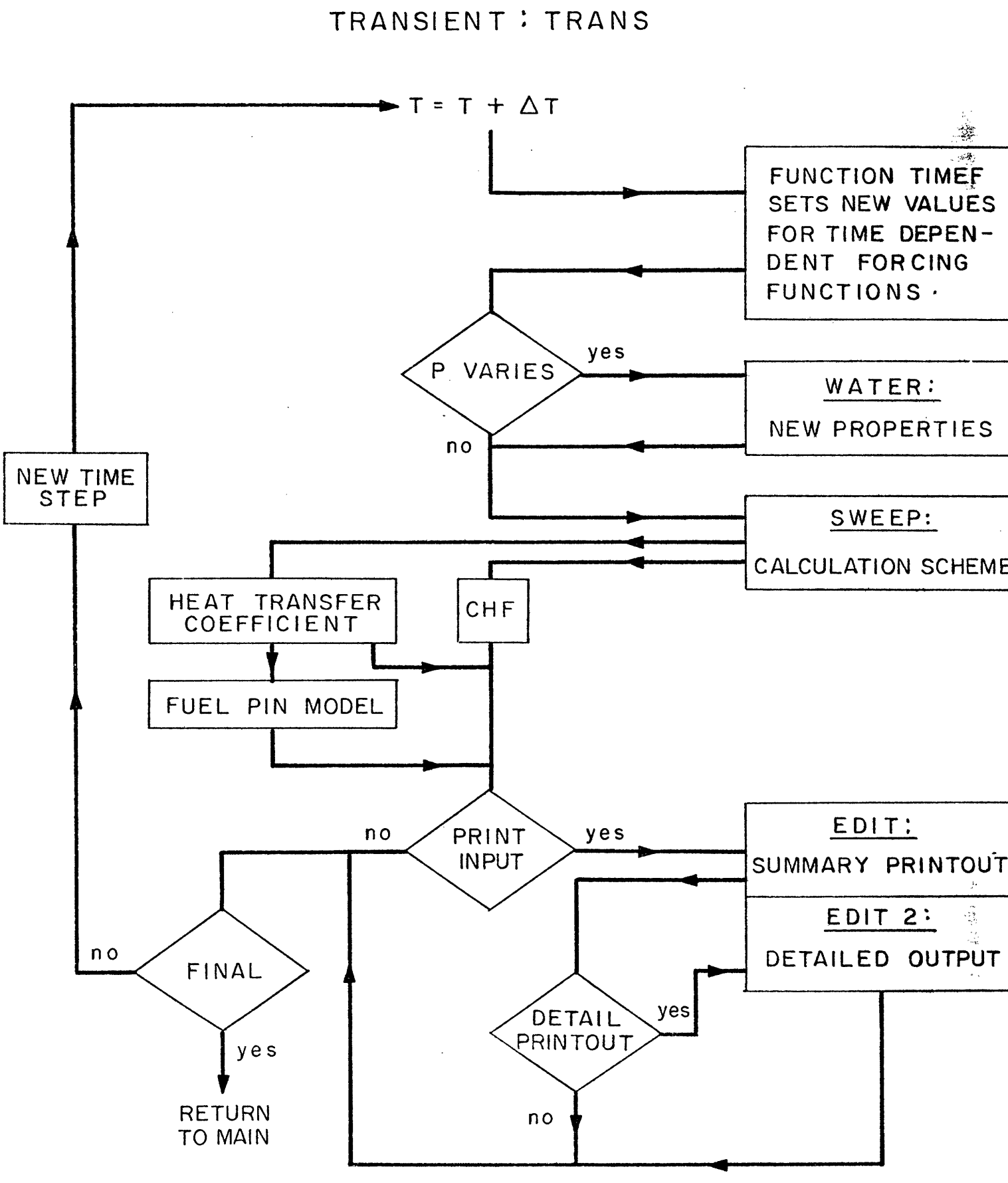

Fig. 5.3: Subroutine TRANS

CALCULATION SCHEME
SUBROUTINE SWEEP

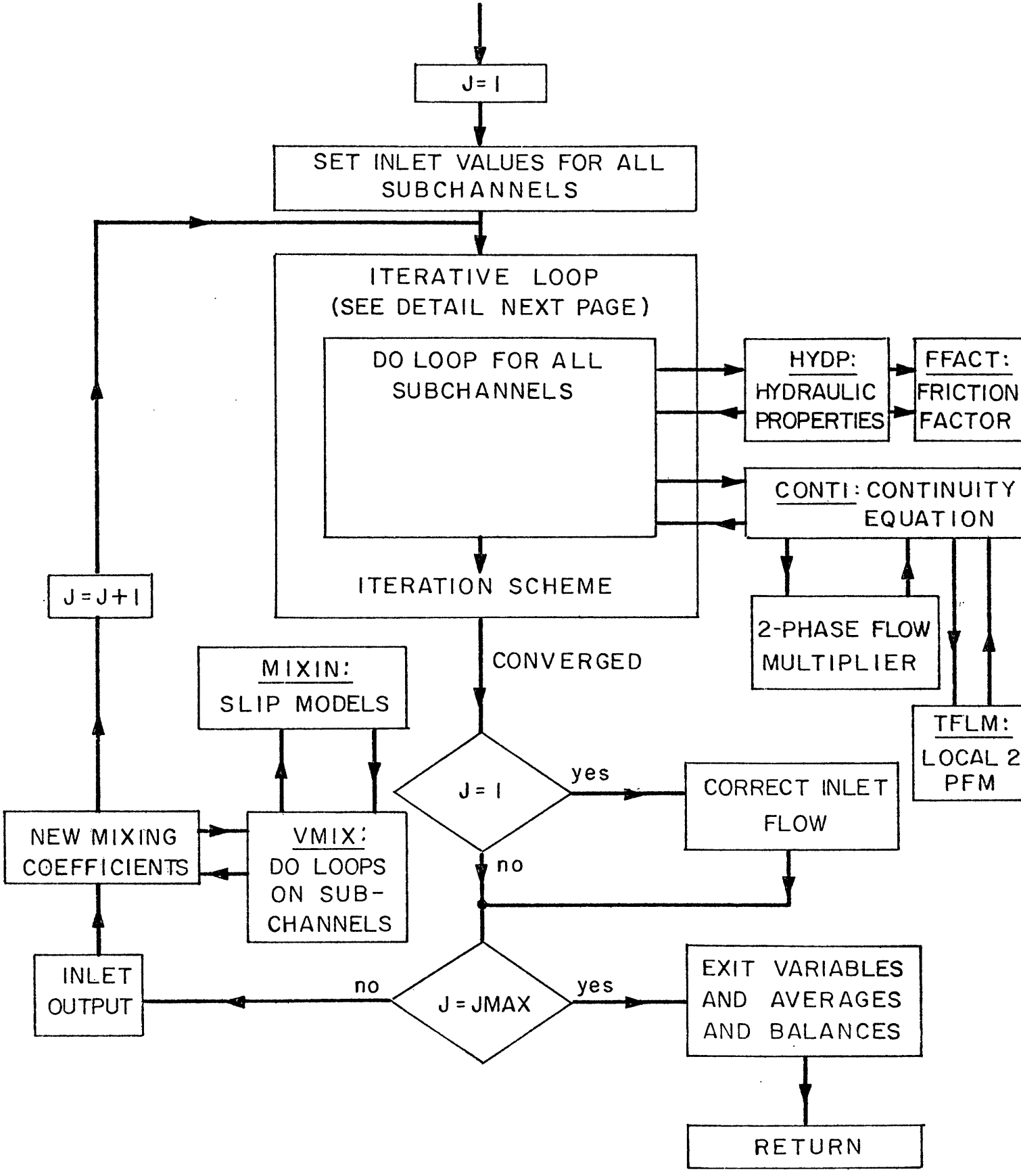

Fig. 5.4: Subroutine SWEEP

ITERATIVE LOOP

DETAIL OF SUBROUTINE SWEEP

ITMAX = 10

REL - RELI (1.) first value of relaxation parameter

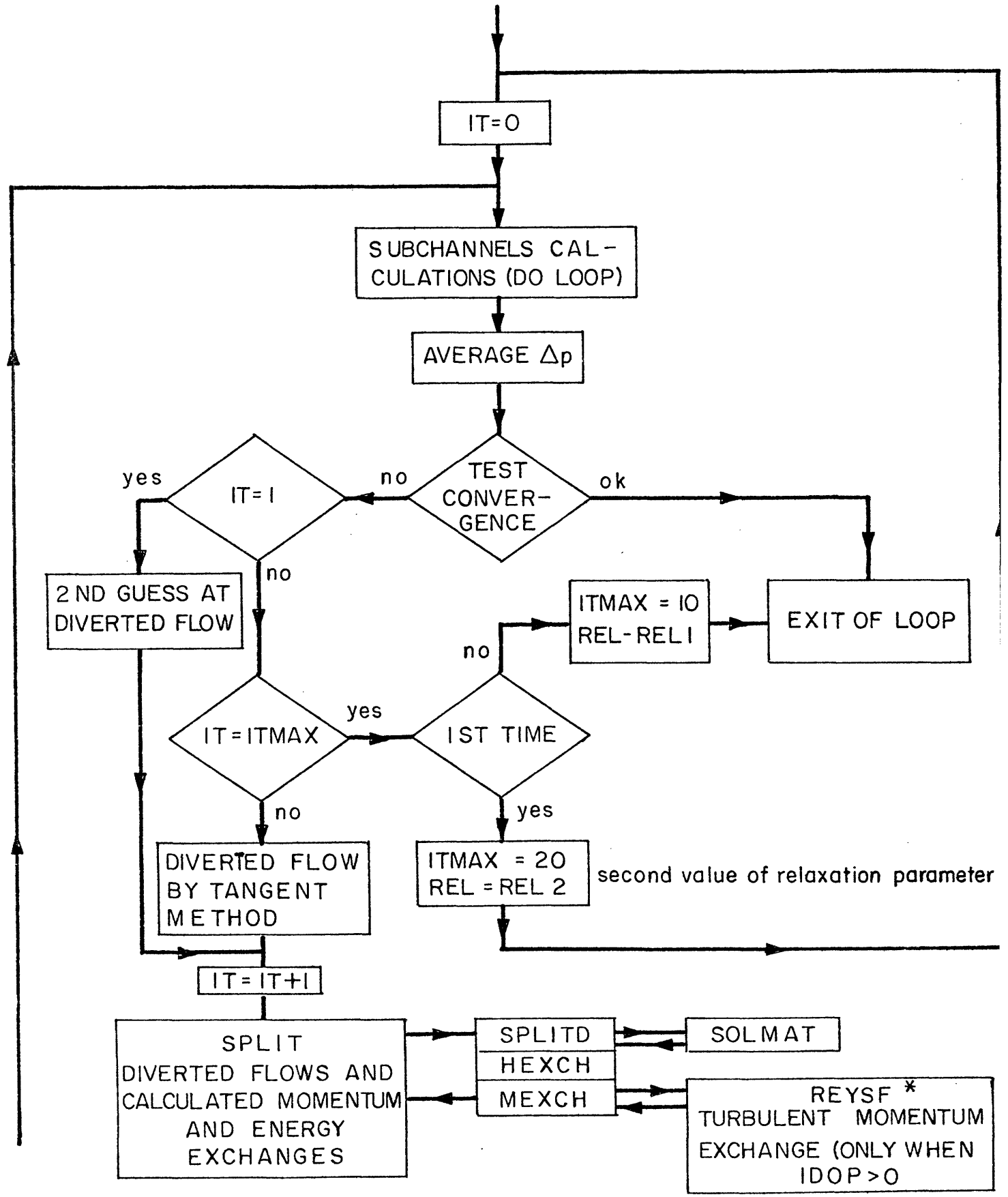

Fig. 5.5: Iterative Solution Procedure in SWEEP

(14) Split of q_i into q_{v_i} and q_{ℓ_i}

(15) Jump to Step 3 for a new iteration.

Figs. 5.1 through 5.5 display the flow charts for the calculations described above.

5.4 The Concept of the Recirculation Loop

As mentioned before, the fully ventilated assumption across the fuel rod bundle implies that the transverse momentum equation is disregarded. In order to completely define the problem by having the same amount of equations as unknowns, the assumption is introduced that the net volumetric flow recirculation around closed loops connecting communicating subchannels is zero. This is not a unique invention by Forti for the MATTEO code but rather a concept which was introduced by Bowring already for the HAMBO code and recently employed again by Whalley for his dryout predictions in a rod-centered subchannel model.

A closed recirculation path or connecting communicating subchannel is defined as being a loop surrounding a rod. The whole entity of those loops can be conveniently displayed as a graph. This concept resembles the swirl flow (secondary vortex) around obstacles where the Gaussian theorem states

$$\oint_S \omega ds = 0$$

with ω being vorticity and s any closed surface.

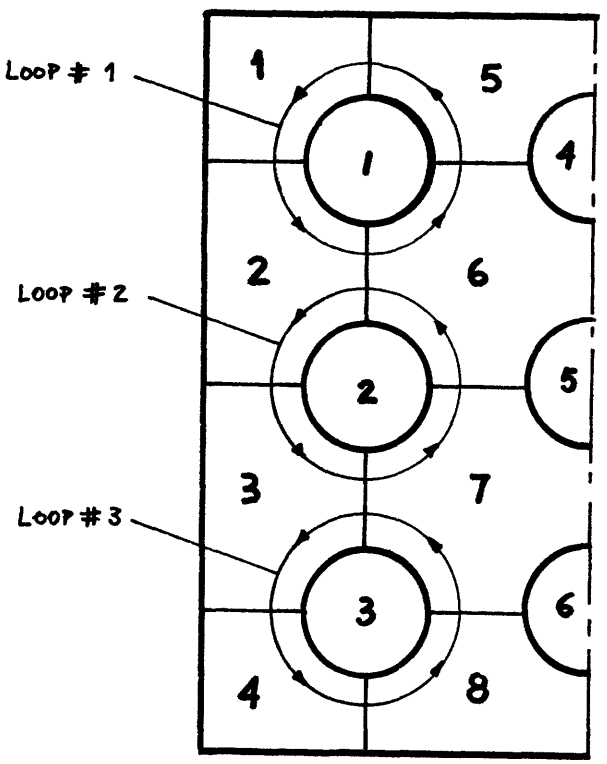

Fig. 5.6: Recirculation loops for 8-subchannel case.

Each rod is essentially surrounded by four net volumetric flows. The method employed in WOSUB consists of setting up the algebraic sum of each set of four net volumetric flows around each rod and requires no net circulation around the loop. Fig. 5.6 shows the recirculation loops for an 8-subchannel case. In general, there are as many recirculation loops in a bundle as there are rods. However, in cases where symmetry applies, there exist rods which cannot be surrounded by complete loops. This is the case for rods #4, 5, 6 in Fig. 5.6. Details about the correct treatment and input for these layouts are fully discussed in the User's Manual, Volume II, of this report series.

In order to more easily comprehend the importance of the recirculation loop concept, a review of the numerical solution scheme as flowcharted in Fig. 5.7 seems to be in order. Once the total volumetric crossflow, q_i, is given, the pressure drop can be predicted for each subchannel. As explained before, a convergence test

$$|\Delta P_i - \overline{\Delta P}| \leq 10^{-3}$$

is applied for the iterative pressure drop calculation.

Suppose that the number of known total volumetric crossflows is N and the number of recirculation loops is k, then the number of boundaries and thus the number of net volumetric flows across adjacent boundaries is (N + k - 1). This is in accordance with Bowring's finding.

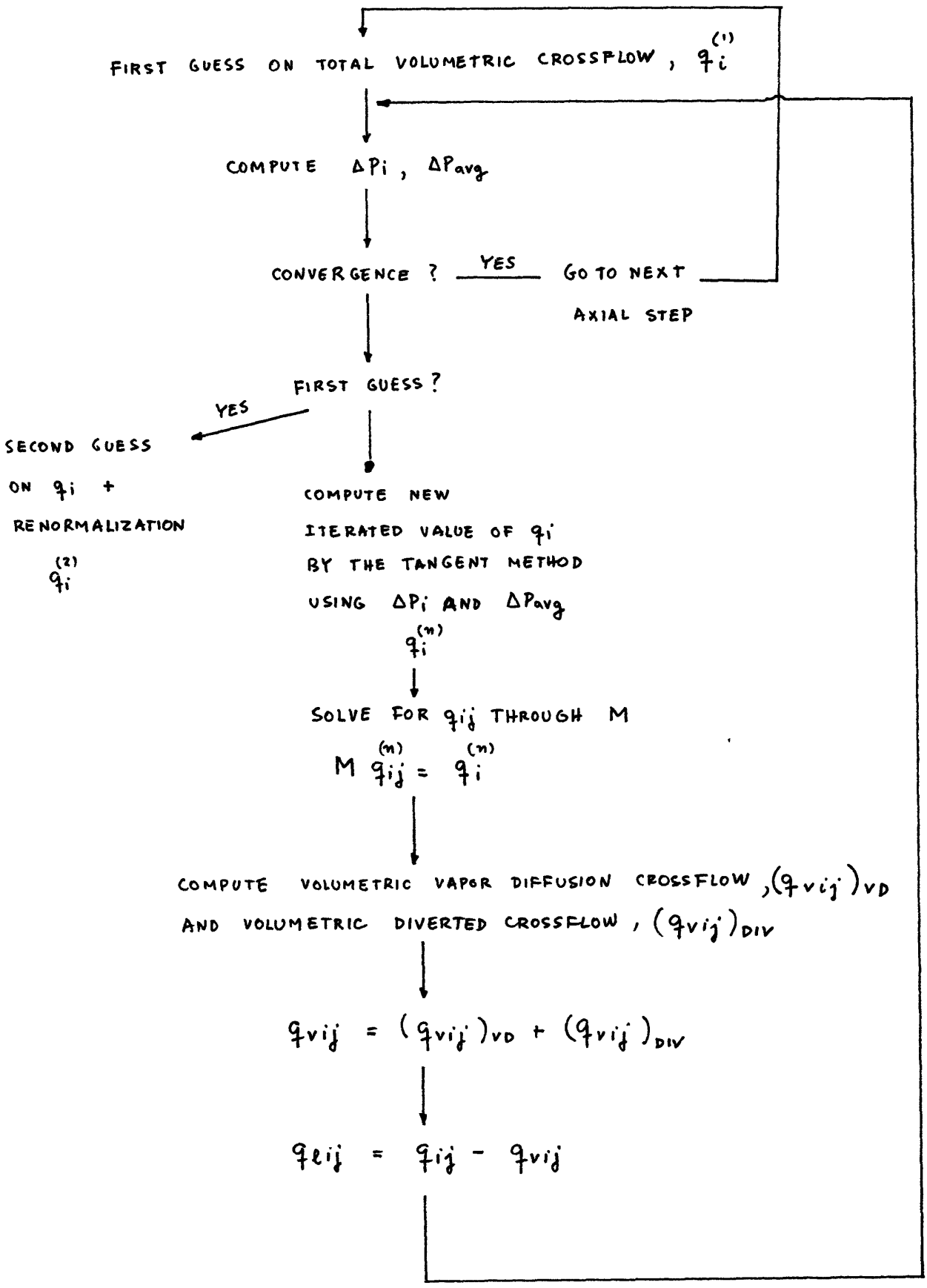

Fig. 5.7: Calculational scheme for the crossflows.

There are then (N + k) dependent relations for (N + k - 1) unknown variables, the q_{ij}'s, as follows:

(1) N relations due to

$$q_i^{(n)} = \sum_j q_{ij} \qquad \text{for } i = 1,2,\ldots,N$$

(2) k recirculation loops imply the following relations

$$|q_{i,m}|_\ell + |q_{m,n}|_\ell + |q_{m,j}|_\ell + |q_{j,i}|_\ell = 0 \qquad \text{for } \ell = 1,2,\ldots,k$$

As a result, one relation is dependent on the others and is merely an expression of overall activity.

The solution method consists then of a simultaneous solution for all the volumetric crossflows in the bundle at a given axial elevation. The advantage of the recirculation loop technique as compared to the crossflow solution method in COBRA-IIIC is that all the volumetric crossflows are accounted for instead of disregarding the crossflows at "secondary" boundaries by assuming they do not affect the calculated crossflows.

In order to more easily comprehend the concept of recirculation loops, the case shown in Fig. 5.6 with 8 subchannels will be set up in full detail.

By recognizing the following definitions:

q_i: volumetric flow rate to subchannel i

q_{ij}: volumetric flow rate to subchannel i from subchannel j

$q_{ij} = -q_{ji}$ for symmetry reasons

the following relations can be established for the sample case

$$q_1 = q_{12} + q_{15}$$

$$q_2 = -q_{12} + q_{23} + q_{26}$$

$$q_3 = -q_{23} + q_{34} + q_{37}$$

$$q_4 + -q_{34} + q_{48}$$

$$q_5 = -q_{15} + q_{56}$$

$$q_6 = -q_{26} + q_{67} - q_{56}$$

$$q_7 = -q_{37} - q_{67} + q_{78}$$

The requirement of overall continuity results in the following relationship:

$$q_1 + q_2 + q_3 + q_4 + q_5 + q_6 + q_7 + q_8 = 0$$

which leads to

$$q_8 = -(q_1 + \ldots\ldots + q_7)$$

By adding the first seven equations as indicated by the expression in the brackets on the RHS, the following is obtained

$$(q_1 + \ldots\ldots + q_7) = q_{48} + q_{78}$$

or

$$q_8 = -q_{48} - q_{78}$$

Therefore, the equation for q_8 is indeed the result of a linear combination of the equations for q_1, q_2,...,q_7 as stated above.

The reader is referred to Volume II of this research report for a more detailed discussion about the type and sizes of matrices involved in the solution procedure of WOSUB.

5.5 Determination of Volumetric Crossflows

Once the net volumetric crossflows, q_{ij}, are known, its vapor part can be deduced. As explained before, there are two contributions, namely,

1) Vapor volumetric flow resulting from the vapor diffusion process, q''_{ij} , and,

2) Vapor volumetric flow resulting from diversion, q'_{ij}.

Therefore, one obtains

$$q_{vap,\ ij} = q''_{ij} + q'_{ij}$$

and consequently for the liquid volumetric flow one gets

$$q_{liq,ij} = q_{ij} - q_{vap,\ ij}$$

It should be noticed that all these flows are derived from a of $q_i^{(n)}$, and thus all of the aforementioned terms are themselves iterate values, i.e.,

$$q_{ij}^{(n)},\ q_{liq,ij}^{(n)},\ q_{vap,ij}^{(n)},\ q_{i,j}^{(n)},\ q_{ij}^{(n)}$$

The pressure drops ΔP_i and $\overline{\Delta P}$ are predicted, then, from $q_i^{(n)}$ and the convergence test is performed. $q_i^{(n)}$ is continuously iterated and so are all of the other liquid and vapor volumetric flows until convergence has been achieved (compare Fig. 5.7). During each iteration, the total volumetric flow iterate, $q_i^{(n)}$, is renormalized as indicated in Section 5.4.

6. Fuel Pin Model

6.1. Introduction

The subroutine which determines the transient temperature fields in fuel and clad employs the collocation method (see Finlayson [6-1]) for the solution of the one-dimensional parabolic partial differential equations using Hermite splines as approximating functions together with Gaussian quadrature points as collocation points. This procedure reduces the partial differential equations to a system of ordinary differential equations. This is further reduced to a set of linear equations by applying a first order finite-difference operator to the temporal derivative. Thus, the basic advantage of using multistep methods in the time variable has been given up for the sake of simplicity for the time being because it was felt that simultaneous changes in the clad-coolant heat transfer coefficient with time might pose some problems in the context of the ordinary differential equation system solver. In any case, the method employed in WOSUB maintains the desirable characteristic of an analytical method because it generates point values as compared to nodal values resulting from finite-difference schemes. This is definitely an advantage compared to fuel pin models used in all the other subchannel codes with the only exception being COBRA-IV which uses the method of weighted residuals in the fuel system.

6.2. Short Review of State-of-the-Art of Fuel Pin Modeling

In the last two decades many numerical methods have

been investigated for solving the linear and nonlinear partial differential equations of transient heat conduction in solids and multi-layered solids. These methods can be roughly categorized into the following groups:

1) Finite Difference Methods
2) Finite Element Methods
3) Methods of Weighted Residuals (MWR)
4) Collocation Methods
5) Various Approximations

The interested reader should consult the book by Finlayson [6-1] for a full account of the advantages and disadvantages of the various methods.

The most commonly employed methods for calculating the fuel pin temperatures in subchannel codes are the finite-difference and the approximate methods. For instance, COBRA-IIIC and COBRA-IIIC/MIT use an implicit finite-difference scheme for the fuel region whereas the MEKIN-code employs an approximate method. The disadvantage of the latter is that it has to be checked against more accurate methods before it is applied to new situations [6-2]. On the other hand, experience with COBRA-IIIC has shown that its fuel pin model lacks computational efficiency. In addition it should be recalled that the fuel-clad gap together with the clad is handled as one lumped node. Furthermore, it should be realized that the respective subroutine is called at each axial elevation at each time step for each axial iteration and rod. Therefore, this process can easily amount to several thousand solutions of the

fuel pin temperature field for one single computer run. As a result, any method which a priori allows larger space step and time step sizes without sacrificing accuracy must be considered superior.

Finite-difference methods are of low order and thus require usually the solution of large systems of equations in order to achieve a satisfactory truncation error. This necessitates large storage requirements. On the other hand finite-element methods based on either the use of Galevkin or weighted residual method achieve high-order accuracy and thus make it possible to reduce the size of the set of equations to be solved. This in turn allows the use of multistep time-differencing procedures. However, the method requires the evaluation of integrals at each time step which means considerably more arithmetic when compared to low-order finite difference techniques. Therefore, the high-order Galevkin procedures although more accurate may not be more effective than finite-difference methods.

The collocation method combined with the use of suitable approximating subspaces has been extensively explored by Villadsen and Stewart [6-3] and Villadsen and Sorenson [6 -4]. These authors employed orthogonal polynomials such as Radau and Legendre to locate the collocation points and showed that the use of Gaussian quadrature points can provide the same accuracy as the Galvekin procedure (see also Finlayson, [6-1], Shalev *et al*. [6-5] and DeBoor and Swartz [6-6]). Chawla *et al*. [6-7] showed that by choosing Hermite piecewise-cubic polynomials as subspaces together with Gaussian quadrature

points as collocation points yields an accuracy of $O(h^4)$ as compared to $O(h^2)$ resulting from finite-difference methods where h denotes the spatial step size.

This fuel heat transfer model in COBRA-IV [6 -8] calculates the internal temperature distribution within a solid material and can include the effects of axial conduction and temperature-dependent fuel thermal conductivity. The solution as proposed by Cena et al. [6 -9] is basically a combination of the Method of Weighted Residuals (MWR) in the radial coordinate and finite-differences in time and the axial coordinate. In MWR, orthogonal collocation as described by Finlayson [6 -1] is employed to determine the form of an approximate polynomial solution. This method affords a higher order of accuracy by using the roots of orthogonal polynomials as the nodal positions. MWR actually maintains the accuracy and computing time of conventional finite-difference schemes as was shown by Cena et al. [6-9] while computer storage is reduced by a factor of two. The formulation of the solution method as given in [6-8] and [6-10] uses also the Kirchhoff transformation to account for temperature-dependent thermal conductivity.

The axial conduction term is calculated by a central finite-difference and the time derivative is approximated by a forward finite-difference scheme.

Despite all of these improvements the fuel pin model as used in COBRA-IV still maintains the technique of lumped resistances for actually calculating an average clad temperature.

The complete matrix equation is solved by virtue of the iterative Gauss-Seidel procedure. The resulting temperature solution supplies the surface heat flux for the fluid energy equation, i.e., the heat flux at the outside clad surface is actually determined by the average clad temperature.

In contrast to what is done in COBRA-IV, WOSUB uses the point value of the temperature at the outside clad. The method used in subroutine is that developed by Chawla *et al.* [6-7] as adopted by Yeung [6-12] for temperature-independent thermal conductivities in fuel and clad.

6.3. Analysis

6.3.1. Differential Equations, Boundary and Initial Conditions

For the present application a typical BWR fuel pin with UO_2 fuel pellets and Zry-cladding is considered as shown in Figure 6.1. The energy transfer across the fuel-cladding gap is simulated by an effective heat transfer coefficient although the gap width is actually modeled. A uniform heat source density is assumed in the fuel region whereas gap and clad regions are considered source free. All physical properties are assumed to be temperature independent and isotropic.

The following assumptions are made:

1) Axial and circumferential heat conduction effects are neglected.

2) All physical properties are considered isotropic and temperature independent.

3) The heat source density in the fuel region is considered to be constant across the cross-section but variable in time.

4) Gap and clad regions are assumed to be heat source free.

5) Although the fuel-clad gap rise is actually modeled the energy transport in the gap region is simulated by using the concept of the effective heat transfer coefficient.

6) The outside surface of the clad is convectively cooled by either single or two-phase fluid for which the heat transfer coefficient is determined from

appropriate correlations.

By virtue of assumptions 1 through 3, the one-dimensional heat conduction equation can be written in cylindical coordinates for the fuel region as

$$\frac{1}{r}\ \frac{\partial}{\partial r}\left(r\frac{\partial T}{\partial r}\right) + \frac{q'''}{k} = \frac{1}{\alpha}\ \frac{\partial T}{\partial t}\quad , \tag{6.1}$$

and with assumption 4 for the clad region as

$$\frac{1}{r}\ \frac{\partial}{\partial r}\left(r\ \frac{\partial T}{\partial r}\right) \ = \ \frac{1}{\alpha}\ \frac{\partial T}{\partial t}$$

The boundary conditions which must be satisfied are

1. $$\left.\frac{\partial T}{\partial r}\right|_{r=0} = 0\quad , \tag{6.2}$$

2. $$-k_f\frac{\partial T}{\partial r}\Big|_{r=r_M} = q''_{gap} = h_{gap}\,[T(r_M) - T(r_{M+1})\,], \tag{6.3}$$

3. $$-k_c\frac{\partial T}{\partial r}\Big|_{r=r_{M+1}} = q''_{gap} = h_{gap}\,[T(r_M) - T(r_{M+1})\,], \text{ and} \tag{6.4}$$

4. $$T(r=r_N) - T_B = \frac{q''_s}{h_{film}} = \frac{k_c}{h_{film}}\ \frac{\partial T}{\partial r}\Big|_{r=r_N} \tag{6.5}$$

As initial condition it is assumed that the transients start from a steady-state temperature distribution as a result of an initial heat source density, i.e.

$$q'''(t = 0) = q_o'''$$

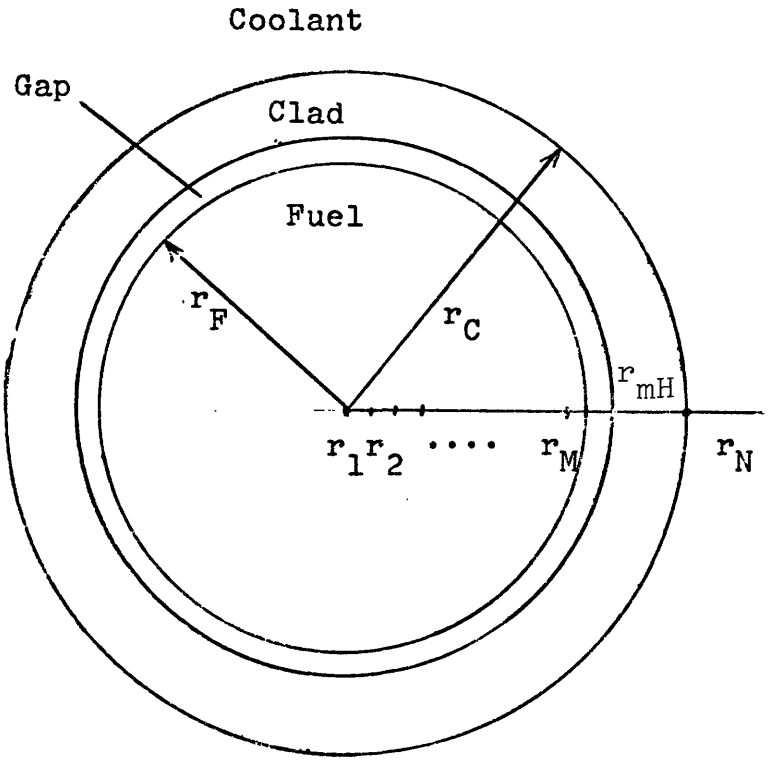

Fig. 6 .1 Cross-Sectional View of The Fuel Pin Model

6.3.2. Approximation for the Temperature Field

An approximate solution for Eq.(6.1) is sought by using the collocation method with Hermite piecewise cubic polynomials for the space variable r. For this purpose the fuel and clad are subdivided by the following set of points:

$$a = r_1 \quad r_2 \quad \cdots \quad r_j \quad r_{j+1} \quad \cdots \quad r_N = r_c$$

with h_j being defined as

$$h_j = r_j - r_{j-1}$$

Relative to this partition the approximating space will consist of all functions f(x) such that:

1) f(x) is equal to a cubic polynomial in each subinterval.

2) f(x) and f'(x) are continuous in each subinterval.

3) f(x) satisfies the appropriate boundary conditions.

A convenient basis for generating the appropriate set of functions is given by the Hermite cubic polynomials. For the j^{th} interval these are

$$V_j(x) = \begin{cases} 1-3x^2 + 2x^3 & 0 \le x \le 1 \\ 1-3x^2 - 2x^3 & -1 \le x \le 0 \\ 0 & |x| > 1 \end{cases} \qquad (6.6)$$

$$S_j(x) = \begin{cases} x(1-x)^2 & 0 \le x \le 1 \\ x(1+x)^2 & -1 \le x \le 0 \\ 0 & |x| > 1 \end{cases} , \qquad (6.7)$$

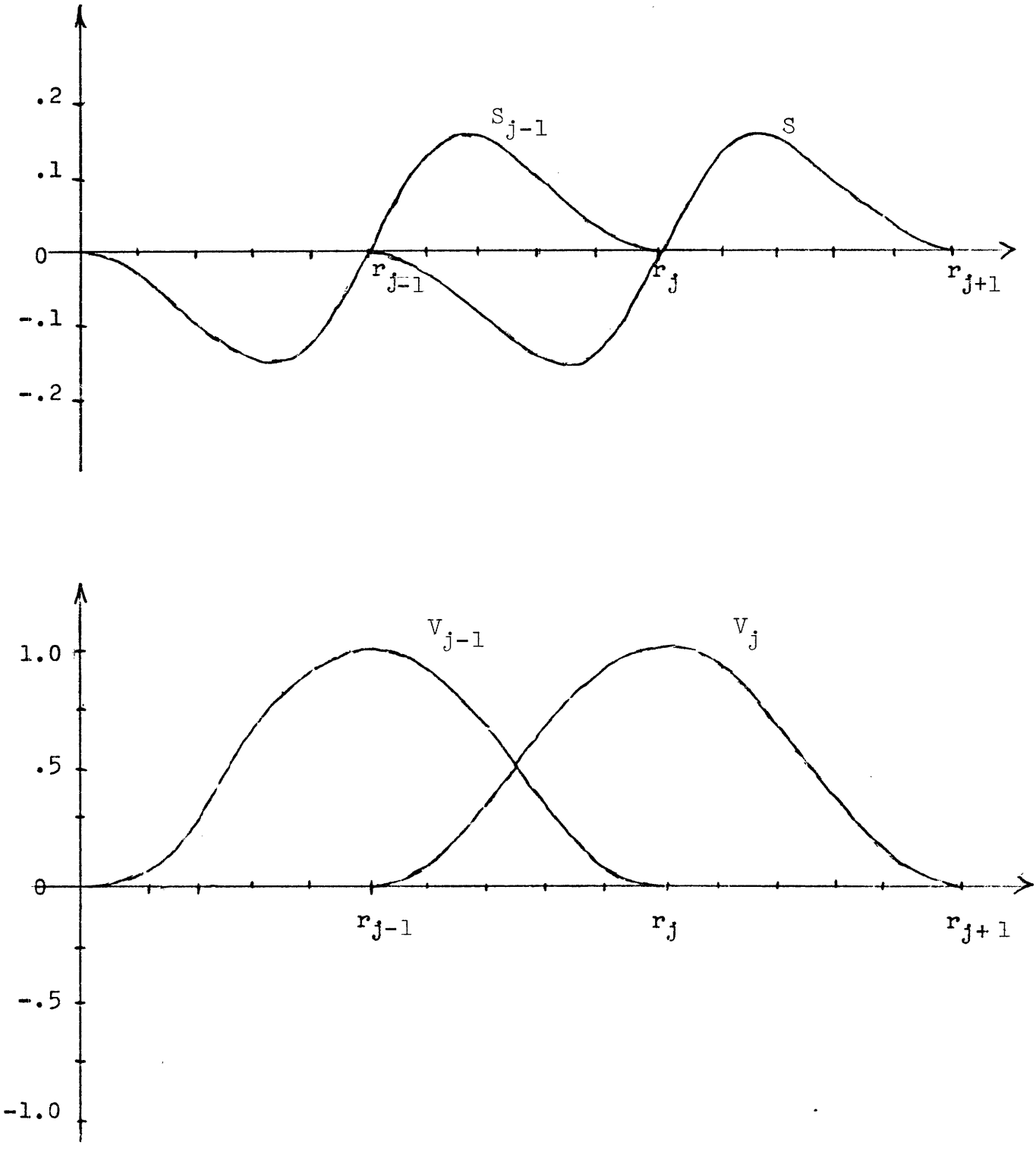

Fig.6.2 Graphs of Hermite Cubic Polynomials

where the variable x is the normalized distance from the j^{th} node and defined as follows

$$x = \frac{r - r_j}{h_j}$$

The four functions $V_{j-1}(x)$, $V_j(x)$, $S_{j-1}(x)$ and $S_j(x)$ are depicted in Figure 6.2. It is assumed that $V_1(x)$ as well as $V_1(x)$ vanish to the left of r_1 whereas $V_{N+1}(x)$ and $S_{n+1}(x)$ vanish to the right of r_{N+1}. The above mentioned functions possess the following properties:

1) Both $V_j(x)$ and $S_j(x)$ are continuous together with their first derivatives in the interval $[a, r_c]$.

2) Each $V_j(x)$ and $S_j(x)$ is a cubic polynomial in each subinterval, and they vanish outside the subinterval $[x_{j-1}, x_{j+2}]$. (6.8)

3) $$\left.\begin{array}{ll} V_i(x_j) = \delta_{ij} & V_i'(x_j) = 0 \\ S_i(x_j) = 0 & S_i'(x_j) = \delta_{ij} \end{array}\right\} \quad 1 \leq i,j \leq N$$

As required before, the set $\left(V_i(x), S_i(x)\right)_{i=1}^{N}$ forms a basis for the functions f(x) such that the temperature field can be put into the following form

$$T(x,t) = \sum_{j=1}^{N} C_1(x_j,t)\, V_j(x) + C_2(x_j,t)\, S_j(x) \quad , \qquad (6.9)$$

with $N = N_F + N_c + 2$ and $\left(C_1(x_j, t), C_2(x_j, t)\right)_{j=1}^{N}$ being the unknown coefficients which have to be determined. These

coefficients represent the unknown temperature and its spatial derivative at each of the knot points, respectively. Since there are N_F subintervals in the fuel and N_c subintervals in the clad region, the total number of unknowns is given by $2(N_F + N_c) + 4$.

In order to obtain a system of $2(N_F + N_c) + 4$ equations for the determination of the unknowns, Eq. (6.9) is required to satisfy Eq. (6.1) at $2N_F$ points in the fuel and Eq. (6.1a) at $2N_c$ points in the clad region along with the four boundary conditions. Following Douglas and Dupont [6-13]and deBoor and Schwartz [6-6], the Gauss-Legendre quadrature points of order two are selected as collocation points in each subinterval. These are given by

$$\xi_{i,k} = \frac{1}{2}(r_i + r_{i+1}) + (-1)^k \frac{h_i}{2\sqrt{3}} \qquad (6.10)$$

where $h_i = r_{i+1} - r_i$, $1 \leq i \leq N$, $K = 1,2$

Shalev, Baruch and Nissim [6-5] demonstrated that the use of the collocation points as given by Eq. (6.10) yields a residual error for the differential equation which satisfies the principle of least squares. Therefore, the accuracy from this collocation method is comparable with that resulting from a least square method. Furthermore, Douglas and Dupont [6-13] have shown that for parabolic equations an accuracy up to $0(h^4)$ can be achieved provided that the thermal conductivity and capacity have bounded third-order derivatives and T(r,t) has bounded sixth-order spatial derivatives over a fixed time interval.

6.3.3. Calculational Procedure

The transient heat conduction equation, Eq. (6.1) can be put into the simplest finite-difference form as

$$\frac{1}{r}\frac{\partial}{\partial r}\left(r\frac{\partial T^{j}}{\partial r}\right) + \frac{q'''^{j}}{k} = \frac{1}{\alpha}\left(\frac{T^{j} - T^{j-1}}{\Delta t}\right) \qquad (6.11)$$

where the superscript j designates the temperature at the j^{th} time step. The initial temperature distribution is obtained by performing the steady-state solution of Eq. (6.11) together with the four boundary conditions and the initial condition.

The solution to the transient heat conduction equation in polar coordinates is assumed to be

$$T(r,t) = \sum_{i=1}^{N} [C_1(r_i,t)\, V_i(x) + C_2(r_i,t)\, S_i(x)] \qquad (6.12)$$

where N = total number of nodes.

Substituting this equation into Eq. (6.11) one obtains

$$\sum_{i=1}^{N}\left\{\frac{1}{h_i} C_1^j(r_i,t)\left[\frac{V_i'(x)}{r} + \frac{1}{h_i} V_i''(x)\right] + \frac{1}{h_i} C_2^j(r_i,t)\left[\frac{S_i'(x)}{r} + \frac{1}{h_i} S_i''(x)\right]\right\}$$

$$+ \frac{q'''}{k} = \frac{1}{\alpha\Delta t}\left\{\sum_{i=1}^{N}\left[C_1^j(r_i,t)\, V_i(x) + C_2^j(r_i,t)\, S_i(x)\right] - \right.$$

$$\left.\sum_{i=1}^{N}\left[C_1^{j-1}(r_i,t)\, V_i(x) + C_2^{j-1}(r_i,t)\, S_i(x)\right]\right\}, \qquad (6.13)$$

This equation can be put into the more convenient form

$$\sum_{i=1}^{N} C_1^j(r_i,t)\,\{V_i(x) - \frac{\alpha\Delta t}{h_i}\,[\,\frac{V_i'(x)}{r} + \frac{1}{h_i}\,V''(x)\,]\} +$$

$$C_2^j(r_i,t)\{S_i(x) - \frac{\alpha\Delta t}{h_i}\,[\frac{S_i'(x)}{r} + \frac{1}{h_i}\,S_i''(x)\,]\} =$$

$$\frac{q'''}{k}\,\alpha\Delta t + \sum_{i=1}^{N}[C_1^{j-1}(r_i,t)V_i(x) + C_2^{j-1}(r_i,t)S_i(x)]. \quad (6.14)$$

This equation is applied to both the fuel and the clad regions by requiring that it be satisfied at $2N_F$ points in the fuel and at $2N_c$ points in the clad. Thus a total of $2N_F + 2N_c$ equations are obtained in the first place. The remaining four equations come from using the boundary conditions, Eqs. (6.2 - 6.5).

Eq. (6.2), namely

$$\left.\frac{\partial T}{\partial r}\right|_{r=0} = 0 \quad (6.2)$$

denotes that due to symmetry the temperature gradient at the fuel pin centerline must be zero. By substituting Eq. (6.12) into this equation it follows that

$$\sum_{i=1}^{N} \frac{1}{h_i}\,\{C_1(r_i,t)\,V_i'(x) + C_2(r_i,t)\,S_1'(x)\}_{r=0} = 0 \quad (6.15)$$

The second boundary condition

$$-k_f \left.\frac{\partial T}{\partial r}\right|_{r=r_M} = h_{gap}\,[T(r_M) - T(r_{M+1})\,]\,. \quad (6.3)$$

relates the temperature gradient at the fuel surface to the temperature difference across the gap. This necessitates the knowledge of the effective gap heat transfer coefficient. Again, by substituting Eq. (6.12) into the above equation the following form is obtained

$$-k_f \sum_{i=1}^{N} \frac{1}{h_i} \left[C_1(r_i,t)\, V_i'(x) + C_2(r_i,t)\, S_i'(x)\right]_{r=r_M} =$$

$$h_{gap} \left\{ \sum_{i=1}^{N} \left[C_1(r_i,t)\, V_i(x) + C_2(r_i,t)\, S_i(x)\right]_{r=r_M} \right.$$

$$\left. - \sum_{i=1}^{N} \left[C_1(r_i,t)\, V_i(x) + C_2(r_i,t)\, S_i(x)\right]_{r=r_{M+1}} \right\} . \qquad (6.16)$$

This can be rearranged as

$$\sum_{i=1}^{N} \left\{ C_1(r_i,t) \left[\frac{1}{h_i h_{gap}} k_f\, V_i'(x) + V_i(x) \right]_{r=r_M} + \right.$$

$$\left. C_2(r_i,t) \left[\frac{1}{h_i h_{gap}} k_f S_i'(x) + S_i(x) \right]_{r=r_M} \right\} =$$

$$= \sum_{i=1}^{N} \left[C_1(r_i,t)\, V_i(x) + C_2(r_i,t)\, S_i(x)\right]_{r=r_{M+1}} . \qquad (6.17)$$

The third boundary condition relates the temperature gradient at the inside clad surface to the temperature difference across the gap, i.e.

$$-k_c \left.\frac{\partial T}{\partial r}\right|_{r=r_{M+1}} = h_{gap} \left[T(r_M) - T(r_{M+1})\right] . \qquad (6.4)$$

Actually, the last equation together with the second boundary continuity of heat fluxes at the fuel-clad interface. As before, Eq. (6.12) is substituted into Eq. (6.4) in order to obtain after rearrangement

$$\sum_{i=1}^{N} \{C_1(r_i,t)\left[\frac{k_c}{h_{gap} h_i} V_i'(x) - V_i(x) \right]_{r=r_{M+1}} + C_2(r_i,t)\left[\frac{k_c}{h_{gap} h_i} S_i'(x) - S_i(x) \right]_{r=r_{M+1}} \} = - \sum_{i=1}^{N} \left[C_1(r_i,t)\, V_i(x) + C_2(r_i,t) S_i(x) \right]_{r=r_M} \quad . \quad (6.18)$$

Finally, the fourth boundary condition, Eq. (6.5), gives a relationship between the temperature and its gradient at the clad surface to the bulk coolant temperature, T_B, as follows

$$- \frac{k_c}{h_{film}} \left. \frac{\partial T}{\partial r} \right|_{r=r_N} = T(r_N) - T_B \quad . \quad (6.5)$$

T_B results from the subchannel analysis, where h_{film} is also determined according to the scheme outlined in Section . Substituting Eq. (6.12) into the above equation results in

$$-k_c \sum_{i=N}^{N} \left[\frac{1}{h_i} C_1(r_i,t) V_i'(x) + \frac{1}{h_i} C_2(r_i,t) S_i'(x) \right]_{r=r_N} = h_{film} \{ \sum_{i=1}^{N} \left[C_1(r_i,t)\, V_i(x) + C_2(r_i,t) S_i(x)\right]_{r=r_N} - T_B \} \quad .$$

(6.19)

which can be arranged into the more convenient form:

$$\sum_{i=1}^{N} \{C_1(V_i,t)[V_i(x) + \frac{k_c}{h_i h_{film}} V_i'(x)]_{r=r_N} + C_2(r_i,t)[S_i(x) + \frac{k_c}{h_i h_{film}} S_i'(x)]_{r=r_N}\} = T_B . \quad (6.20)$$

Thus, the total set of $2N_F + 2N_c + 4$ linear equations is finally complete.

6.3.4 Matrix Formulation

By noting that the set of functions $V_i(x)$, $S_i(x)$ has its support in $[x_i, x_{i+1}]$ Eq. (6.14) is rewritten for

$$x = \xi_{ik} \qquad (i = 1, \ldots, N-1;\ k = 1,2)$$

which results in

$$C_1^j(r_i)\,\phi_i(\xi_{ik}) + C_1^j(r_{j+1})\,\phi_{i+1}(\xi_{ik}) + C_2^j(r_i)\,\psi(\xi_{ik}) + C_2^j(r_{i+1})\,\psi(\xi_{ik}) = C_1^{j-1}(r_i)V_i(\xi_{ik}) + C_1^{j-1}(r_{i+1})V_{i+1}(\xi_{ik}) + C_2^{j-1}(r_i)\,S_i(\xi_{ik}) + C_2^{j-1}(r_{i+1})S_{i+1}(\xi_{ik}) \quad (6.21)$$

where ϕ_i and ψ_i are defined as

$$\phi_i = V_i(x) - \frac{\alpha\Delta t}{h_i}\left[\frac{V_i'(x)}{r} + \frac{1}{h_i} V_i''(x)\right] \quad (6.22)$$

$$\psi_i = S_i(x) - \frac{\alpha\Delta t}{h_i}\left[\frac{S_i'(x)}{r} + \frac{1}{h_i} S_i''(x)\right] \quad (6.23)$$

The four boundary conditions are reformulated as follows. Eq. (6.15) becomes simply

$$C_2(r_1) = 0 \quad (6.24)$$

by recalling that

$$V_1'(x=0) = 0$$

$$S_1'(x=0) = 1$$

Eq. (6.17) becomes

$$C_1(r_m) + \frac{k_f}{h_M h_{gap}} C_2(r_m) = C_1(r_{m+1}) \qquad (6.25)$$

and similarly Eq. (6.18) reads as

$$C_1(r_{m+1}) - \frac{k_c}{h_{M+1} h_{gap}} C_2(r_{M+1}) = -C_1(r_M) \qquad (6.26)$$

Finally, Eq. (6.20) is rewritten as

$$C_1(r_N) + \frac{k_c}{h_N h_{film}} C_2(r_N) = T_B \qquad (6.27)$$

Naturally, the unknown C's are functions of time. Eqs. (6.21, 6.24, 6.25, 6.26, and 6.27) can be put into the following more convenient matrix formulation

$$[A]\,(C^j) = (B^{j-1}) \qquad (6.28)$$

where the right-hand side source vector and the vector of the unknown C's have the following structure

$$(C^j) = \begin{bmatrix} C_1^j(r_1) \\ C_2^j(r_1) \\ C_1^j(r_2) \\ C_2^j(r_2) \\ \vdots \\ C_1^j(r_N) \\ C_2^j(r_N) \end{bmatrix} \qquad \begin{bmatrix} 0 \\ B_{11} \\ B_{12} \\ B_{21} \\ B_{22} \\ \vdots \\ B_{N-1,1} \\ B_{N-1,2} \\ T_B \end{bmatrix} \qquad (6.29)$$

and the coefficient matrix (A) is of the form

$$
[A] = \begin{bmatrix}
0 & 1 & 0 & 0 & & & & & & \\
\phi_1'' & \psi_1'' & \phi_2'' & \psi_2'' & & & & & & \\
\phi_1^{12} & \psi_1^{12} & \phi_2^{12} & \psi_2^{12} & & & & & & \\
 & & \phi_{M-1}^{M-1,1} & \psi_{M-1}^{M-1,1} & \phi_M^{M-1,1} & \psi_M^{h-1,1} & & & & \\
 & & \phi_{M-1}^{h-1,2} & \psi_{h-1}^{h-1,2} & \phi_M^{h-1,2} & \psi_h^{h-1,2} & & & & \\
 & & 0 & 1 & \gamma_M & -1 & 0 & & & \\
 & & 0 & -1 & 0 & 1 & \gamma_{M+1} & & & \\
 & & & & \phi_{M+1}^{M+1,1} & \psi_{h+1}^{h+1,1} & \phi_{M+1}^{h+1,1} & \psi_{h+1}^{M+1,1} & & \\
 & & & & & & \phi_{N-1}^{N-1,2} & \psi_{N-1}^{N-1,2} & \phi_N^{N-1,2} & \psi_N^{N-1,2} \\
 & & & & & & 0 & 1 & \gamma_N & 0
\end{bmatrix}
$$

(6.30)

The following abbreviations have been used in Eqs. (6.29) and (6.30)

$$B_{ik} = C_1^{j-1}(V_i)V_1(\xi_{ik}) + C_1^{j-1}(r_{i+1})V_{i+1}(\xi_{ik}) + C_2^{j-1}(r_i)S_i(\xi_{ik}) + C_2(r_{i+1})S_{i+1}(\xi_{ik}) \quad (i = 1,2, \ldots, h-1, M+1, \ldots, N-1)$$

$$B_{M_1} = B_{h_2} = 0 \qquad (6.31)$$

$$\phi_j^{ik} = \phi_j(\xi_{ik}) \qquad (6.32)$$

$$\psi_j^{ik} = \psi_j(\xi_{ik}) \qquad (6.33)$$

$$\gamma_M = \frac{k_f}{h_M h_{gap}} \qquad (6.34)$$

$$\gamma_{h+1} = \frac{k_c}{h_N h_{gap}} \qquad (6.35)$$

and

$$\gamma_N = \frac{k_c}{h_N h_{film}} \qquad (6.36)$$

6.3.5. Method of Solution

As denoted by Eq. (6 .28), for each time step a new set of coefficients must be obtained. The Gauss-Krout algorithm is employed for solving this equation. At this point in time, no efforts have been made to take advantage of the obviously banded structure of the coefficient matrix during the solution procedure simply because it is felt that the matrix is too small (usually 12 x 12) to get a tremondous pay-off. However, it should be recognized that further improvements in the solution method are possible which definitely lead to smaller computation times.

6.4. Numerical Results

Before this subroutine was implemented into WOSUB it has been extensively tested. Table 6.1 summarizes the test case actually run by Yeung [6-12]. The transient is initiated by letting the linear heat generation rate increase exponentially with time as specified below

$$q'(t) = q'(0) \exp(0.1t)$$

Table 6.1 Fuel Pin Physical Properties and Dimensions

1. Transport properties of fuel and cladding

a) Properties of fuel

k_f = 1.50 BTU/hr-ft °F

c_{pf} = 0.080 BTU/lbm °F

ρ_f = 684 lbm/ft^3

b) Properties of cladding

k_c = 9.50 BTU/hr-ft °F

c_{pc} = 0.071 BTU/lbm °F

ρ_c = 409 lbm/ft^3

c) Heat transfer coefficients

h_{film} = 3000 BTU/ft^2-hr °F

h_{gap} = 1000 BTU/ft^2-hr °F

d) Dimensions of fuel pin

R_{cs} = clad outer surface radius = 0.212"

R_c = clad thickness = 0.024"

R_g = gap width = .002"

e) Power transient

$q'(t) = q'(0) \exp(0.1t)$

where $q'(0)$ = 14 kw/ft

and t is the time in seconds

with

$$q'(0) = 14 \text{ kw/ft}$$

being about representative for the hottest channel in a BWR.

The effect of spatial discretization, i.e. number of subintervals, on the accuracy of the solution has been studied by performing a set of three calculations. For the first run, two knots were placed into the fuel and two into the clad region. Since two points were placed in one subinterval, the temperature distribution is approximated by one subinterval in the fuel and the clad, respectively. For the second run four collocating points were put into the fuel and two into the clad while the third run used six points in the fuel and four in the clad. A time step size of 1 ms was chosen for all calculations.

Parallel to these runs the same problem was solved using an explicit finite-difference method in time and a nodal spatial subdivision as described by El-Wakil [6-14]. A calculation using 45 nodes in the fuel and five nodes in the clad with the same time step size of 1 ms has been performed for the conditions as summarized in Table .1.

Table 6.2 shows a comparison of the temperature distributions as calculated by the two methods at 2 s. after the initiation of the transient whereas Table 6.3 shows the temperatures at 4 s. Among the thirteen radial positions denoted in the tables are some of those used as original nodal positions for the finite-difference calculation. Thus, additional interpolations are not necessary. For the collocation

Table 6.2

Comparison of a Finite-Difference Method with the Collocation Method at time = 2.0 seconds

Δt = 0.001 seconds

Radial Distance (in)	Finite-Difference 45 Pts in Fuel 5 Pts in Clad T(°F)	Collocation Method: 2 pts in Fuel 2 pts in Clad T(°F)	% Error	4 pts in Fuel 2 pts in Clad T(°F)	%Error	6 pts in Fuel 2 pts in Clad T(°F)	% Error	
0	3868	3877	0.233	3878	0.258	3878	0.258	
0.211×10^{-1}	3838	3845	0.182	3846	0.208	3846	0.208	
0.423×10^{-1}	3740	3749	0.241	3748	0.214	3748	0.214	
0.634×10^{-1}	3577	3587	0.280	3585	0.224	3584	0.196	fuel
0.846×10^{-1}	3348	3359	0.329	3356	0.239	3355	0.209	
1.06×10^{-1}	3053	3064	0.360	3061	0.262	3059	0.197	
1.27×10^{-1}	2691	3700	0.334	2699	0.297	2697	0.223	
1.48×10^{-1}	2262	2267	0.221	2269	0.309	2267	0.211	
1.69×10^{-1}	1762	1763	0.057	1767	0.284	1766	0.227	
1.86×10^{-1}	1308	1309	0.077	1312	0.306	1312	0.306	
1.88×10^{-1}	804.2	800.3	0.485	801.3	0.361	801.3	0.361	
2.00×10^{-1}	752.0	748.5	0.465	749.3	0.359	749.3	0.359	clad
2.12×10^{-1}	703.0	699.8	0.455	700.4	0.371	700.4	0.370	

Table 6.3

Comparison of a Finite-Difference Method with the Collocation Method at time = 4.0 seconds

Δt = 0.001 seconds

Radial Distance (in)	Finite-Difference 45 Pts in Fuel 5 Pts in Clad	Collocation Method					
		2 pts in Fuel 2 pts in Clad		4 pts in Fuel 2 pts in Clad		6 pts in Fuel 4 pts in Clad	
	T(°F)	T(°F)	%Error	T(°F)	% Error	T(°F)	% Error
0	4092	4100	0.196	4099	0.171	4098	0.147
0.211×10^{-1}	4061	4068	0.172	4067	0.148	4065	0.099
0.423×10^{-1}	3961	3972	0.278	3967	0.152	3966	0.126
0.634×10^{-1}	3795	3809	0.369	3801	0.158	3798	0.079
0.846×10^{-1}	3559	3575	0.450	3565	0.169	3563	0.112
1.06×10^{-1}	3254	3268	0.430	3260	0.184	3257	0.092
1.27×10^{-1}	2875	2885	0.348	2882	0.243	2878	0.104
1.48×10^{-1}	2420	2422	0.082	2426	0.248	2423	0.124
1.69×10^{-1}	1880	1878	0.106	1886	0.319	1884	0.213
1.86×10^{-1}	1383	1382	0.072	1388	0.362	1388	0.362
1.83×10^{-1}	829.4	824.2	0.627	826.2	0.386	826.1	0.398
2.00×10^{-1}	772.0	767.4	0.596	769.0	0.389	768.9	0.402
2.12×10^{-1}	718.1	714.0	0.571	715.2	0.404	715.2	0.404

method which results in point values, the temperatures at these positions are obtained by means of interpolation which is entirely consistent with the approximation procedure being used. As additional information, a column is given which shows the deviation

$$\frac{T_{f.d} - T_{c.m}}{T_{f.d}} \times 100\%$$

As can be seen from the tables the accuracy obtained from the collocation method is surprisingly high even in the case of the simplest approximation where the calcualtion results agree within 0.5%. This seems more than adequate for most engineering applications. It should be kept in mind that the values obtained by the finite-difference method have to interpreted as nodal ones. Consistently higher accuracy is observed in the fuel region than in the clad. The reason for this is the higher thermal diffusivity in the fuel compared with that of the clad. A higher accuracy of the results in the clad can be achieved naturally by increasing the number of subintervals or by reducing the time step size.

Fig. 6.1 summarizes the results previously given in the tables and compares the collocation method with the finite-difference method for different times during the transient.

More information about the accuracy of the collocation method has been provided by Chawla et al [6-7]. However, it should be recalled that these authors treated the nonlinear heat conduction equation and finally ended up with a set of nonlinear ordinary differential equations which

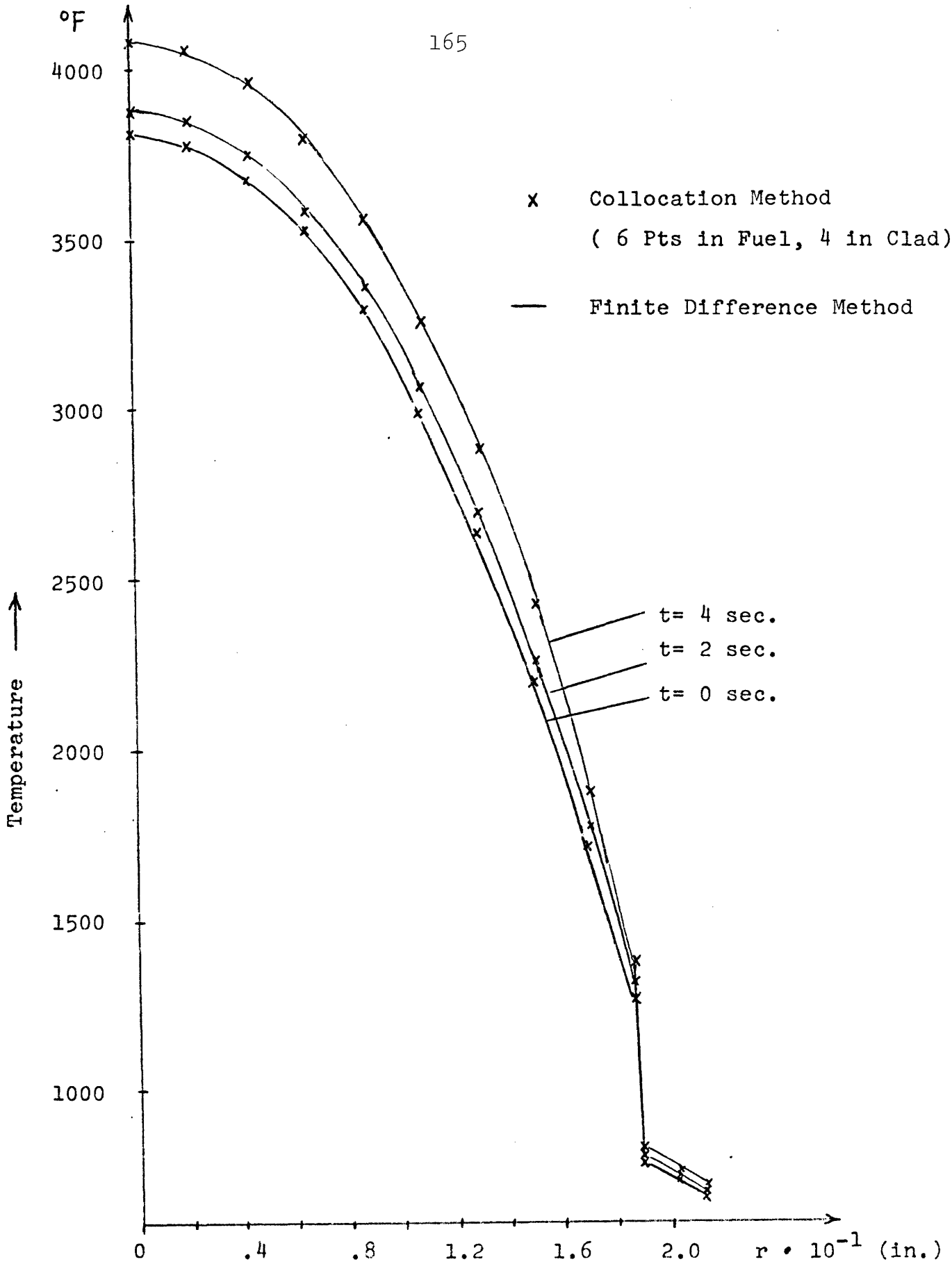

Fig. 6.3 Temperature Distributions in a Fuel Rod During Transient

is solved using the GEAR [6-15] package. Nevertheless, their findings also support our results showing the great advantage of using the collocation method. For the purpose of comparison the THTB [6-16]program has been used by these authors which incorporates an implicit time differencing scheme. Even so, their results indicate that the accuracy obtained with only 12 equations in the collocation method is comparable with the accuracy obtained with 41 equations in the finite-difference method corresponding to a time step of 0.01 s. However, the collocation method needed only 3 s. CPU-time whereas the finite-difference method required 67 s.!

6.5. Conclusion

The integration of a collocation method for solving the transient fuel pin temperatures into the subchannel code WOSUB, should be considered as a major step forward in the direction of the use of more effective and money-saving numerical methods.

Although the fuel pin model now incorporated into WOSUB works on the basis of temperature-independent physical properties, there remains still the possibility to easily extend this procedure in order to account for temperature dependencies by applying Kirchhoff's transformation. What this amounts to is simply replacing the subroutine now in the code by one which has been provided by Chawla [6-17]. This has the additional feature of taking melting into account by a procedure described in [6-18], a phenomenon totally neglected in standard subchannel codes, thus far.

6.6 REFERENCES

[6-1] B.A. Finlayson, "The Method of Weighted Residuals and Variational Principles with Application in Fluid Mechanics, Heat and Mass Transfer," Academic Press, N.Y., 1972.

[6-2] T. Rodack and L. Wolf, "Sensitivity Study of the Assembly Averaged Thermal-Hydraulic Models of the MEKIN Computer Code in Power Transients," MITNE-206, MIT Department of Nuclear Engineering, August, 1977.

[6-3] I.V. Villadsen and W.E. Stewart, "Solution of Boundary-Value Problems by Orthogonal Collocation," Chemical Engineering Science, 22, 1483-1501 (1967).

[6-4] I.V. Villadsen and I.P. Sorenson, "Solution of Parabolic Differential Equations by a Double Collocation Method," Chemical Engineering Science, 24, 1337-1349 (1969).

[6-5] A. Shalev, M. Baruch and E. Nissim, "Buckling Analysis of Hydrostatically Loaded Conical Shells by the Collocation Method," AIAA Journal, 11, 1603-1607 (1973).

[6-6] C. DeBoor and B. Swartz, "Collocation at Gaussian Points," SIAM J. Numerical Analysis, 10, 582, (1973).

[6-7] T.C. Chawla et al, "The Application of the Collocation Method Using Hermite Cubic Splines to Nonlinear Transient One-Dimensional Heat Conduction Problems," ASME Paper 76-HT-B, also J. Heat Transfer, 562-569, (1975).

[6-8] C.W. Stewart et al, "COBRA-IV: The Model and the Method," BNWL-2214, 1975.

[6-9] R.J. Cena et al, "Predicting Fuel Rod Temperature Response by Orthogonal Collocation," Trans. ANS, 21, 205-206 (1975).

[6-10] C.L. Wheeler et al, "COBRA-IV-I: An Interim Version of COBRA for Thermal-Hydraulic Analysis of Rod Bundle Nuclear Fuel Elements and Cores," BNWL-1962, 1976.

[6-11] M.-K. Yeung, "The Application of the Collocation Method Using Hermite Cubic Polynomials to LWR Fuel-Pin Transient Conduction Problems," Special Problem in Nuclear Engineering, Department of Nuclear Engineering, September 1975.

[6-12] I. Douglas and T. Dupont: "A Finite Element Collocation Method for Quasi-linear Parabolic Equations," Math. Comp., 27, 121, (1973).

[6-13] M.M. El-Wakil, "Nuclear Heat Transport," International Textbook Co., 1971.

[6-14] A.C. Hindmarsh, "GEAR: Ordinary Differential Equation System Solver," UCID-30001, Rev. 3, 1974.

[6-15] G.L. Stephens and D.I. Campbell, "Program THTB for Analysis of General Transient Heat Transfer Systems," R60FPD647, General Electric Co., 1961.

[6-16] T.C. Chawla, "FUELMELT" personal communication, July 1976.

[6-17] T.C. Chawla, G. Leaf and W. Chen, "A Collocation Method Using B-Splines for One-Dimensional Heat or Mass-Transfer-Controlled Moving Boundary Problems," Nuclear Engineeering Design, 35, 163-180 (1975).

APPENDIX A

Derivation of the Conservation Equations

A.1 Continuity of Mass

A.1.1 Vapor Phase

The balance equation for the continuity of vapor mass is set up for the control volume shown below:

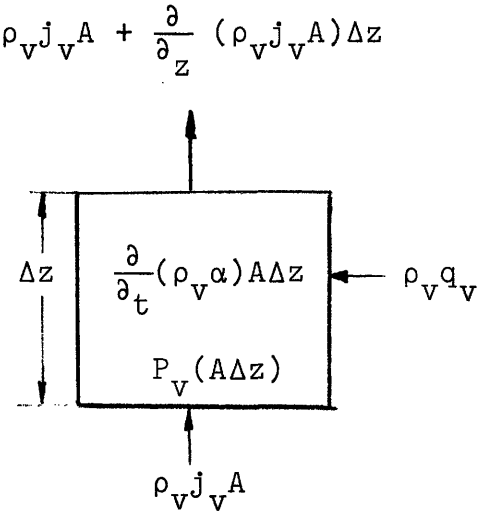

Collecting terms and reordering results in

$$\frac{\partial}{\partial t}(\rho_v \alpha) A \Delta z = \rho_v j_v A - \rho_v j_v A - \frac{\partial}{\partial z}(\rho_v j_v A)\Delta z + \rho_v q_v \Delta z + \Gamma_v (A \Delta z)$$

In case the cross-sectional flow area is constant, i.e., A = const., the above equation simplifies to

$$\frac{\partial}{\partial t}(\rho_v \alpha) + \frac{\partial}{\partial z}(\rho_v j_v) = \Gamma_v + \frac{\rho_v q_v}{A} \qquad \text{(A-1)}$$

If the vapor is assumed to be incompressible, then

$$\frac{\partial j_v}{\partial z} = \frac{1}{\rho_v}\left[\Gamma_v + \frac{\rho_v q_v}{A} - \frac{\partial}{\partial t}(\rho_v \alpha)\right] \tag{A-2}$$

A.1.2 Liquid Phase

In a similar manner, the equation can be derived for the liquid phase.

$$\frac{\partial j_\ell}{\partial z} = \frac{1}{\rho_\ell}\left\{-\Gamma_v + \frac{\rho_\ell g_\ell}{A} - \frac{\partial}{\partial t}\left[\rho_\ell(1-\alpha)\right]\right\} \tag{A-3}$$

A.1.3 Mixture Volumetric Flux

By adding Eqs. (A-2) and (A-3) one obtains the balance equation for the total mixture volumetric flux

$$\frac{\partial j}{\partial z} = \left(\frac{1}{\rho_v} - \frac{1}{\rho_\ell}\right)\Gamma_v + \frac{q}{A} - \frac{1}{\rho_v}\frac{\partial}{\partial t}(\rho_v \alpha) - \frac{1}{\rho_\ell}\frac{\partial}{\partial t}\left[\rho_\ell(1-\alpha)\right] \tag{A-4}$$

where

$$j = j_v + j_\ell$$

and

$$q = q_v + q_\ell$$

The drift flux formulation for the void fraction is

$$\alpha = \frac{j_v}{C_o j + V_{gj}} \tag{A-5}$$

A.1.4 Finite Difference Formulation

With this information, Eqs. (A-2) and (A-4) can be put into finite difference equations, namely for the latter one obtains

$$j_{out} = j_{in} + z[(1-\mu)\Psi + \frac{q}{A}] - \frac{\Delta z}{\Delta t}(1-\frac{\overline{\rho_v}}{\rho_v})\bar{\alpha} - \frac{\Delta z}{\Delta t}(1-\frac{\overline{\rho_\ell}}{\rho_\ell})(1-\bar{\alpha}) \tag{A-6}$$

whereas for the latter one gets

$$j_v = \frac{j+V_{gj}}{C_o j+V_{gj}+\frac{\Delta z}{\Delta t}} \{j_{v_{in}} + \Delta z(\Psi + \frac{q_v}{A}) + \frac{\Delta z}{\Delta t}\frac{\overline{\rho_v}}{\rho_v}\bar{\alpha}\} \tag{A-7}$$

where

$$\mu = \frac{\rho_v}{\rho_\ell} \qquad \text{and} \qquad \Psi = \frac{\Gamma_v}{\rho_v}$$

Eq. (A-5) was used to derive Eq. (A-7).

A.2 Conservation of Energy

Again, starting point is the central volume shown below together with all incoming and exiting energy fluxes.

$$A\{\rho_\ell j_\ell H_\ell + \rho_v j_v H_g + \frac{\partial}{\partial z}(\rho_\ell j_\ell H_\ell + \rho_v j_v H_g)\Delta z\}$$

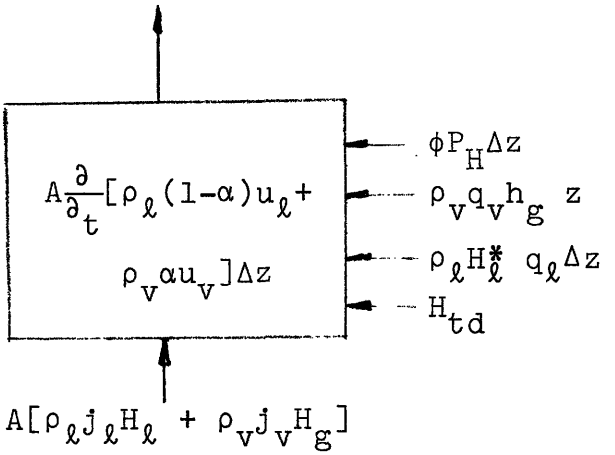

where $u_\ell = h_\ell - P/\rho_\ell$

The assumption is made that the vapor is always saturated, i.e., $H_v = H_g$. The balance on the control volume yields

$$\frac{\partial}{\partial t}[\rho_\ell(1-\alpha)H_\ell + \rho_v \alpha H_v] + \frac{\partial}{\partial z}[\rho_\ell j_\ell H_\ell + \rho_v j_v H_v]$$

$$= \phi\frac{P_H}{A} + \frac{\partial P}{\partial t} + \frac{\rho_\ell H_\ell^* q_\ell}{A} + \frac{\rho_v H_v q_v}{A} + \frac{H_{td}}{A} \qquad \text{(A-8)}$$

APPENDIX B

Drift Velocity Formulation for Annular Two-Phase Flow

B.1 Annular Correlation

B.1.1 Introduction

The latest formulation of the drift velocity in two-phase annular flow by Ishii, Chawla and Zuber [B-1] offers an interesting range of extended application for the WOSUB code.

The goal of Ishii's formulation is to establish empirical correlation of the drift velocity for annular flow conditions. The correlation is based on parameters describing the effects of gravity, interfacial shear stress as function of interfacial roughness and the flow regime effect on the liquid film.

As discussed in Chapter 3, the built-in correlation for the drift velocity is limited to the churn turbulent bubbly flow. The addition of a correlation for annular flow would greatly facilitate the application of WOSUB in transient analyses where this flow regime may prevail.

In what follows, some ideas are presented as to how the annular correlation can be implemented into the WOSUB code.

B.1.2 Assumptions and Range of Validity

The assumptions underlying the annular correlation are as follows:

1) Steady state and adiabatic conditions;
2) Effects of heat transfer and phase changes are considered secondary. It must be concluded then, that for diabatic and transient conditions, i.e., conditions for

which the correlation would be most helpful, it must be considered an approximation.

B.2 Equations

B.2.1 Drift Velocity as Function of Liquid Volumetric Flux

The liquid film may be either in laminar or turbulent flow.

a) For laminar flowing film, the vapor drift velocity is given by

$$V_{gj}^2 = \frac{16\alpha}{\rho_g f_i \xi}\left[\frac{\mu_\ell j_\ell}{D} + \frac{\Delta\rho_g D(1-\alpha)^3}{48}\right] \qquad \text{(B-1)}$$

where $f_i = \pm\, 0.005[1 + \varepsilon]$ + for $V_{gj} \geq 0$, - for $V_{gj} \leq 0$

interfacial friction factor

$\varepsilon = 300\ \delta/D \simeq 75(1-\alpha)$ roughness parameter

$\delta =$ thickness of liquid film

$\xi = P_i/P_{wf} \simeq 1$

where

$P_i = \pi(D + \delta)$

$P_{wf} = \pi D$

b) For turbulent flowing film, the vapor drift velocity is given by

$$V_{gj}^2 = \frac{\alpha(1-\alpha)^3 D}{\xi f_i \rho_\ell} \left[\left(\frac{0.0791}{Re_\ell^{0.25}}\right) \frac{\rho_\ell j_\ell |j_\ell|}{D(1-\alpha)^3} + \frac{1}{3}\Delta\rho g\right] \qquad \text{(B-2)}$$

This equation can be put into a simpler form by defining a turbulent wall friction factor such as:

$$f_{wf} = \begin{cases} 16/Re & \text{if } Re \leq 3200 \\ 0.005 & \text{if } Re > 3200 \end{cases}$$

then

$$V_{gj}^2 = -\frac{(1-\alpha)^3 D}{f_i \rho g} \left[\frac{0.005\ \rho_\ell j_\ell |j_\ell|}{D(1-\alpha)^3} + \frac{1}{3}\Delta\rho g\right] \qquad \text{(B-3)}$$

It is proposed to use Eq. (B-3) as a first step in WOSUB, thereby always assuming a turbulent liquid film thickness and only concurrent flow.

B.2.2 Drift Velocity as Function of Mixture Velocity

When the drift velocity is expressed as function of the mixture velocity, V_m, a more general formulation is obtained which is also capable of accounting for countercurrent flow situations.

Table B.I presents all the equations which are suggested to be implemented into WOSUB as a second step.

B.3 Discussion About Programming Technique

The following steps are suggested to implement the iterative scheme shown in Fig. B.I into the code:

1) In subroutine WATER

   before VDRIFT calc. in WATER (correlation)

   put a switch (JTRANS) to continue the calculation in case of transients to

   VDAF = vapor drift for annular flow = f (correlation)

2) Use the same procedure in CONTI, i.e.,

   set up (JTRANS) in TRANS such as

   JTRANS = .TRUE.

   IN CONTI, or WATER:

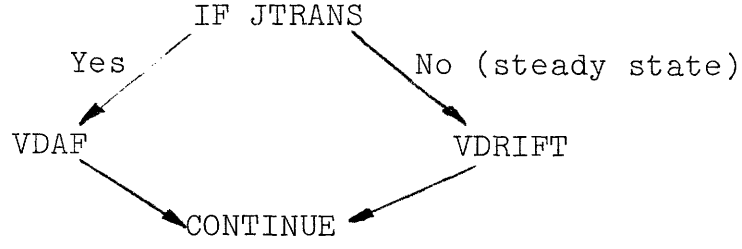

LAMINAR FLOW	TURBULENT FLOW
$$V_{gj} = \frac{8\mu_f \alpha^2}{\rho_m D f_i \xi}\left\{-1+\left(1+\frac{f_i D \rho_m^2 (1-\alpha)\xi}{4\mu_f \alpha^3 \rho_g}\times\left[v_m+\frac{\Delta\rho g D^2 (1-\alpha)^2}{48\mu_f}\right]\right)^{1/2}\right\}$$ Valid for cocurrent or countercurrent flow with V_{gj} such as $$\frac{(1-\alpha)\rho_m v_m - \rho_m j_{ftr}}{\alpha\rho_g} \leq V_{gj} \leq \frac{(1-\alpha)\rho_m v_m + \rho_m j_{ftr}}{\alpha\rho_g}$$	For $v_m = \left\{\frac{\Delta\rho g D (1-\alpha)^3 \alpha^3 \rho_g}{3\rho_m^2 f_i \xi}\right\}^{1/2}$ $$V_{gj} = \begin{cases} \frac{-b v_m + [a v_m^2 + (a-b^2)c]^{1/2}}{a-b^2} & \text{if } a-b^2 \neq 0 \\ (v_m^2 + c)/2b v_m & \text{if } a-b^2 = 0 \end{cases}$$ where $a \equiv \frac{f_i \xi \rho_g}{0.05 \alpha \rho_f (1-\alpha)^2}$; $b \equiv \frac{\alpha\rho_g}{\rho_m(1-\alpha)}$; $c \equiv \frac{\Delta\rho g D (1-\alpha)^3}{0.015\rho_f}$ Upwards liquid flow for $-\sqrt{c} < v_m < \sqrt{cb^2/a}$, $$V_{gj} = \frac{-b v_m + [-a v_m^2 + (a+b)^2 c]^{1/2}}{a+b^2}$$

Table B.I: Relations for V_{gj} when $V_{gj} = f(v_m)$

MODIFICATION IN SUBROUTINE CONTI FOR A DIFFERENT VELOCITY DRIFT CALCULATION

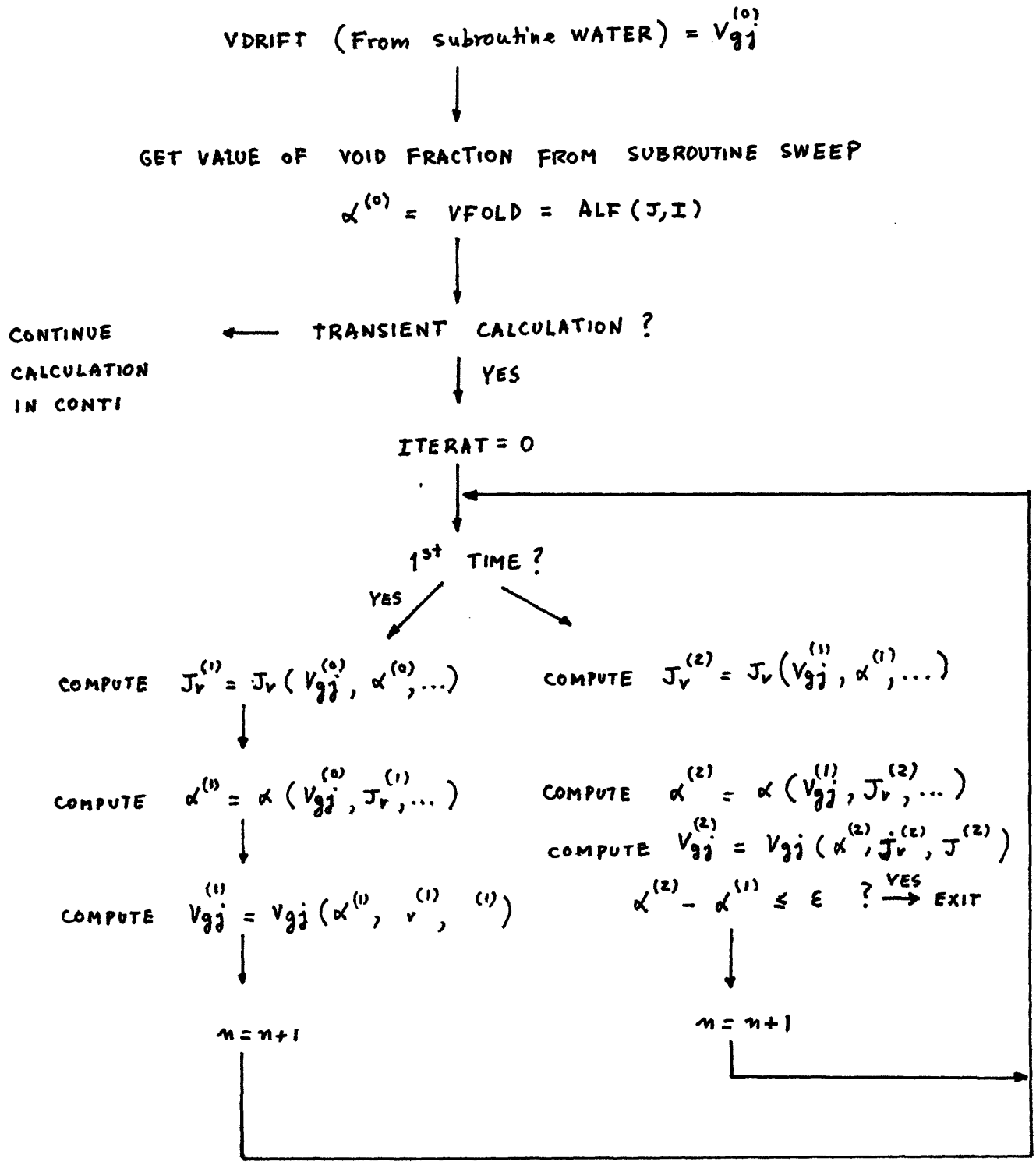

Fig. B.1: Iterative scheme for the calculation of V_{gj} in annular flows.

B.4 Programming

1. Put SWITCH in TRANS for a transient calculation of the velocity drift: this switch is JTRANS

```
LOGICAL   JTRANS
JTRANS = .TRUE.
```
} in subroutine TRANS

```
LOGICAL   JTRANS
JTRANS = .FALSE.
```
} in MAIN

```
LOGICAL  JTRANS
```
in CONTI , SWEEP

2. Put in CONTI , MAIN SWEEP

```
LOGICAL    ITERAT
      Put in CONTI
DATA  ETA/1./
      After line    00001662:
      ITERAT = 0.
1000  IF (ITERAT -1)  998, 998, 1003
998   SAVE = AJVIN + DZ*PS± + QV/AA
      SAVJ = AJ + AK* VDRIFT
 44   CONTINUE
      IF (NOT.JTRANS) GO TO 1200
      YFUSED = VF
      AJUSED = AJ
      AJVUSE = AJV
      SAVIR = 0.
```

```
1003  SAVOR = 0.
C     CALCULATE VAPOR DRIFT VELOCITY FOR TRANSIENT
      CONDITION
      EPSI = 75 * (1.-VFUSED)
      FINTER = 0.005*(1. + EPSI)
      SAVOR = VFUSED* HYDRO/ETA*ROVAP
      SAVOR = SAVOR*(1-VFUSED)**3
      PABS = ABS(AJUSED - AJVUSE)
      PABS = PABS* (AJUSED -AJVUSE)* RO* 0.005
      PABS = PABS/ HYDRO* (1- VFUSED) ** 3
      PABS = PABS + (RO - ROVAP) * 9.81/3
      VDANF = SAVOR * PABS
      VDANF = SQRT (VDANF)
      SAVO = 0.
      SAVA = 0.
      AJNEW = AJIN + DZUMG*PSI + Q/AA
      IF (ITRA) AJNEW = AJNEW - VZERO* (1-ROVRA)*VFOLD
C     VAPOR CONTINUITY
      SAVO = AJVIN.+ DZ*PSI+QU/AA
      SAVJO = AJNEW + AK*VDANF
      IF (.NOT. ITRA) GO TO 1002
      SAVO = SAVO + VEERO * ROVRA * VFUSED
      SAVO = SAVJO * SAVO-VZERO*ZE*PSIS
      SAVO = SAVO/ (SAVJO+AK*VZERO)
1002  AJVNEW = SAVO
C     VOID FRACTION CALCULATION WITH VDANF
      VFNEW = (AK * AJVNEW + ZE*PSIS)/SAVJO.
```

```
      DELTA = VFNEW - VFUSED
      DELTA = DELTA/VFNEW
      IF (DELTA - 0.001) 1001, 1001, 1200
1002  VFUSED = VFNEW
      AJUSED = AJNEW
      AJVUSE = AJVNEW
      ITERAT = ITERAT + 1
      GO TO 1000
1200  CONTINUE
C     LIQUID CONTINUITY                    line 00001681
```

3. IN SWEEP PUT: (IN LOOPE 10)

   After line 00001137

```
HYDRO = HYD(I).
Put also
LOGICAL JTRANS
LOGICAL ITERAT
```

NOMENCLATURE

A	Subchannel Flow Area $[L^2]$
C_o	Zuber's void concentration parameter
C	Constant
D_H	Hydraulic Diameter $[L]$
h	Convective heat transfer coefficient $[E/(L^2.T.^oR)]$
f	Friction factor
G	Mass flux $[M/L^2.T)]$
g	Acceleration of gravity $[L/T^2]$
$\hat{H}_\ell$	Liquid enthalpy $[E/M]$
$\hat{H}^*_\ell$	Enthalpy of the liquid entering subchannel $\underline{i}$ from all other subchannels $[E/M]$
$\hat{H}_v$	Vapour enthalpy $[E/M]$
H_{td}	Energy transfer due to liquid-liquid mixing $[E/(T.L)]$
H_{fg}	Latent heat of evaporation $[E/M]$
H_{sat}	Enthalpy of saturated liquid $[E/M]$
j	Total volumetric flux $[L/T]$
j	Liquid flux (superficial velocity) $[L/T]$
j_v	Vapour flux $[L/T]$
K	Thermal conductivity
K	Constant appearing in the velocity potential term
K''	Mixing parameter
M_ℓ	Correction factor for the liquid momentum
M_v	Correction factor for the vapour momentum

M Matrix specifying the geometrical layout of the subchannels

n Constant in nucleate boiling correlation

P Pressure $[F/L^2]$

P_h Heated perimeter $[L]$

$q_i = q_{\ell i} + q_{v_i}$ Total diverted flow to subchannel $\underline{i}$ per unit length $[L^2/T]$

q_{ℓ_i} Liquid volume flow to subchannel $\underline{i}$ from all other subchannels per unit length $[L^2/T]$

q_{v_i} Vapour volume flow to subchannel $\underline{i}$ from all other subchannels per unit length $[L^2/T]$

$q_{v_{i,k}}$ Vapour volume flow to subchannel $\underline{i}$ from subchannel $\underline{k}$ per unit length $[L^2/T]$

q_{ik} Total flow to subchannel $\underline{i}$ from subchannel $\underline{k}$ per unit length $[L^2/T]$

R_{ij} Diffusion coefficient characterizing transport from subchannel $\underline{i}$ to $\underline{j}$ $[L^2/T]$

R_e Reynolds shear stress due to turbulence $[F/L^2]$

R Recondensation coefficient

S_{ij} Transverse slip ratio relating the vapour flow to total flow

t Time $[T]$

$\overline{V}_{gj}$ Vapour drift velocity $[L/T]$

V Velocity potential term

Z Space coordinate in the axial flow direction $[L]$

Z_e Relaxation Length $[L]$

Greek Symbols

α Void fraction

γ Density ratio = p_v/p_l

ϵ Eddy diffusivity $[L^2/T]$

ϕ Heat flux $[E/(L^2.T)]$

χ Two phase friction multiplier

λ Latent heat of evaporation $[E/M]$

ψ Vapour volume generation term per unit volume

ρ Density $[M/L^3]$

θ Temperature referred to saturation $[^0R]$

ς Momentum transferred due to diverted flow $[F/L^2]$